CONSEIL INTERNATIONAL DES UNIONS SCIENTIFIQUES

UNION GEODESIQUE ET GEOPHYSIQUE INTERNATIONALE

ASSOCIATION DE SÉISMOLOGIE ET DE PHYSIQUE DE L'INTÉRIEUR DE LA TERRE

PUBLICATIONS DU BUREAU CENTRAL SÉISMOLOGIQUE INTERNATIONAL

Sous la direction de J. P. ROTHÉ

SECRÉTAIRE DE L'ASSOCIATION DE SÉISMOLOGIE ET DE PHYSIQUE DE L'INTÉRIEUR DE LA TERRE

SÉRIE A

TRAVAUX SCIENTIFIQUES

Fascicule 23

TOULOUSE
ÉDOUARD PRIVAT & Cie Libraire-Éditeur
14, RUE DES ARTS, 14

1964

AVERTISSEMENT

Dans le présent fascicule on trouvera le texte de quelques-unes des communications scientifiques qui ont été présentées au cours de l'Assemblée Générale de Berkeley (15 août au 31 août 1963).

Les communications publiées se rapportent aux sujets suivants :

Propagation des ondes séismiques;

Constitution de la croûte continentale et de la croûte océanique;

Séismicité et tectonique;

Microséismes.

Les autres communications présentées sont destinées à paraître dans différents périodiques scientifiques. On en trouvera les références bibliographiques dans les Comptes Rendus n° 14, Association de Séismologie et de Physique de l'Intérieur de la Terre; Comptes Rendus des séances de la XIII[e] conférence réunie à Berkeley du 15 au 31 août 1963, Strasbourg, 1964 (sous presse).

J.-P. Rothé,

Secrétaire général
de l'Association Internationale de Séismologie
et de Physique de l'Intérieur de la Terre.

ASSEMBLÉE GÉNÉRALE DE BERKELEY

(15 au 31 août 1963)

COMMUNICATIONS PUBLIÉES DANS LE FASCICULE 23 DES TRAVAUX SCIENTIFIQUES DU BUREAU CENTRAL INTERNATIONAL DE SÉISMOLOGIE

TABLE DES MATIÈRES

SEISMIC WAVES PROPAGATION

PAGES

CONSTITUTION OF THE CONTINENTAL AND OCEANIC CRUST

SEISMICITY AND TECTONICS

MICROSEISMS

THE THEORY OF SURFACE WAVE DIFFRACTION BY SYMMETRIC CRUSTAL DISCONTINUITIES*

by J. KANE** and J. SPENCE**

SUMMARY

A major barrier in comparing seismic theory with observed wave trains, stems from the fact that elastic wave characteristics are influenced by discontinuities along the propagation path, and any understanding of such signal corruption would require a knowledge of the diffracted fields at the appropriate obstacles. However, even a relatively simple crustal feature such as a discontinuous change in terrain presents major difficulties if the relevant problem of diffraction in a wedge-shaped region is considered. Although some first-order calculations have been made by Lapwood (1961), Kane and Spence (1963), and Hudson and Knopoff (1963), the theoretical discussion of the diffraction effects are hampered by the intractability of the associated boundary value problems. In this report, we show how one can take advantage of symmetry considerations and variational techniques to rapidly estimate reflection, transmission, and conversion coefficients for elastic wave diffraction at symmetric wedge-shaped obstacles. In Part I, we illustrate the ideas by a discussion of the vector problem of Rayleigh wave propagation along the faces of an elastic wedge with free boundaries. In Part II, we analyze the scalar problem of multi-mode Love wave diffraction in a symmetric layered wedge.

PART I

Rayleigh waves on an elastic wedge

1. *Fundamental equations*

The tremors $s(u, v, w)$ of an elastic solid characterized by the Lame parameters λ, μ, and density ρ, can be derived from a scalar potential $\varnothing (x, y, z)$, and a vector potential $\Psi\ [\psi_x (x, y, z), \psi_y (x, y, z), \psi_z (x, y, z)]$ by the relation

$$s(u, v, w) = \Delta . \varnothing + \Delta \times \Psi. \qquad (1.1)$$

For two-dimensional motions wich are independant of the z-coordinate, both $\varnothing$ and Ψ are but functions of x and y, or $\varnothing = \varnothing (x, y)$, and $\Psi = \Psi (x, y)$. Furthermore, we can neglect pure distorsions by setting $\psi_x = \psi_y = 0$, so that the vector potential $\Psi = \Psi\ [0, 0, \psi_z (x, y)]$ is characterized by one scalar component and the subscript on ψ_z can be dropped without confusion. If we assume that the vibrations

---

* Preliminary version of a paper to appear in the Geophysical Journal of the Royal Astronomical Society.

** Univ. of Rhode Island; Kingston, R. I., U.S.A.

are harmonic, we can suppress a time factor $e^{-i\omega t}$, and it can be shown that $\varnothing$, and ψ the z-component of the vector potential, satisfy the reduced wave equations

$$(\Delta^2 + k^2_c)\,\varnothing = 0, \qquad k^2_c = \omega^2\rho/(\lambda + \mu), \tag{1.2}$$

$$(\Delta^2 + k^2_s)\,\psi = 0, \qquad k^2_s = \omega^2\rho/\mu \quad . \tag{1.3}$$

Once the potentials $\varnothing$ and ψ are known, the displacement vector s is given by (1.1), and the resultant stress dyadic $\mathfrak{S}$ $(\varnothing, \psi)$ can be given in symbolic notation as

$$\mathfrak{S}\,(\varnothing, \psi) = \lambda\,\mathfrak{I}\ \Delta . s + \mu\,(\Delta s + s\Delta) \tag{1.4}$$

where $\mathfrak{I}$ is the unity dyadic, the idemfactor.

2. *The Rayleigh wave potentials*

A time harmonic Rayleigh wave, or $\mathcal{R}$-wave for brevity, is comprised of a pair of exponential solutions of (1.2) and (1.3), $\mathcal{R} = \mathcal{R}$ $(\varnothing_R, \psi_R)$. If the elastic solid lies within the half-space $y \leqslant 0$ (*cf.* Fig. 1 *a*), then these solutions, in polar coordinates $x = r \cos \theta$, $y = r \sin \theta$, assume the form

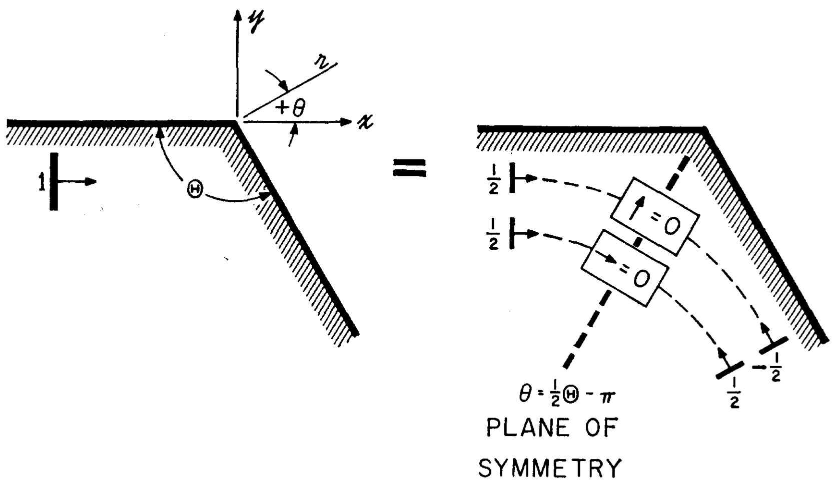

FIG. 1. — A unit Rayleigh wave incident along one face of an elastic wedge is equivalent to four partial waves. The partial waves of like parity comprise the excitation for the even problem, and the partial waves of unlike parity furnish the initial disturbance for the odd problem.

$$\mathcal{R}\,(\varnothing_R, \psi_R) = \begin{cases} \varnothing_R = e^{\alpha(\theta)\Xi} & (1.5) \\ \psi_R = -\,i\,\Gamma\,e^{\beta(\theta)\Xi} & (1.6) \end{cases}$$

wherein the exponential variation is given by

$$\alpha\,(\theta) = \sqrt{1 - (v_R/v_c)^2}\,\sin\theta + i\cos\theta, \quad v^2_c = \frac{\lambda + \mu}{\rho} \tag{1.7}$$

$$\beta(\theta) = \sqrt{1-(v_R/v_s)^2}\,\sin\theta + i\cos\theta,\; v_s^2 = \frac{\mu}{\rho} \qquad (1.8)$$

and Γ, the magnitude of the ratio of the shear potential coefficient of ψ_R to the compressional one $\varnothing_R$ is

$$\Gamma = \frac{\sqrt{1-(v_R/v_c)^2}}{1-{}^1/{}_2(v_R/v_s)^2}\,, \qquad (1.9)$$

and Ξ is a dimensionless distance parameter

$$\Xi = k_R\, r = \frac{\omega}{v_R}\, r. \qquad (1.10$$

The parameters v_c and v_s represent the velocities of the compressional and shear body waves respectively. For a given Poisson's ratio σ

$$\sigma = \frac{\lambda}{2(\lambda+\mu)} \qquad (1.11)$$

one needs choose the Rayleigh wave velocity v_R, which is less than v_s, so that the stresses induced by $\varnothing_R$ and ψ_R vanish at the surface $y = 0$

$$\mathfrak{S}\,(\varnothing_R,\, \psi_R) = 0, \qquad y = 0. \qquad (1.12)$$

With this choice of v_R, the $\varnothing_R$ and ψ_R given by (1.5) and (1.6) are the vector and scalar potentials characterizing a Rayleigh wave traveling to the right with unit amplitude (we shall speak of the coefficient of the compressional potential as the amplitude). It is very convenient to note that *we can reverse the direction of any harmonic wave by the operation of complex congugation;* thus

$$R\,\mathcal{R}\,(\varnothing^*_R,\, \psi^*_R) = \left\{ \begin{array}{ll} R\,\varnothing^*_R = R\, e^{\alpha^*(\theta)\Xi} & (1.13) \\ R\,\psi^*_R \;= +\, iR\Gamma\, e^{\beta^*(\theta)\Xi} & (1.14) \end{array} \right.$$

represents a Rayleigh wave traveling in the opposite direction with amplitude R.

3. *Formulation of the boundary value problems*

a) *The major problem*

The conundrum posed by Rayleigh wave diffraction in a wedge-shaped region is to find additional solutions $\varnothing_d$ and ψ_d, of (1.2) and (1.3) which represent diffracted fields in the interior of the wedge such that the stress dyadic $\mathfrak{S}\,(\varnothing_R + \varnothing_d,\, \psi_r + \psi_d)$ vanishes on both faces of the wedge for $\mathcal{R}$-wave excitation along one face. In our geometry (*cf.* Fig. 1 *a*), the $\mathcal{R}$-wave is incident from infinity along the negative x-axis. We shall be principally concerned with calculating the complex amplitudes of the reflected and transmitted

$\mathcal{R}$ waves as a function of the wedge angle Θ and Poisson's ratio σ. This task can be substantially eased by reducing the major problem to a pair of minor problems involving even and odd symmetries. Consider the incident $\mathcal{R}$-wave along the left wedge face to be the sum of two waves, each of half amplitude. Likewise, the absence of any excitation along the right wedge face is equivalent to a pair of incident $\mathcal{R}$-waves along it, each of half amplitude, *but opposed in sign*, (*cf.* Fig. 1 *b*). The four partial $\mathcal{R}$-waves can be separated into two groups : First, a pair of $\mathcal{R}$ waves on either face of like parity wich serves as the excitation of what we call *the even minor problem*. Second, another pair of $\mathcal{R}$-waves whose amplitudes are of unlike parity which constitutes the excitation of the *odd minor problem*. If we designate the diffracted fields of the even and odd problems by the subscripts e and o respectively, then since we are dealing with linear equations, the desired major potentials $\varnothing_d$ and ψ_d can be expressed as a superposition of the minor potentials

$$\varnothing_d = \varnothing_e + \varnothing_o, \tag{1.15}$$

$$\psi_d = \psi_e + \psi_o, \tag{1.16}$$

and likewise the displacement vector $\mathbf{s} = \mathbf{s}_e + \mathbf{s}_o$ can be decomposed into even and odd components.

b) *The even minor problem*

In the even problem, the wedge will suffer only *even displacements** $\mathbf{s}_e$ about the plane of symmetry, and as a result, there can be no component of normal displacement along the plane of symmetry at $\theta = \Theta/2 - \pi$. It follows that the even problem is equivalent to finding the potentials in a *bisected wedge* with one face free of stresses which supports the incident Rayleigh wave, and the other face so constrained that the *normal* displacement vanishes there. That is, we seek solutions $\varnothing_e$ and ψ_e of (1.2) and (1.3) in a wedge of half-angle $\Theta/2$

$$\text{EVEN} \begin{cases} \mathfrak{S}\,(\varnothing_R + \varnothing_e, \psi_r + \varnothing_e) = 0. & \theta = \pi \qquad (1.17) \\ \dfrac{1}{r}\dfrac{\partial}{\partial\theta}(\varnothing_R + \varnothing_e) + \dfrac{\partial}{\partial r}(\psi_R + \psi_e) = 0, & \theta = \Theta/2 - \pi \qquad (1.18) \end{cases}$$

c) *The odd minor problem*

By the same arguments, the odd problem wich involves $\varnothing_o$, ψ_o is a complementary version in the bisected wedge, wherein the

---

* N. B. — The displacements, and the compressional potential will be even about the plane of symmetry, but the shear potential will be an odd function, and *vice versa* for the odd problem.

tangential displacements must vanish identically along the plane of symmetry, i.e.,

$$\text{ODD}\left\{\begin{array}{lll} \mathfrak{S}\,(\varnothing_R + \varnothing_o,\ \psi_R + \varnothing_o) = 0 & \theta = \pi & (1.19) \\ \dfrac{\partial}{\partial r}\,(\varnothing_R + \varnothing_o) + \dfrac{1}{r}\,\dfrac{\partial}{\partial \theta}\,(\psi_R + \psi_o) = 0 & \theta = \Theta/2 - \pi & (1.20) \end{array}\right.$$

d) *The Reflection Coefficients*

For either the even or the odd problem, the solution will contain a reflected Rayleigh wave. Let $\rho_e\ (\Theta/2,\ \sigma)$ and $\rho_o\ (\Theta/2,\ \sigma)$ be the complex ratios of the reflected to the incident Rayleigh wave amplitude for the even and odd minor problems in the bisected wedge. The reflection coefficient R $(\Theta,\ \sigma)$ for the original major problem will be

$$R\,(\Theta,\sigma) = \tfrac{1}{2}\,[\rho_e\,(\Theta/2,\sigma) + \rho_o\,(\Theta/2,\sigma)], \qquad (1.21)$$

and likewise the overall transmission coefficient T $(\Theta,\ \sigma)$ will be

$$T\,(\Theta,\sigma) = \tfrac{1}{2}\,[\rho_e\,(\Theta/2,\sigma) - \rho_o\,(\Theta/2,\sigma)]. \qquad (1.22)$$

Formulas (1.21) and (1.22) can be verified by a glance at Figure 1 *b* which indicates that the overall reflection coefficient R results from a superposition of the partial reflection coefficients $\frac{1}{2}\,(\rho_e + \rho_o)$, and the transmission coefficient T from their interference $\frac{1}{2}\,(\rho_e - \rho_o)$.

4. *The Variational Principle*

a) *Discussion*

Variational procedures consist of assuming a suitable trial function containing unspecified coefficients, and then choosing these parameters to minimize certain quantities. One major advantage of the variational method is that first-order accuracy in the trial function usually gives results which are accurate to second-order, because of the stationary character of the approximation.

A natural aperture in the present problem is the plane of symmetry and we can assume it to be illuminated by an incident $\mathcal{R}$-wave, and a reflected one with an adjustable amplitude. In the even problem, the net angular displacement must vanish along the plane of symmetry. A unit $\mathcal{R}$-wave traveling to the right gives rise to the angular component of the displacement

$$s_\theta^{\text{inc}} = k_R \left[\frac{\partial \alpha}{\partial \theta}\, e^{\alpha \Xi} + \beta e^{\beta \Xi} \right], \qquad (1.23)$$

and likewise an $\mathcal{R}$-wave of amplitude ρ_o moving to the left generates the disturbance

$$\rho_e\, s_\theta^{\text{ref}} = \rho_e\, (s_\theta^{\text{inc}})^* \qquad (1.24)$$

which apart from an amplitude factor is the complex conjugate of (1.23). Only if there is no discontinuity, or if $\Theta = \pi$ can we make the angular displacement of the trial function

$$s_\theta^{T} = s_\theta^{inc} + \rho_e \left(s_\theta^{inc}\right)^* \tag{1.25}$$

vanish for all r along the plane of symmetry by properly choosing ρ_e. Otherwise $\alpha \neq \alpha^*$, $\beta \neq \beta^*$, and no choice of ρ_e can make s_Θ^T vanish at more than an isolated set of points. There are at least two ways by which we can improve matters : We could use a more complex trial function which acknowledges body-wave contributions to the diffracted field, or, since the residual displacement s_Θ^T is explicitly known, we can use it as the aperture illumination of a Green's theorem type calculation to correct the variational estimate.

However, the practical seismic interest is in the realm of small discontinuities, and for this case we shall see that the elementary trial function yields satisfactory results.

b) *Definition of the scalar product*

While there are many gauges by which s_Θ^T can be minimized, we shall choose a ρ_e which minimizes s_Θ^T in the mean square sense. For this purpose, let us define the complex scalar product of two functions $u\,(r\,,\theta)$ and $v\,(r,\,\theta)$ to be

$$(u, v) \equiv \int_0^\infty u\,(r, \theta)\; v^*\,(r, \theta)\; dr, \tag{1.26}$$

where the integration is to be carried out along the plane of symmetry $\theta = \Theta/2 - \pi$. To each complex function $u\,(r,\,\theta)$ we can attach a positive definite number, the norm of u or $\|\, u \,\|$ which is defined to be $\sqrt{(u, u)}$. The norm $\|\, u \,\|$ depends on the wedge angle, and is to be distinguished from $u^2 = (u,\, u^*)$ which is in general complex.

c) *The Even Subsidiary Reflection Coefficient*

With this notation, the mean square value of the angular displacement of the trial function s_Θ^T is

$$\|\, s_\theta^T \,\|^2 = (s_\theta^{inc}) + \rho_e\ (s_\theta^{inc})^*,\ s_\theta^{inc} + \rho_e\,(s_\theta^{inc})^*), \tag{1.27}$$

and this will be a minimum if and only if ρ_e is chosen as

$$\rho_e\ (\Theta/2, \sigma) = \frac{\left(s_\theta^{inc\,2}\right)}{\|\ s_\theta^{inc}\,\|^2}\,, \tag{1.28}$$

or explicity in terms of $\alpha\,(\theta)$, $\beta\,(\theta)$ and Γ,

$$\rho_e\,(\Theta/2,\sigma) = \frac{-\dfrac{1}{2\alpha}\left(\dfrac{\partial\alpha}{\partial\theta}\right)^2 + \dfrac{\Gamma^2\beta}{2} - \dfrac{2\,i\,\Gamma\,\beta}{\alpha+\beta}\left(\dfrac{\partial\alpha}{\partial\theta}\right)}{\dfrac{1}{\alpha+\alpha^*}\left|\dfrac{\partial\alpha}{\partial\theta}\right|^2 + \dfrac{\Gamma^2\,|\,\rho\,|^2}{\beta+\beta^*} + i\,\Gamma\left[\dfrac{\beta}{\alpha^*+\beta}\dfrac{\partial\alpha^*}{\partial\theta} - \dfrac{\beta^*}{\alpha+\beta^*}\left(\dfrac{\partial\alpha}{\partial\theta}\right)\right]} \tag{1.29}$$

d) *The Odd Subsidiary Reflection Coefficient*

If we use an analogous trial function, and similar reasoning, we find that if ρ_o is to be an optimal choice we need make the selection

$$\rho_o\,(\Theta/2,\,\sigma) = \frac{\left(s_r^{\mathrm{inc}}\right)^2}{\|\,s_r^{\mathrm{inc}}\,\|^2}\,, \tag{1.30}$$

or

$$\rho_o\,(\Theta/2,\sigma) = \frac{-\dfrac{\alpha^2}{2\alpha} + \dfrac{\Gamma^2}{2\beta}\left(\dfrac{\partial\beta}{\partial\theta}\right) + \dfrac{2\,i\,\alpha\,\Gamma}{\alpha+\beta}\left(\dfrac{\partial\beta}{\partial\theta}\right)}{\dfrac{|\alpha|^2}{\alpha+\alpha^*} + \dfrac{\Gamma^2}{\beta+\beta^*}\left|\dfrac{\partial\beta}{\partial\theta}\right|^2 - i\,\Gamma\left[\dfrac{\alpha^*}{\alpha^*+\beta}\left(\dfrac{\partial\beta}{\partial\theta}\right) - \dfrac{\alpha}{\alpha+\beta^*}\left(\dfrac{\partial\beta^*}{\partial\theta}\right)\right]} \tag{1.31}$$

5. *Discussion of the overall reflection and transmission coefficients*

With an explicit ρ_e and ρ_o at our disposal, we can evaluate the R (Θ, σ) and T (Θ, σ) germane to our elementary trial function. For reference, their complex variation is plotted as a function of the discontinuity angle $\Theta - \pi$, in Figure 2 for Poisson's ratio $\sigma = \frac{1}{4}$. The present magnitudes $|\,\mathrm{T}\,|$ are somewhat smaller than that given by earlier first-order calculations (Kane and Spence 1963), which do not simultaneously yield R and T. Since we evaluate both R and T together, we must, in effect, withdraw some energy from the transmitted field to allow for the reflected wave. Furthemore, it is the nature of the variational technique to underestimate the subsidiary diffraction coefficients ρ_e and ρ_o since it only yields their projection in the sub-space spanned by the trial function.

Although the analysis is certainly valid for a small enough discontinuity in wedge angle, the utility of the procedure can not be established until there is some estimate of the errors committed. A feature of the present procedure is that it suggests a natural gauge of the accuracy. While ρ_e and ρ_o are so chosen that $\|\,s_\Theta^{\mathrm{T}}\,\|$ and $\|\,s_r^{\mathrm{T}}\,\|$ are minimized, both s_Θ^{T} and s_r^{T} are non-zero along aperture plane. These residuals, which are explicitly known, can not be farther reduced without introducing new features such as body wave contributions into be analysis. Since $[1 - |\mathrm{R}|^2 - |\mathrm{T}|^2]$ represents that fraction of energy unaccounted for, we can estimate the need for improving the calculations by examining this quantity.

This error estimate is a very generous one because only part of it implies higher-order corrections to R and T, the remainder representing energy which is accounted for by $\mathcal{R}$-wave to body wave conversion. The data of Figure 2 shows that if $|\,\Theta - \pi\,| < 10°$, the present analysis accounts for at least 92 percent of the energy, and therefore the theory should not require further improvement within this range. We can also compare the present theory with experiment, but we must be very careful if we do so, because there are fundamental distinctions between analysis in the harmonic domain and pulse measurements (*cf.* Appendix).

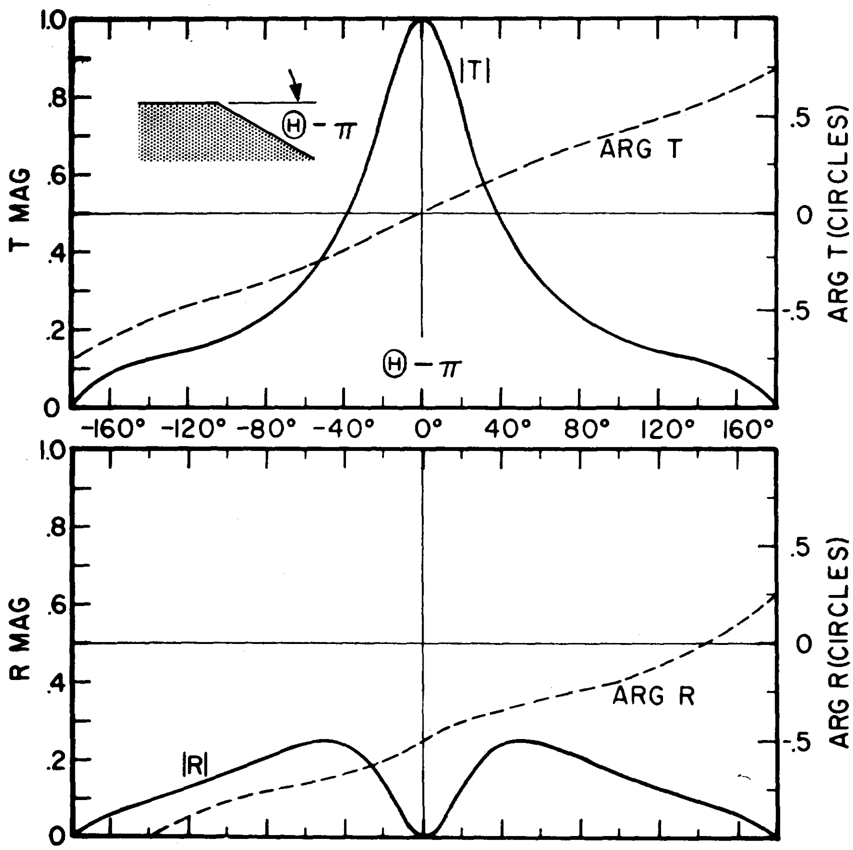

FIG. 2. — The diffraction coefficients R and T for a trial function consisting of but an incident and reflected wave. In this case, Poisson's ratio $\sigma = 1/4$.

PART II

Love waves on an elastic wedge

1. *Introduction*

A layered solid can support surface waves which are horizontally polarized shear waves trapped in the superficial layer. Since these Love waves, as they are known, have no compressional component, it is not necessary to introduce potentials, and it is possible to work directly with one scalar function $w\ (x, y)$, the z-component of the displacement vector

$$\mathbf{s} = \mathbf{s}\ [0, 0, w\,(x, y)]. \tag{2.1}$$

Within the E_1 layer, w satisfies the wave equation

$$(\Delta^2 + k^2{}_1)\ w\,(x, y) = 0, \qquad k^2{}_1 = \omega^2\rho_1/\mu_1, \qquad (2.2)$$

and within the E_2 substrate, w obeys

$$(\Delta^2 + k^2{}_2)\ w\,(x, y) = 0, \qquad k^2{}_2 = \omega^2\rho_2/\mu_2. \qquad (2.2)$$

At the free surface of E_1, the normal stress must vanish, which will be true provided that the normal derivative

$$\frac{\partial w}{\partial n} = 0 \qquad (2.4)$$

vanishes there.

We assume the $E_1 — E_2$ interface to be welded so that the displacement and normal stress must be continuous across this boundary. Along the left wedge face, these conditions will be satisfied provided that the Love waves, or $\mathfrak{L}_i$-waves of amplitude A_i have the form

$$A_i\,\mathfrak{L}_i = \begin{cases} A_i \cos\sqrt{k^2{}_1 - \lambda^2{}_i}\; y\, e^{i\lambda_i x}, & 0 \geqslant y \geqslant -H \qquad (2.5)\\ A_i \cos\sqrt{k^2{}_1 - \lambda^2{}_i}\; H \exp\sqrt{\lambda^2{}_i - k^2{}_2}\; y\, e^{i\lambda_i x}, & y \leqslant -H, \qquad (2.6)\end{cases}$$

and the propagation constants λ_i are the real roots of the period equation

$$\tan\sqrt{k^2{}_1 - \lambda^2{}_i}\; H = \frac{\mu_2}{\mu_1}\sqrt{\frac{\lambda^2{}_i - k^2{}_2}{k^2{}_1 - \lambda^2{}_i}} \qquad (2.7)$$

If the shear wave is to be trapped in the layer, or if the Love wave is to propagate, we need $|k_2| \leqslant |\lambda_i| \leqslant |k_1|$. For any thickness however small, there is at least one root λ_1 corresponding to an acceptable solution — the fundamental $\mathfrak{L}_1$-wave. As the acoustic thickness k_1H increases, other modes can propagate. In our discussion, we shall assume that the thickness is such that only two modes propagate, the fundamental, and one harmonic : the $\mathfrak{L}_2$-wave with a propagation constant λ_2. The analysis proceeds in a similar fashion if an arbitrary number of modes can propagate.

2. *Formulation of the boundary value problem*

We assume than an $\mathfrak{L}_1$-wave is incident along one face of a symmetrically layered wedge. At the discontinuity, four surface waves will be excited : A reflected and transmitted $\mathfrak{L}_1$-wave with amplitude coefficients R_{11} and T_{11} respectively, and reflected and reflected and transmitted $\mathfrak{L}_2$ waves whose amplitudes are the convesion coefficients R_{12} and T_{12} respectively. Our task will be to determine these diffraction coefficients as functions of the wedge angle Θ, the layer thickness H, and the elastic constants ρ_1, ρ_2, μ_1, μ_2.

By the same argument as in Part I, we can add and subtract a symmetric $\mathfrak{L}_1$-excitation on the right wedge face which leads us to

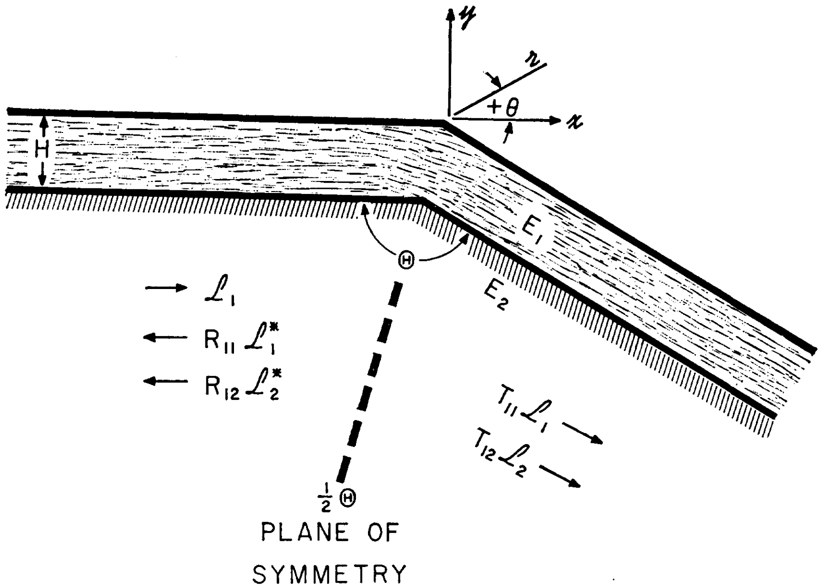

FIG. 3.

consider a pair of even and odd problems in a bisected wedge. Since Love wave diffraction is a scalar problem, the subsidiary boundary conditions along the aperture or plane of symmetric are simply

$$\text{EVEN}: \frac{1}{r}\frac{\partial w}{\partial \theta} = 0, \qquad \theta = \Theta/2 - \pi \tag{2.8}$$

$$\text{ODD}: \quad w = 0, \qquad \theta = \Theta/2 - \pi \tag{2.9}$$

for the even and odd problems. The trial function will consist of an incident $\mathfrak{L}_1$-wave, and reflected $\mathfrak{L}^*_1$ and $\mathfrak{L}^*_2$-waves, with unknown amplitudes. If we denote the subsidiary reflection and conversion coefficient for the even problem in the bisected wedge as r^e_{11} and r^e_{12}, and similary r^0_{11} and r^0_{12} for the odd problem, then the desired major coefficients are

$$R_{11} = \tfrac{1}{2}(r^e_{11} + r^0_{11}), \tag{2.10}$$

$$R_{12} = \tfrac{1}{2}(r^e_{12} + r^0_{12}), \tag{2.11}$$

$$T_{11} = \tfrac{1}{2}(r^e_{11} - r^0_{11}), \tag{2.12}$$

$$T_{12} = \tfrac{1}{2}(r^e_{12} - r^0_{12}). \tag{2.13}$$

As in Part I, we shall determine these coefficients by a variational procedure which ignores body wave contributions.

3. *Solution*

In the odd problem we shall choose r_{o11} and r_{o12} so that the residual variation $\varepsilon(r)$ along the aperture plane

$$\varepsilon(r) = \mathcal{L}_1 + r^o_{11}\, \mathcal{L}^*_1 + r^o_{12}\, \mathcal{L}^*_1, \qquad \theta = \Theta/2 - \pi \tag{2.14}$$

is as small as possible in the mean square sense. Using the same definition of scalar product as in Part I, we have

$$\| \varepsilon(r) \|^2 = (\mathcal{L}_1 + r^o_{11}\, \mathcal{L}^*_1 + r^o_{12}\, \mathcal{L}^*_2,\ \mathcal{L}_1 + r^o_{11}\, \mathcal{L}^*_1 + r^o_{12}\, \mathcal{L}^*_2), \tag{2.15}$$

and this expression will be a minimum if and only if r^o_{11} and r^o_{12} satisfy the normal equations

$$(\mathcal{L}_1, \mathcal{L}_1) + r^o_{11}(\mathcal{L}^*_1, \mathcal{L}_1) + r^o_{12}(\mathcal{L}^*_2, \mathcal{L}_1) = 0, \tag{2.16}$$

$$(\mathcal{L}_1, \mathcal{L}_2) + r^o_{11}(\mathcal{L}^*_1, \mathcal{L}_2) + r^o_{12}(\mathcal{L}^*_2, \mathcal{L}_2) = 0. \tag{2.17}$$

Equations (2.16) and (2.17) can immediately be solved for r^o_{11} and r^o_{12}

$$r^o_{11} = -\frac{1}{\mathrm{DET}^o} \begin{vmatrix} (\mathcal{L}_1, \mathcal{L}_1) & (\mathcal{L}^*_2, \mathcal{L}_1) \\ (\mathcal{L}_1, \mathcal{L}_2) & (\mathcal{L}^*_2, \mathcal{L}_2) \end{vmatrix}, \tag{2.18}$$

and

$$r^o_{12} = -\frac{1}{\mathrm{DET}^o} \begin{vmatrix} (\mathcal{L}^*_1, \mathcal{L}_1) & (\mathcal{L}_1, \mathcal{L}_1) \\ (\mathcal{L}^*_1, \mathcal{L}_2) & (\mathcal{L}_1, \mathcal{L}_2) \end{vmatrix} \tag{2.19}$$

where

$$\mathrm{DET}^o = \begin{vmatrix} (\mathcal{L}^*_1, \mathcal{L}_1) & (\mathcal{L}^*_2, \mathcal{L}_1) \\ (\mathcal{L}^*_1, \mathcal{L}_2) & (\mathcal{L}^*_2, \mathcal{L}_2) \end{vmatrix} \tag{2.20}$$

$$r^e_{11} = -\frac{1}{\mathrm{DET}^e} \begin{vmatrix} \left(\frac{1}{r}\frac{\partial \mathcal{L}_1}{\partial \theta}, \frac{1}{r}\frac{\partial \mathcal{L}_1}{\partial \theta}\right) & \left(\frac{1}{r}\frac{\partial \mathcal{L}^*_2}{\partial \theta}, \frac{1}{r}\frac{\partial \mathcal{L}_1}{\partial \theta}\right) \\ \left(\frac{1}{r}\frac{\partial \mathcal{L}_1}{\partial \theta}, \frac{1}{r}\frac{\partial \mathcal{L}_2}{\partial \theta}\right) & \left(\frac{1}{r}\frac{\partial \mathcal{L}^*_2}{\partial \theta}, \frac{1}{r}\frac{\partial \mathcal{L}_2}{\partial \theta}\right) \end{vmatrix}, \tag{2.21}$$

and

$$r^e_{12} = -\frac{1}{\mathrm{DET}^e} \begin{vmatrix} \left(\frac{1}{r}\frac{\partial \mathcal{L}^*_1}{\partial \theta}, \frac{1}{r}\frac{\partial \mathcal{L}_1}{\partial \theta}\right) & \left(\frac{1}{r}\frac{\partial \mathcal{L}_1}{\partial \theta}, \frac{1}{r}\frac{\partial \mathcal{L}_1}{\partial \theta}\right) \\ \left(\frac{1}{r}\frac{\partial \mathcal{L}^*_1}{\partial \theta}, \frac{1}{r}\frac{\partial \mathcal{L}_2}{\partial \theta}\right) & \left(\frac{1}{r}\frac{\partial \mathcal{L}_1}{\partial \theta}, \frac{1}{r}\frac{\partial \mathcal{L}_2}{\partial \theta}\right) \end{vmatrix}, \tag{2.22}$$

where

$$\mathrm{DET}^e = \begin{vmatrix} \left(\frac{1}{r}\frac{\partial \mathcal{L}^*_1}{\partial \theta}, \frac{1}{r}\frac{\partial \mathcal{L}_1}{\partial \theta}\right) & \left(\frac{1}{r}\frac{\partial \mathcal{L}^*_2}{\partial \theta}, \frac{1}{r}\frac{\partial \mathcal{L}_1}{\partial \theta}\right) \\ \left(\frac{1}{r}\frac{\partial \mathcal{L}^*_1}{\partial \theta}, \frac{1}{r}\frac{\partial \mathcal{L}_2}{\partial \theta}\right) & \left(\frac{1}{r}\frac{\partial \mathcal{L}^*_2}{\partial \theta}, \frac{1}{r}\frac{\partial \mathcal{L}_2}{\partial \theta}\right) \end{vmatrix}, \tag{2.23}$$

With this knowledge, the reflection, transmission and conversion coefficients are given by (2.10) — (2.13).

C. *Discussion of the results*

1. *Numerical Data*

We have used the preceeding formulas to calculate the diffraction coefficients for an E_1-layer and E_2-substrate for which $k_1/k_2 = 1.297$ and $\mu_2/\mu_1 = 2.159$. The phase and group velocities for this case have been given by Stoneley and are available in a standard reference (p. 213, Ewing, Jardetsky, and Press). Figures 4 through 7 illustrate the variation of the magnitude of the diffraction coefficients which are *even* functions of the discontinuity angle Θ-π. The curves are indexed by four values of the dimensionless parameter $\lambda_1 H$, namely 5, 6, 7, 8; if $\lambda_1 H = 5$, then the second mode is just above cut-off, and if $\lambda_1 H = 8$, the third mode is just below cut-off. It is very interesting to note that the conversion coefficient T_{12} exceeds the reflection coefficient by an order of magnitude. That is, there is a tendency for the energy to continue to propagate in the same direction even if it necessitates a transfer of modal characteristics.

2. *Interpretation*

If we compare any two waves of identical characteristics, then their relative energy is proportional to the absolute square of any corresponding amplitude. On the other hand, before we can compare the energy in the fundamental $\mathfrak{L}_1$-wave to that of an $\mathfrak{L}_2$-wave, its first harmonic, we need make some further calculations. With no loss in generality, let us specialize our discussion to the horizontal wedge face for which the $\mathfrak{L}_i$-waves are given explicitly by (2.5) and (2.6), and evaluate the scalar product along the wavefront $y = 0$. Thus $|A_i|^2 \, \| \mathfrak{L}_i \|^2$ represents the mean square energy flux transported by an $\mathfrak{L}_i$-wave of amplitude A_i. If we denote the group velocity of an $\mathfrak{L}_i$-wave as Λ_i it follows that the ratio

$$\frac{|A_1|^2 \Lambda_1 \| \mathfrak{L}_1 \|^2}{|A_2|^2 \Lambda_2 \| \mathfrak{L}_2 \|^2} \tag{2 24}$$

compares the power flow of an $A_1\mathfrak{L}_1$-wave to an $A_2\mathfrak{L}_2$-wave. In particular, a mode near cut-off behaves like an unbounded plane wave in the E_2-medium; hence such a wave can carry large amounts of power even if its amplitude is deceptively small. As a

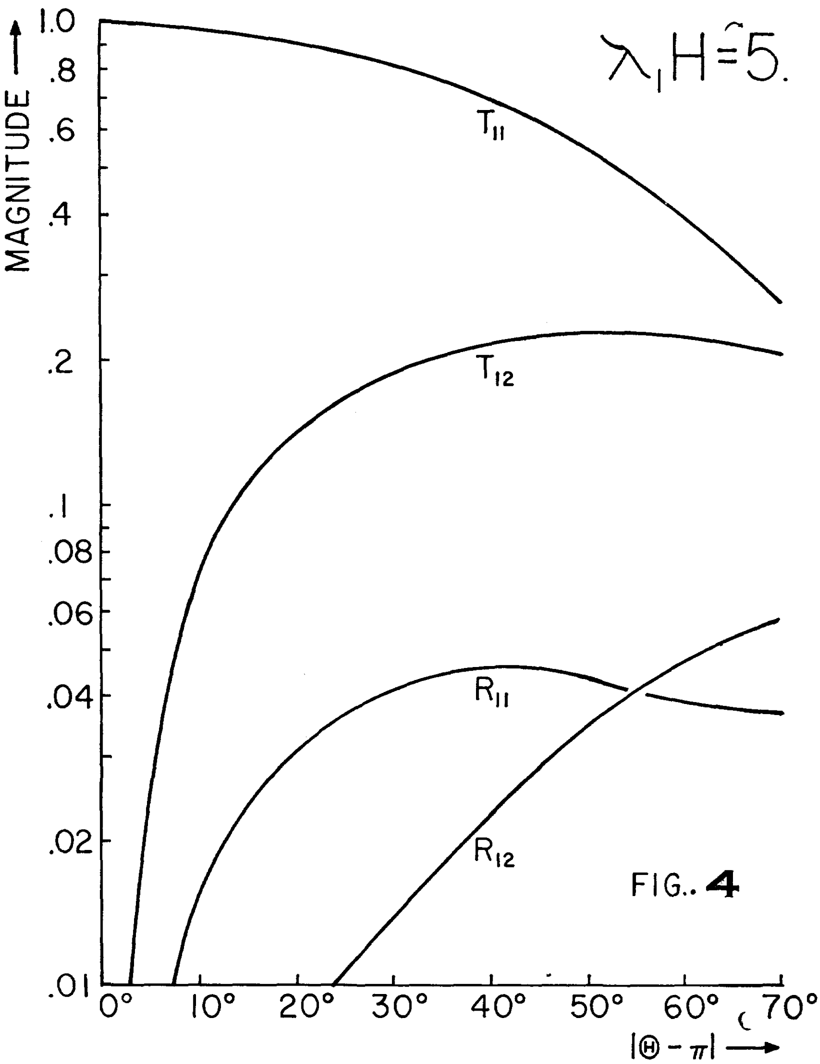

FIG. 4. — The magnitude of the Love wave diffraction coefficients for $\lambda_1 H = 5$; they are even functions of the discontinuity angle $\Theta - \pi$. In this case $k_2/k_1 = 1.297$, $\mu_2/\mu_1 = 2.159$; the normalization value $N = 2.0$.

result, if we are to discuss power transfer, we should renormalize the amplitudes of the conversion coefficients

$$R^N_{12} = NR_{12}, \qquad T^N_{12} = NT_{12} \tag{2.25}$$

where

$$N^2 = \frac{\Lambda_2}{\Lambda_1} \frac{\| \mathcal{L}_2 \|}{\| \mathcal{L}_1 \|} \tag{2.26}$$

so that $|R^N_{12}|^2$ and $|T^N_{12}|^2$ are proportional to the power transferred by the diffraction of a $\mathfrak{L}_1$-wave of unit amplitude at a wedge discontinuity. The appropriate values of N for the previous numerical example are cited in the captions of Figures 4-7.

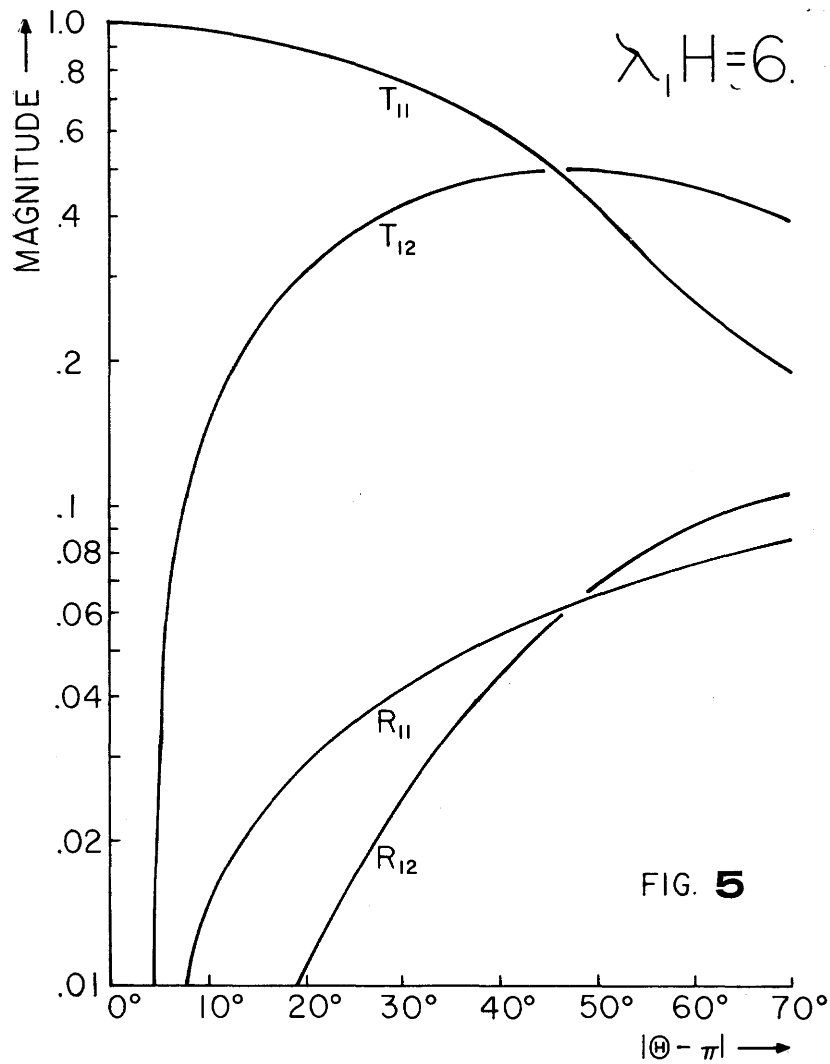

FIG. 5

FIG. 5. — The magnitude of the Love wave diffraction coefficients for $\lambda_1 H = 6$; they are aven functions of the discontinuity angle $\Theta - \pi$. In this case $k_2/k_1 = 1.297$, $\mu_2/\mu_1 = 2.159$; the normalization value $N = 1.2$.

In a fashion similar to the error analysis of Part I, the function $[1 - |R_{11}|^2 - |R^N_{12}|^2 - |T_{11}|^2 - |T^N_{12}|^2]$ represents the amount of ambiguous energy. These values are far more satisfactory in the present analysis than in Part I; this can be explained by the

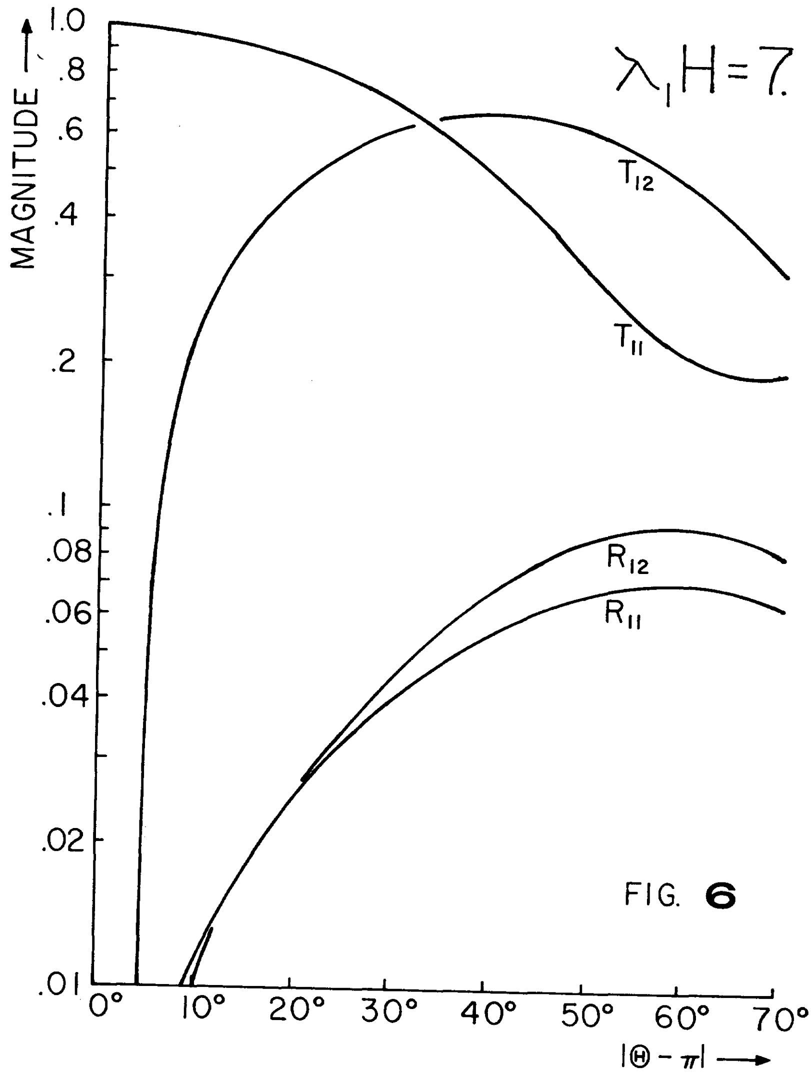

FIG. 6

FIG. 6. — The magnitude of the Love wave diffraction coefficients for $\lambda_1 H = 7$; they are even functions of the discontinuity angle $\Theta - \pi$. In this case $k_2/k_1 = 1.297$, $\mu_2/\mu_1 = 2.159$; the normalization value $N = 1.1$.

fact that we have a more flexible trial function since we can vary the coefficients of *two* reflected modes.

APPENDIX

Love wave diffraction coefficients would be very difficult to measure in the laboratory, but the techniques of two-dimensional

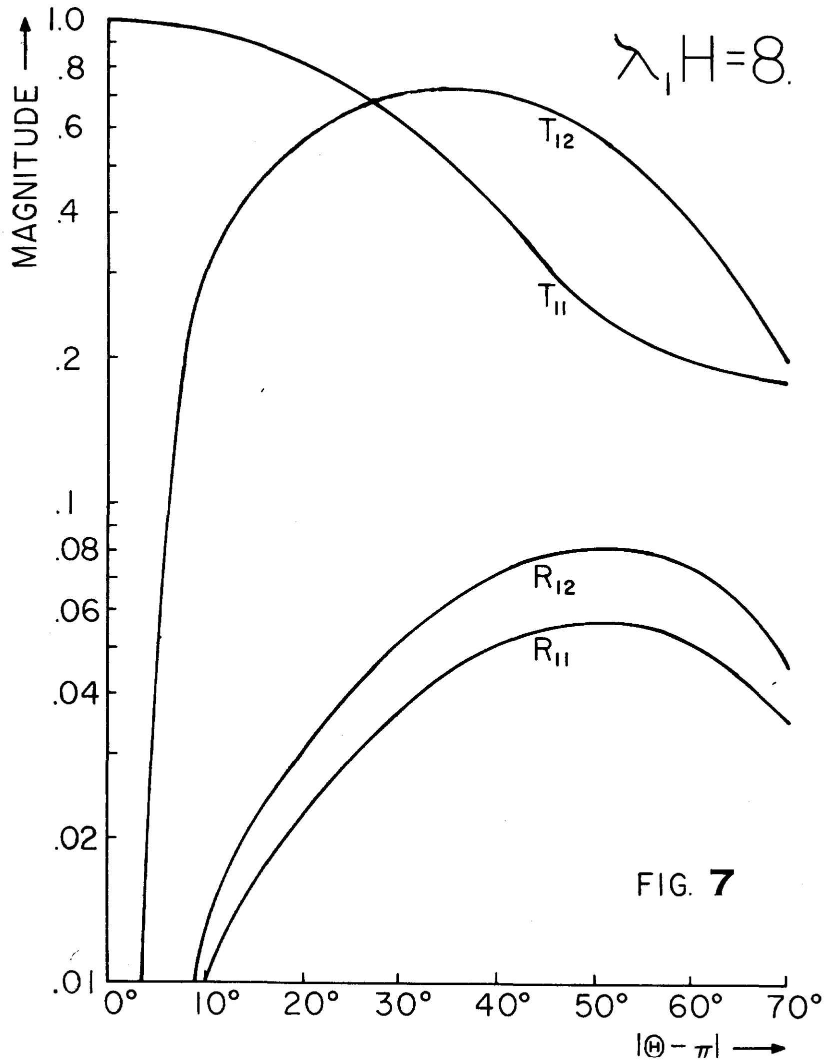

FIG. 7. — The magnitude of the Love wave diffraction coefficients for $\lambda_1 H = 8$; they are even functions of the discontinuity angle $\Theta - \pi$. In this case $k_2/k_1 = 1.297$, $\mu_2/\mu_1 = 2.159$; the normalization value $N = 1.0$

model seismology offer a means of determining Rayleigh wave reflection and transmission coefficients with an accuracy of about 10-20 per cent. The present theory and experiment agree if $\Theta \sim \pi$, but outside this range, there are experimental features which are not duplicated by the results of the present elementary variational procedure. The analysis in the harmonic domain could be refined by employing various devices to reduce the amount of unexplained energy. Such calculations would probably require substantial effort, and the idealized formulation of the present problem should be reviewed if the labor is to have relevance to pulse measurements.

There are major distinctions between analysis in the harmonic and time domain. For example, whereas a harmonic Rayleigh wave is a uniquely defined entity, Friedlander (1948) has pointed out that a Rayleigh pulse can assume a variety of waveforms. Furthermore, any Rayleigh pulse can not have a sharply defined wavefront, and theoretically must give infinite advance notice of its arrival, unless it merges continuously with a precursor, typically the shear pseudo-surface wave (Cagniard 1939). Although the amplitude of this shear wave decays with distance, *its integrated flux remains constant.* It is difficult to separate the far-field effects due to the arrival of a Rayleigh pulse and its shear companion at the second wedge face. In other words, in addition to Rayleigh/Rayleigh interactions, there will be some shear/Rayleigh conversions. What contributions might this shear wave introduce? Whereas we can not give a rigorous answer to this question, we can however make a rough, but simple, estimate.

We first note that if the wedge angle Θ is π or $\pi/2$, then we would expect little or no shear/Rayleigh conversion. In the first case, there is no discontinuity, and the second case corresponds to a geometry for which the shear wave is essentially normal to the second wedge face, and we know that for normal incidence, a shear wave is reflected as a shear wave. Then, from Equation (1.6), we note that we can easily add some additional shear potential to the original excitation by incrementing the Rayleigh wave's shear coefficient Γ by an additional contribution $f(\Theta)$ depending on the wedge angle

$$\Gamma' = \Gamma\,[1 + f(\Theta)]$$

Quite arbitrarily, we have chosen

$$f(\Theta) = \cos\Theta + \cos^2\Theta$$

whose sole merit is that it is the simplest function we could think of that vanishes for $\Theta = \pi, \pi/2$. It is then a trivial matter to repeat the calculations appropriate for Figure 2, and the results are plotted in Figure 8. The shaded area indicates the range of experimental points as measured by Knopoff and Gangi (1960), De Bremaecker (1958), and Viktarov (1958). Of course there is limited justification for this heuristic procedure, but it is remarkable that with this naive device the coefficients R and T adopt many of the characteristics of the experimental data. In any event, we conclude that more refined calculations should use a more realistic excitation.

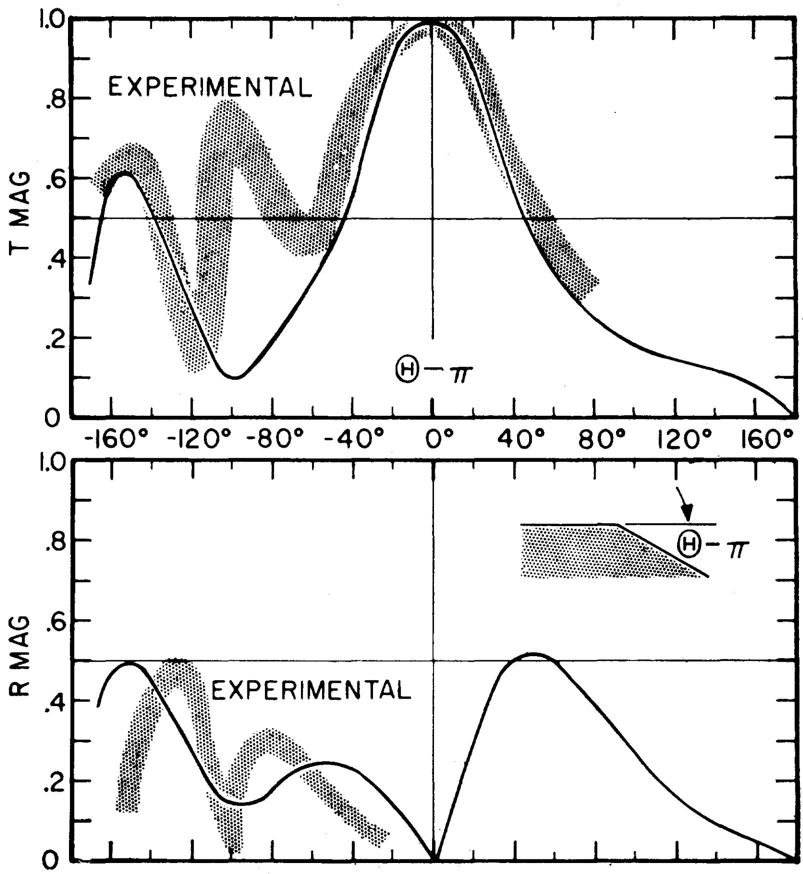

FIG. 8. — The diffraction coefficients R and T for a trial function consisting of an incident and reflected Rayleigh wave. However, the shear coefficient Γ of the incident Rayleigh wave has been incremented by a factor $(1 + \cos \Theta + \cos^2 \Theta)$. In this case, Poisson's ratio $\sigma = 1/4$.

Acknowledgement : The research in this report has been sponsored by the Air Force Cambridge Research Laboratories (Bedford Mass., U.S.A.) as part of project Vela-Uniform.

REFERENCES

BREMAECKER (J. Cl. DE), 1958. *Geophysics, 23,* 253.
CAGNIARD (L.), Thèse, 1939. Translation, 1962, *Reflection and Refraction of Seismic Waves,* McGraw-Hill.
EWING (M.). Jardetsky, W., and Press, F., 1957. *Elastic Waves in Layered Media,* McGraw-Hill.
FRIEDLANDER (F. G.), 1948. *Quart. J. Mech. Appl. Math., 1,* 376.
HUDSON (J. A.) and KNOPOFF (L.), 1963. Contributions 1177 and 1178, Division of Geological Sciences, California Institute of Technology.
KANE (J.) and SPENCE (J.), 1963. *Geophysics, 28,* 715.
KNOPOFF (L.) and GANGI (A. F.), 1960. *Geophysics, 25,* 1203.
LAPWOOD (E. R.), 1958. *Geophysics. J., 4,* 174.
VIKTAROV (I. A.), 1958. *Soviet Physics-Doklady, 3,* 304.

A THEORY OF RAYLEIGH WAVES BASED ON A VISCOELASTIC-PLASTIC MODEL OF EARTH'S CRUST AND MANTLE*

by Paul LIEBER* and K. T. YEN**
* University of California, Berkeley; ** Space Research Laboratories General Electric Company Valley Forge, Pennsylvania

INTRODUCTION

This paper is written in two sections, I and II. Section I outlines the scope and some results of a comprehensive investigation relating to the inelastic constitution of the earth. The theory presented here on Rayleigh Waves in a Maxwell Body constitutes a segment of this investigation and in section I we attempt to communicate its position and role in this context.

Section II presents in detail the mathematical development leading to the conditions of admissibility of harmonic Rayleigh Waves propagating in a Maxwell Body. These imply conditions, on period selectivity, attenuation, and dispersion not rendered by the corresponding Rayleigh Wave theory for a perfectly elastic body. A similar conclusion was obtained from an earlier investigation on Love Waves propagating in a two layered earth consisting of a Sesawa crust supported by a Maxwell halfspace. Our work on Love Waves first pointed up a fundamental observation; namely, that *inelastic constitution in conjunction with layered structure* leads to selectivity conditions and dispersion phenomena which in principle cannot be represented by elastic models of the layered earth and therefore attempting to do so is tantamount to curve fitting. It then follows that the adequacy of a layered elastic model of the earth *cannot in principle* be decided in the framework of elastic seismology, since the effect of inelastic constitution in conjunction with layering on information contained in seismic data cannot be determined in this way.

These theoretical studies on Love Waves and Rayleigh Waves were both prompted by a viscoelastic-plastic model of the crust and mantle. This model accommodates a mechanism for progressively and repeatedly storing and releasing strain-energy in the crust. The

* This paper corresponds to the paper presented at the International Union of Geodesy and Geophysics Meeting at Berkeley during August 1963 under the title « On the Propagation, Dispersion, and Attenuation of Rayleigh Waves for a Maxwell Body ».

object of these theoretical wave studies is to determine whether significant observable manifestations of this model may be expected in seismic data, and if so, whether they can be used for identifying numerically the inelastic moduli ascribed by this model to the two layers.

The considerations which led to the conception of this model and to the selection of adequate members of the class of viscoelastic materials in its formal representation follow a principle of reconciliation and accommodation. Accordingly, the selection is made by choosing the *simplest* members which reconcile what we know by direct experience and accommodate plausible hypotheses suggested by large scale and indirect observations. Thus the progressive and repeated accumulation of strain-energy in the crust terminating in seismic disturbances constitute direct experience whereas the existence of convection currents in the mantle is conjectured by hypothesis based on the compilation of indirect evidence. Accordingly, although the Maxwell Body provides a simplified representation of the mechanical properties of the mantle it is nevertheless sufficient to accommodate the seismic mechanism cited and reconcile it at least in principle with the existence of convection currents in the mantle. We say in principle since in the final analysis the reconciliation must be made numerically by linking the moduli with direct measurements such as obtained from seismic data. The numerical values of the material constants determined from such measurements may be incompatible with convection currents if they should necessitate, for example, unreasonable temperature gradients.

The theory presented here on Rayleigh Waves was made with the view of enhancing a capability for critically evaluating the Sesawa-Maxwell model of crust and mantle, rather than as a mathematical curiosity. For this reason we feel it is preferable to present it in the context of a comprehensive study in geophysics rather than as a boundary value problem.

I. — *The Geophysical Basis and Background of Theory.*

The work reported here on Rayleigh Waves in a Maxwell Body was carried out and completed at the Rensselaer Polytechnic Institute in 1952. It is a segment of a comprehensive investigation on relaxation phenomena and inelastic processes in the earth. This was initiated in 1948 as a subject of a doctoral dissertation, and culminated in a thesis in 1951 (ref. 1). Some of the results are outlined in refs 2 and 3. We attempt here to present theoretical results on Rayleigh Waves in a Maxwell Body in the context of this comprehensive study, as their primary function is to assist in the numerical identification of the material constants and depth of a Maxwell Body ascribed in the thesis to the mantle. It is therefore relevant first to outline the central observations and ideas of this comprehensive study, the questions they pose, and the manner and extent to which we are able to resolve these questions at this juncture.

A central phenomenological fact relevant to seismology and to the task of elucidating the physical state of the mantle is the progressive and repeated accumulation of strain energy in portions of the crust which lead to states of critical stress producing plastic yield and/or sudden fault displacements manifested in earthquakes.

This observation leads to a crucial question in mechanics, namely, under what conditions, necessary and sufficient, can a continously extended body progressively accumulate strain energy in some finitely extended part of it, when it is subjected to a temporally constant and spatially dependent macroscopic environment in the applied forces and other phenomenological parameters which describe it. Once the question is put this way it follows almost directly that a necessary condition is inelastic constitution and inhomogeneity. On reflection one sees then immediately that such progressive accumulation cannot take place under these environmental conditions in an ideally elastic body. If we exclude resonance as a phenomenon (ref. 4) the same conclusion appears to hold under more general environmental conditions, namely when a body is subjected to a temporally periodic and spatially non-uniform macro-environment in which the forces are bounded in magnitude.

From these considerations it follows that inelastic constitution is a property that is essential to the tectonic and seismic processes of the earth. This immediately presents some crucial questions and the need for constructing conceptual and theoretical frameworks which may lead to the identification of the specific inelastic properties that are both necessary and sufficient for these processes to occur.

This leads to a twofold task. First, the *selection* of appropriate members of the class of conceivable inelastic materials for modeling the layered materials of the earth and secondly, the construction of a mathematical scheme by which such models can be identified with observation and thus subjected to the test of experimentation. Conversely, by so doing we should be able to derive from information obtained by measurements at the surface of the earth, numerical information on the constants of the materials used in modeling the layers.

In responding to the first task we immediately encounter a difficult situation. The class of inelastic bodies are, at this point, defined in negative terms, that is, by saying that it is composed of members none of which belong to the class of elastic bodies. Furthermore we note that every member of the class of elastic bodies is defined positively in the sense that we ascribe to each member definite physical attributes which they all share and which are representable in precise mathematical terms. Correspondingly, before we can derive calculatable consequences of a *layered inelastic model* of the earth amenable to the test of observation and measurement we must describe the inelastic models of the materials of the individual layers in precise mathematical terms. This leads to the consideration of a *sub-class* of the class of inelastic materials consisting of members positively described by precise mathematical statements. This sub-class is of course larger than the class of elastic bodies, and the task of selecting from it members that appropriately model the layered earth is consequently more difficult than for a corresponding elastic model, which according to most investigators should account in principle for all significant observable information contained in seismic data.

In facing up to the task of selection we have followed a principle of accommodation and reconciliation, according to which we select the simplest inelastic materials which reconcile and accommodate geophysical and geological information. A model of the crust and mantle was thus conceived which is endowed with a mechanism for progressively and repeatedly accumulating strain energy in the crust, when said configuration is subjected to a spatially dependent but temporally constant macroscopic force environment identified with a spatially non-uniform distribution of gravitational forces (ref. 1). The simplest member of the sub-class of inelastic materials which can do the job called for is a Maxwell Body, a body which can relax stress under conditions of constant strain and which equally can support shear waves, which we know from observation the mantle is capable of doing. The upper layer, i. e. the crust was modeled as a Sesawa Body. However, from the standpoint of mechanism noted it can also be modeled as a Maxwell Body endowed with a much higher coefficient of viscosity than is the Maxwell material of the mantle.

With the object of relating this model to experimental seismology we then put the question : Can this model accommodate a harmonic progressive Love Wave and, if so, under what conditions? This led to a simple theory of Love Waves which shows that such a wave is addmissible but under more restrictive conditions than in the elastic case. These restrictions imply dispersion and selectivity conditions not included in the elastic theory of Love Waves. Furthermore, it is obvious that in principle these conditions cannot be accounted for by an elastic model without resorting to curve fitting. This led to the realization that we can expect to find significant information in seismic data revealing the inelastic, as well as the elastic, properties of individual layers of an appropriate inelastic model of the layered earth. This motivated the formulation of a theory for calculating surface waves on a multi-layered inelastic earth. The central ideas behind this theory are outlined in (ref. 5). It effects a reduction to the procedure for calculating surface waves over a layered elastic earth introduced by Thomsen and extended by Haskell, Anderson and others.

In this regard, we wish to emphasize again that our study on Love Waves first showed that it is the juxtaposition of inelasticity and layering which imply a number of observable manifestations of inelasticity in seismic data. These include dispersion, period selection and attenuation and are especially prominent when inelastic properties change abruptly across interfaces.

In this context and with the principle of accommodation and reconciliation in mind we put the following question : Can a Maxwell Body admit Benard-Rayleigh convection, since there is growing evidence for the existence of convection currents in the mantle? We have recently examined this question analytically and have found that Benard-Rayleigh convection in the sense of the principle of exchange of stability is definitely addmissible in a Maxwell Body under an impressed and sustained temperature gradient provided its coefficient of viscosity is sufficiently small. This means that we should expect a marked change in the viscosity coefficient across the interface joining the crust and mantle. It follows from the above that we may expect significant observable manifestation of Love Waves which cannot in principle be accounted for by an elastic model.

In the same context our work on Rayleigh Waves is designed to determine whether or not significant observable seismic implications bearing on the representation and modeling of the mantle as a Maxwell Body may be expected. The answer is found in the mathematical solution of this boundary value problem which shows again that the Maxwell Body is endowed with dispersion, selectivity and attenuation characteristics with respect to Rayleigh Waves that are absent in an elastic body.

In conclusion it should be pointed out that there is a theoretical basis for saying that some plastic as well as viscoelastic behavior of inelastic materials can be modeled by complicated networks of linearly viscoelastic elements. This does not however afford a practical way of treating the problem of modeling the earth as a elasto-plastic viscoelastic body because the mathematics it presents is too difficult for extracting information. The principle of reconciliation and accommodation followed in this paper appears both effective and necessary in the construction of inelastic models of the layered earth, which can realistically furnish by calculation observable and testable explicit information.

II. — *Mathematical Development and Results on Rayleigh Waves in a Maxwell Body.*

We shall limit ourselves here to the case when the Maxwell material occupies a half space, i. e., in Cartesian coordinates, extending from the plane $x_1 = 0$ to infinity in the positive direction. We are interested in the effect of the viscosity elements as they are arranged in a Maxwell material upon the speed of propagation, attenuation and dispersion of Rayleigh Waves.

For a Maxwell material the stress-strain law is given by :

$$\sigma_{ij} = \lambda\, e^e{}_{kk}\, \delta_{ij} + 2\mu\, e^e{}_{ij} \tag{1}$$

Where $e^e{}_{ij}$ are the strain components of the elastic elements, and

$$\sigma_{ij} = \lambda'\, \dot{e}^v{}_{kk}\, \delta_{ij} + 2\mu'\, \dot{e}^v{}_{ij} \tag{2}$$

where $e^v{}_{ij}$ are the strain components of the viscous element.

The components of the total strain rate tensor $\dot{e}_{ij} = \dot{e}^e{}_{ij} + \dot{e}^v{}_{ij}$ are obtained from 1 and 2 as follows.

We have

$$\sigma_{ii} = (3\lambda + 2\mu)\, e^e{}_{ii}$$

$$\therefore \quad e^e{}_{ij} = \frac{1}{2\mu}\left\{\sigma_{ij} - \frac{\lambda\sigma_{kk}}{3\lambda+2\mu}\,\delta_{ij}\right\}$$

$$\therefore \quad \dot{e}^e{}_{ij} = \frac{1}{2\mu}\left\{\dot{\sigma}_{ij} - \frac{\lambda\,\dot{\sigma}_{kk}}{3\lambda+2\mu}\,\delta_{ij}\right\} \tag{2 a}$$

Similarly,

$$\dot{e}''_{ij} = \frac{1}{2\mu'} \left\{ \sigma_{ij} - \frac{\lambda' \sigma_{kk}}{3\lambda' + 2\mu'} \delta_{ij} \right\}$$

Further $\dot{e}_{ij} = \dot{e}^e_{ij} + \dot{e}^v_{ij}$

$$= \frac{\dot{\sigma}_{ij}}{2\mu} + \frac{\sigma_{ij}}{2\mu'} - \left\{ \frac{\lambda}{2\mu\,(3\lambda+2\mu)} \frac{\partial}{\partial t} + \frac{\lambda'}{2\mu'\,(3\lambda'+2\mu')} \right\} \sigma_{kk}\, \delta_{ij} \tag{3}$$

The differential equations of equilibrium are :

$$\sigma_{ij,j} = \rho \frac{\partial^2 u_i}{\partial t^2} \tag{4}$$

Introducing the symbol

$$\chi \equiv \frac{3\lambda + 2\mu}{3\lambda' + 2\mu'} \tag{5}$$

and the operator notations

$$D_1 \equiv \frac{\partial}{\partial t} + \chi$$

$$D_2 \equiv \lambda \frac{\partial}{\partial t} + \lambda' \chi \frac{\mu}{\mu'} \tag{6}$$

one obtains from (3) by differentiation

$$\dot{e}_{ij.j} = \frac{1}{2\mu} \dot{\sigma}_{ij,j} + \frac{1}{2\mu'} \sigma_{ij,j} - \frac{1}{2\mu(3\lambda+2\mu)} \left\{ \lambda \frac{\partial}{\partial t} + \lambda' \frac{2\mu(3\lambda+2\mu)}{2\mu'(3\lambda'+2\mu')} \right\} \frac{\partial}{\partial x_i} (\sigma_{kk})$$

$$= \frac{\dot{\sigma}_{ij,j}}{2\mu} + \frac{\sigma_{ij,j}}{2\mu'} - \frac{1}{2\mu\,(3\lambda + 2\mu)} D_2\,(\sigma_{kk,i})$$

and

$$\dot{e}_{kk,i} = \left\{ \frac{1}{2\mu} \dot{\sigma}_{kk} + \frac{1}{2\mu'} \sigma_{kk} - \left(\frac{3\lambda}{2\mu(3\lambda+2\mu)} \frac{\partial}{\partial t} \sigma_{kk} + \frac{\lambda'}{2\mu'(3\lambda'+2\mu')} 3\sigma_{kk} \right) \right\}_{,i}$$

$$= \left\{ \frac{\dot{\sigma}_{kk}}{2\mu} - \frac{3\lambda}{2\mu(3\lambda+2\mu)} \dot{\sigma}_{kk} + \frac{1}{2\mu'} \sigma_{kk} - \frac{3\lambda'}{2\mu'(3\lambda'+2\mu')} \sigma_{kk} \right\}_{,i}$$

$$= \left\{ \frac{3\lambda+2\mu-3\lambda}{2\mu} \cdot \frac{\dot{\sigma}_{kk}}{3\lambda+2\mu} + \frac{3\lambda'+2\mu'-3\lambda'}{2\mu'} \cdot \frac{\sigma_{kk}}{3\lambda'+2\mu'} \right\}_{,i}$$

$$= \frac{1}{3\lambda + 2\mu} \left\{ \frac{\partial}{\partial t} + \frac{3\lambda + 2\mu}{3\lambda' + 2\mu'} \right\} \sigma_{kk,i}$$

$$= \frac{1}{3\lambda + 2\mu} D_1\,(\sigma_{kk,i})$$

From the above equations by eliminating $\sigma_{kk,i}$ one obtains

$$D_1\left(\ddot{e}_{ij,j}-\frac{1}{2\mu}\dot{\sigma}_{ij,j}-\frac{1}{2\mu'}\sigma_{ij,j}\right)+\frac{1}{2\mu(3\lambda+2\mu)}D_1 D_5(\sigma_{kk,i})=0$$

$$\therefore\ D_1\left(2\mu\,\dot{e}_{ij,i}-\dot{\sigma}_{ij,j}-\frac{\mu}{\mu'}\sigma_{ij,j}\right)+D_2\left\{\frac{1}{3\lambda+2\mu}D_1(\sigma_{kk,i})\right\}=0$$

$$\therefore\ D_1\left(2\mu\,\dot{e}_{ij,j}-\dot{\sigma}_{ij,j}-\frac{\mu}{\mu'}\sigma_{ij,j}\right)+D_2(\dot{e}_{kk,i})=0$$

Now from (4) and the relation $2e_{ij}=u_{i,j}+u_{j,i}$ the following equations are obtained.

$$D_1\left\{2\mu\frac{1}{2}(\dot{u}_{i,j}+\dot{u}_{j,i}),_j-\rho\frac{\partial^3 u_i}{\partial t^3}-\frac{\mu}{\mu'}\rho\frac{\partial^2 u_i}{\partial t^2}\right\}+D_2(\dot{u}_{k,ki})=0$$

$$\rightarrow\frac{\partial}{\partial t}\left\{D_1\left\{\mu(u_{i,jj}+u_{j,ij})-\rho\frac{\partial^2 u_i}{\partial t^2}-\rho\frac{\mu}{\mu'}\frac{\partial u_i}{\partial t}\right\}+D_2(u_{k,ki})\right\}=0 \qquad (8)$$

Differentiating (8) with respect to x_i yields

$$\frac{\partial}{\partial t}\left[D_1\left\{\mu(u_{i,jji}+u_{j,iji})-\rho\frac{\partial^2 u_{i,i}}{\partial t^2}-\rho\frac{\mu}{\mu'}\frac{\partial u_{i,i}}{\partial t}\right\}+D_2(u_{k,kii})\right]=0 \qquad (9)$$

$$\rightarrow\frac{\partial}{\partial t}\left[D_1\left\{2\mu\,\nabla^2 u_{i,i}-\rho\frac{\partial^2 u_{i,i}}{\partial t^2}-\rho\frac{\mu}{\mu'}\frac{\partial u_{i,i}}{\partial t}\right\}+D_2(\nabla^2 u_{i,i})\right]=0$$

where $\nabla^2\equiv\dfrac{\partial^2}{\partial x_i\,\partial x_i}$

If the curl operator is applied to (8), one obtains

$$\frac{\partial}{\partial t}\left[D_1\left\{\mu e_{lmi}(u_{i,jj}+u_{j,ij}),_m-\rho\frac{\partial^2}{\partial t^2}\left(e_{lmi}\frac{\partial u_i}{\partial x_m}\right)-\rho\frac{\mu}{\mu'}\frac{\partial}{\partial t}\left(e_{lmi}\frac{\partial\mu_i}{\partial x_m}\right)\right\}\right.$$
$$\left.+D_2\left(e_{lmi}\frac{\partial\mu_{k,ki}}{\partial x_m}\right)\right]=0$$

$$\therefore\ \frac{\partial}{\partial t}\left[D_1\left\{\mu\,\nabla^2(\text{curl }u_i)-\rho\frac{\partial^2}{\partial t^2}(\text{curl }u_i)-\rho\frac{\mu}{\mu'}\frac{\partial}{\partial t}(\text{curl }u_i)\right\}\right]=0$$

Because curl (div u) $=0$ i. e. $e_{lmi}\dfrac{\partial}{\partial x_m}(u_{k,ki})=0.$

$$\therefore\ \frac{\partial}{\partial t}\left\{D_1\left(\mu\nabla^2\omega_i-\rho\frac{\partial^2\omega_i}{\partial t^2}-\rho\frac{\mu}{\mu'}\frac{\partial\omega_i}{\partial t}\right)\right\}=0\ ;\quad \omega_i\equiv\text{curl }u_i=e_{ijl}\frac{\partial u_l}{\partial x_j} \qquad (10)$$

Eqs. (9) and (10) form the basic differential equations for our problem.

Let us now restrict our solutions as follows :

$u_i=u_i(x_1,x_3)$ $\quad i=1,2,3$ and introduce $\varnothing$

and ψ such that

$$u_1 = \frac{\partial \varnothing}{\partial x_1} + \frac{\partial \psi}{\partial x_3}$$

$$u_3 = \frac{\partial \varnothing}{\partial x_3} - \frac{\partial \psi}{\partial x_1}$$

It follows then

$$\nabla^2 \varnothing = \frac{\partial^2 \varnothing}{\partial x_1^2} + \frac{\partial^2 \varnothing}{\partial x_3^2}$$

$$= \frac{\partial u_1}{\partial x_1} - \frac{\partial^2 \psi}{\partial x_1 \partial x_3} + \frac{\partial u_3}{\partial x_3} + \frac{\partial^2 \psi}{\partial x_1 \partial x_3} \qquad (11)$$

$$= u_{i,i} \qquad i = 1,\ 3$$

$$\nabla^2 \psi = \frac{\partial^2 \psi}{\partial x_1^2} + \frac{\partial^2 \psi}{\partial x_3^2}$$

$$= \frac{\partial^2 \varnothing}{\partial x_1 \partial x_3} - \frac{\partial u_3}{\partial x_1} + \frac{\partial u_1}{\partial x_3} - \frac{\partial^2 \varnothing}{\partial x_1 \partial x_3}$$

$$= \frac{\partial u_1}{\partial x_3} - \frac{\partial u_3}{\partial x_1}$$

Hence if we can find $\varnothing$ which satisfies (9) and u_2 and ψ which satisfy (10), the functions u_1, u_2, u_3 obtained from (11) are the desired solutions, provided the appropriate boundary conditions are satisfied.

Let us consider (10) first. A possible form of solution is assumed to be

$$\psi = T_1(t)\, R(x_1, x_3)$$

Substituting yields :

We consider in (10) the component in x_1, x_3 plane : which is $\nabla^2\psi$.

$$\omega_i = \text{curl}\ \dot{u}_k = e_{ijk} \frac{\partial u_k}{\partial x_j} \quad \rightarrow \quad \omega_2 = \frac{\partial u_1}{\partial x_3} - \frac{\partial u_3}{\partial x_1} = \nabla^2 \psi$$

$$\therefore \frac{\partial}{\partial t}\left[D_1 \left\{ \mu \nabla^4 \psi - \rho \frac{\partial^2 \nabla^2 \psi}{\partial t^2} - \rho \frac{\mu}{\mu'} \frac{\partial \nabla^2 \psi}{\partial t} \right\} \right] = 0$$

$$\therefore \frac{\partial}{\partial t}\left[D_1 \left\{ (\mu \nabla^4 R)\, T_1 - \rho\, T_1'' \nabla^2 R - \rho \frac{\mu}{\mu'} T_1' \nabla^2 R \right\} \right] = 0$$

$$\therefore \frac{\partial}{\partial t}\left[\left(\frac{\partial}{\partial t} + \chi \right) \left\{ (\mu \nabla^4 R)\, T_1 - \rho\, T_1'' \nabla^2 R - \rho \frac{\mu}{\mu'} T_1' \nabla^2 R \right\} \right] = 0$$

$$\therefore \quad \Big[\mu \nabla^4 R T_1'' + \chi \mu \nabla^4 R T_1' - \rho \nabla^2 R T_1'''' - \rho \nabla^2 R \chi T_1'''$$

$$- \rho \frac{\mu}{\mu'} \nabla^2 R T_1''' - \rho \frac{\mu}{\mu'} \nabla^2 R \chi T_1'' \Big] = 0$$

$$\therefore \ \mu(T_1''+\chi T_1')\,\nabla^4 R=\rho\,\nabla^2 R\left\{T_1''''+\chi\,T_1'''+\frac{\mu'}{\mu}\,T_1'''+\frac{\mu}{\mu'}\,\chi\,T_1''\right\}$$

$$\therefore \ \frac{\mu}{\rho}\,\frac{\nabla^4 R}{\nabla^2 R}=\frac{T_1''''+\left(\chi+\frac{\mu}{\mu'}\right)T_1'''+\chi\frac{\mu}{\mu'}\,T_1''}{T_1''+\chi\,T_1'}=-\,C_1^2$$

Where c^2_1 is an arbitrary positive constant, with dimension $(\text{time})^{-2}$, to be determined.

Hence

$$\left(\nabla^2+C_1^2\,\frac{\rho}{\mu}\right)\left(\nabla^2 R\right)=0 \tag{13}$$

$$T_1''''+\left(\chi+\frac{\mu}{\mu'}\right)T_1'''+\left(C_1^2+\chi\,\frac{\mu}{\mu'}\right)T_1''+C_1^2\chi T_1'=0. \tag{14}$$

Let $T_1=e^{pt}$ Then, if $p\neq 0$, and since

$$\left[p^4+\left(\chi+\frac{\mu}{\mu'}\right)p^3+\left(C_1^2+\chi\,\frac{\mu}{\mu'}\right)p^2+C_1^2\,\chi p\right]e^{pt}=0$$

We get p to satisfy

$$p^3+\left(\chi+\frac{\mu}{\mu'}\right)p^2+\left(C_1^2+\chi\,\frac{\mu}{\mu'}\right)p+C_1^2\chi=0 \tag{15}$$

From (9) we get

$$\frac{\partial}{\partial t}\left[D_1\left\{2\mu\nabla^4\varnothing-\rho\,\frac{\partial^2\nabla^2\varnothing}{\partial t^2}-\rho\,\frac{\mu}{\mu'}\,\frac{\partial\nabla^2\varnothing}{\partial t}\right\}+D_2\left(\nabla^4\varnothing\right)\right]=0$$

Letting $\varnothing=T_2(t)\,S(x_1,x_3)$ we get

$$\frac{\partial}{\partial t}\left[\left(\frac{\partial}{\partial t}+\chi\right)\left\{2\mu\,T_2\nabla^4 S-\rho\,T_2''\nabla^2 S-\rho\,\frac{\mu}{\mu'}\,T_2'\,\nabla^2 S\right\}\right.$$
$$\left.+\left(\lambda\frac{\partial}{\partial t}+\lambda'\chi\,\frac{\mu}{\mu'}\right)\left(\nabla^4 S\right)T_2\right]=0$$

$$\therefore \ \frac{\partial}{\partial t}\left[2\mu\nabla^4 S\,(T_2'+\chi\,T_2)-\rho\,\nabla^2 S\left(T_2'''+\chi T_2''+\frac{\mu}{\mu'}\,T_2''+\chi\,\frac{\mu}{\mu'}\,T_2'\right)\right.$$
$$\left.+\nabla^4 S\left(\lambda\,T_2'+\lambda'\,\chi\,\frac{\mu}{\mu'}\,T_2\right)\right]=0$$

$$\therefore \ 2\mu\,\nabla^4 S\,(T_2''+\chi T_2')-\rho\nabla^2 S\left(T_2''''+\chi\,T_2'''+\frac{\mu}{\mu'}\,T_2'''+\chi\,\frac{\mu}{\mu'}\,T_2''\right)$$
$$+\nabla^4 S\left(\lambda\,T_2''+\lambda'\chi\,\frac{\mu}{\mu'}\,T_2'\right)=0$$

$$\therefore \quad \nabla^4 S \left\{ (\lambda+2\mu)\, T''_2 + \chi \left(\frac{\lambda'\mu}{\mu'} + 2\mu \right) T'_2 \right\}$$

$$= \rho\, \nabla^2 S \left\{ T_2'''' + \left(\chi + \frac{\mu}{\mu'} \right) T_2''' + \chi \frac{\mu}{\mu'} T_2'' \right\}$$

$$\therefore \quad 2\mu \nabla^4 S \left\{ \left(1 + \frac{\lambda}{2\mu} \right) T_2'' + \chi \left(1 + \frac{\lambda'}{2\mu'} \right) T_2' \right\}$$

$$= \rho\, \nabla^2 S \left\{ T_2'''' + \left(\chi + \frac{\mu}{\mu'} \right) T_2''' + \chi \frac{\mu}{\mu'} T_2'' \right\}$$

$$\therefore \quad \frac{2\mu \nabla^4 S}{\rho \nabla^2 S} = \frac{T_2'''' + \left(\chi + \frac{\mu}{\mu'} \right) T_2''' + \chi \frac{\mu}{\mu'} T_2''}{\left(1 + \frac{\lambda}{2\mu} \right) T_2'' + \chi \left(1 + \frac{\lambda'}{2\mu'} \right) T_2'} = - d^2$$

$$\therefore \quad \left(\nabla^2 + \frac{\rho}{2\mu} d^2 \right) \nabla^2 S = 0 \tag{16}$$

$$T_2'''' + \left(\chi + \frac{\mu}{\mu'} \right) T_2''' + \left\{ \chi \frac{\mu}{\mu'} + d^2 \left(1 + \frac{\lambda}{2\mu} \right) \right\} T_2'' + \chi \left(1 + \frac{\lambda'}{2\mu'} \right) d^2\, T'_2 = 0 \tag{17}$$

where d^2 is an arbitrary constant to be determined. By comparing equations (14) and (17), in order that the dilatational wave and distortional wave propagate with the same speed, it is necessary that

$$c_1^2 + \frac{\lambda\mu}{\mu'} = \lambda \frac{\mu}{\mu'} + d^2 \left(1 + \frac{\lambda}{2\mu} \right); \quad c_1^2 \chi = d^2 \chi \left(1 + \frac{\lambda'}{2\mu'} \right)$$

$$\rightarrow \quad \frac{\lambda}{\lambda'} = \frac{\mu}{\mu'} \quad \text{and} \quad c_1^2 = d^2 \left(1 + \frac{\lambda}{2\mu} \right) \tag{18}$$

It follows then that $\chi \equiv \dfrac{3\lambda + 2\mu}{3\lambda' + 2\mu'} = \dfrac{\mu}{\mu'} = \dfrac{\lambda}{\lambda'}$ (19)

and equation (15) becomes

$$p^3 + 2\chi p^2 + (c^2_1 + \chi^2)\, p + c^2_1 \chi = 0 \tag{20}$$

Let us consider the equation

$$\left(\nabla^2 + C_1^2 \frac{\rho}{\mu} \right) R = 0 \tag{13 a}$$

The solution of (13a) is taken as $R = X(x_1)\, Z(x_3)$
Then

$$X''Z + XZ'' + C_1^2 \frac{\rho}{\mu} XZ = 0$$

$$\rightarrow \quad \frac{X''}{X} + C_1^2 \frac{\rho}{\mu} = - \frac{Z''}{Z} = q^2 \quad \text{where } q \text{ is real.}$$

Hence we have

$$X = A \exp. \left[\sqrt{q^2 - \frac{\rho c_1^2}{\mu}}\; x_1\right] + B \exp. \left[\sqrt{q^2 - \frac{\rho c_1^2}{\mu}}\; x_1\right]$$

$$Z = C \exp\,[iqx_3] + D \exp\,[iqx_3]$$

The desired solutions for R satisfying (13a) and hence (13) also, are

$$R = A \exp. \left[\sqrt{q^2 - \frac{\rho c_1^2}{\mu}}\; x_1 - iq\,x_3\right] \tag{21}$$
$$+ B \exp. \left[-\sqrt{q^2 - \frac{\rho c_1^2}{\mu}}\; x_1 + iqx_3\right]$$

Similarly for S, we have from (16a) viz : $\left(\nabla^2 + \frac{\rho}{2\mu} d^2\right) S = 0$

$$S = E \exp\left[\sqrt{l^2 - \frac{\rho d^2}{2\mu}}\; x_1 - i\,l\,x_3\right] \tag{22}$$
$$+ F \exp.\left[-\sqrt{l^2 - \frac{\rho d^2}{2\mu}}\, x_1 + il\,x_3\right] \quad , \qquad l \text{ is real.}$$

It is clear that in order to have equal speeds of propagation for these two waves, one requires

$$l = q \tag{23}$$

Let us consider the b. c. : At $x_1 = 0$ the coundary conditions on the stresses are :

$$\sigma_{11} = \sigma_{13} = \sigma_{12} = 0$$

From $\sigma_{12} = 0$ one sees that $u_2 = 0$
From the form of the solutions chosen above we see that the condition $\sigma_{13} = 0$ at $x_1 = 0$ yields

$$\left[\frac{\partial u_1}{\partial x_3} + \frac{\partial u_3}{\partial x_1}\right]_{x_1=0} = 0 \quad \rightarrow \quad 2\,\frac{\partial^2 \varnothing}{\partial x_1\,\partial x_3} + \frac{\partial^2 \psi}{\partial x_3^2} - \frac{\partial^2 \psi}{\partial x_1^2} = 0$$

We have

$$\frac{\partial\varnothing}{\partial x_1} = T_2\,\frac{\partial S}{\partial x_1} = T_2\left(\sqrt{l^2 - \frac{\rho d^2}{2\mu}}\right)\left\{E \exp.\left(\sqrt{l^2 - \frac{\rho d^2}{2\mu}}\; x_1 - i\,l\,x_3\right)\right.$$
$$\left. - F \exp.\left(-\sqrt{l^2 - \frac{\rho d^2}{2\mu}}\; x_1 + i\,l\,x_3\right)\right\}$$

$$\therefore \quad \frac{\partial^2 \varnothing}{\partial x_1\,\partial x_3} = -\,i\,l\left(\sqrt{l^2 - \frac{\rho d^2}{2\mu}}\right) S T_2$$

$$\therefore \quad \left[\frac{\partial^2 \varnothing}{\partial x_1\,\partial x_3}\right]_{\substack{x_1=0\\ x_3=0}} = -\,i\,l\left(\sqrt{l^2 - \frac{\rho d^2}{2\mu}}\right) T_2\,(E + F)$$

Suppose $F = 0$, then $\left.\frac{\partial^2 \varnothing}{\partial x_1 \, \partial x_3}\right|_{\substack{x_1=0\\x_3=0}} = -\, i\, l \sqrt{l^2 - \frac{\rho\, d^2}{2\mu}}\; T_2\, E$

We have

$$\frac{\partial^2 \psi}{\partial x_1^2} = T_1 \frac{\partial^2 R}{\partial x_1^2} = \left(\sqrt{q^2 - \frac{\rho\, c_1^2}{2\mu} 2}\right)^2 R\, T_1 = \left(q^2 - \frac{\rho\, c_1^2}{\mu}\right) R\, T_1$$

$$\frac{\partial^2 \psi}{\partial x_3^2} = T_1 \frac{\partial^2 R}{\partial x_3^2} = -\, q^2\, R T_1$$

$$\therefore \left[\frac{\partial^2 \psi}{\partial x_3^2} - \frac{\partial^2 \psi}{\partial x_1^2}\right]_{\substack{x_1=0\\x_3=0}} = \left[-\, q^2 - \left(q^2 - \frac{\rho\, c_1^2}{\mu}\right)\right] (A+B)\, T_1$$

With $B = 0$,

$$\left[\frac{\partial^2 \psi}{\partial x_3^2} - \frac{\partial^2 \psi}{\partial x_1^2}\right]_{\substack{x_1=0\\x_3=0}} = \left[-\, q^2 - \left(q^2 - \frac{\rho c_1^2}{\mu}\right)\right] A T_1$$

Hence we have the condition that

$$-\, 2 i l \sqrt{l^2 - \frac{\rho\, d^2}{2\mu}}\; E + \left\{-\, q^2 - \left(q^2 - \frac{\rho\, c_1^2}{\mu}\right)\right\} A = 0 \quad \text{if we take } T_1 = T_2$$

Since $l = q$ and $c_1^2 = d^2\left(1 + \frac{\lambda}{2\mu}\right)$, we get

$$2\, i\, q \sqrt{q^2 - \frac{\rho\, c_1^2}{\lambda + 2\mu}}\; E + \left\{q^2 + \left(q^2 - \frac{\rho\, c_1^2}{\mu}\right)\right\} A = 0 \qquad (24)$$

We now consider the condition $\sigma_{11} = 0$. From the stress strain law (3) we get for $\sigma_{11} = 0$:

$$\dot{e}_{11} = -\left[\frac{\lambda\, \dot{\sigma}_{kk}}{2\mu(3\lambda+2\mu)} + \frac{\lambda'\, \sigma_{kk}}{2\mu'\,(3\lambda' + 2\mu')}\right] \qquad (i)$$

But we have

$$\dot{e}_{kk} = \frac{\dot{\sigma}_{kk}}{3\lambda + 2\mu} + \frac{\sigma_{kk}}{3\lambda' + 2\mu'} \qquad (ii)$$

$$\therefore \frac{\sigma_{kk}}{3\lambda' + 2\mu'} = \dot{e}_{kk} - \frac{\dot{\sigma}_{kk}}{3\lambda + 2\mu} \qquad (iii)$$

$$\frac{\dot{\sigma}_{kk}}{3\lambda + 2\mu} = \dot{e}_{kk} - \frac{\sigma_{kk}}{3\lambda' + 2\mu'} \qquad (iv)$$

Using (iii) in (i) we get

$$\dot{e}_{11} = -\left[\frac{\lambda}{2\mu} \frac{\dot{\sigma}_{kk}}{3\lambda + 2\mu} + \frac{\lambda'}{2\mu'} \dot{e}_{kk} - \frac{\lambda'}{2\mu'} \dot{\sigma}_{kk} \frac{1}{3\lambda + 2\mu}\right]$$

$$= -\left[\frac{\lambda'}{2\mu'}\dot{e}_{kk} + \frac{\lambda\mu' - \lambda'\mu}{2\,\mu\mu'}\,\frac{\dot{\sigma}_{kk}}{3\lambda + 2\mu}\right]$$

$$\therefore\quad 2\mu'\,\dot{e}_{11} + \lambda'\,\dot{e}_{hk} = -\,\frac{\lambda\mu' - \lambda'\mu}{2\,\mu\mu'}\,2\,\mu'\,\dot{\sigma}_{kk}\,\frac{1}{3\lambda + 2\mu}.$$

$$\therefore\quad \frac{\partial}{\partial t}\left\{(2\mu' e_{11} + \lambda'\,e_{kk})\right\} = \frac{\partial}{\partial t}\left[\left\{-\,\frac{\lambda\mu' - \lambda'\mu}{\mu}\,\sigma_{kk}\right\}\frac{1}{3\lambda + 2\mu}\right] \qquad (\mathrm{V})$$

$$\therefore\quad \sigma_{kk} = -\,\frac{\mu\,(3\lambda + 2\mu)}{\lambda\mu' - \lambda'\mu}\,(2\mu'\,e_{11} + \lambda'\,e_{kk}) \qquad (\mathrm{VI})$$

Using (iv) in (i) we get

$$\dot{e}_{11} = -\left[\frac{\lambda}{2\mu}\,\dot{e}_{kk} - \frac{\lambda}{2\mu}\,\frac{\dot{\sigma}_{kk}}{(3\lambda' + 2\mu')} + \frac{\lambda'}{2\mu'}\,\frac{\dot{\sigma}_{kk}}{(3\lambda' + 2\mu')}\right]$$

$$= -\,\frac{\lambda}{2\mu}\,\dot{e}_{kk} + \left[\frac{\lambda\mu' - \lambda'\mu}{2\,\mu\mu'}\,\frac{\dot{\sigma}_{kk}}{3\lambda' + 2\mu'}\right]$$

$$\therefore\quad 2\mu\,\dot{e}_{11} + \lambda\,\dot{e}_{kk} = \frac{\lambda\mu' - \lambda'\mu}{\mu'\,(3\lambda' + 2\mu')}\,\dot{\sigma}_{kk}.$$

$$\therefore\quad \sigma_{kk} = \frac{3\lambda' + 2\mu'}{\lambda\mu' - \lambda'\mu}\,\mu'\,(2\mu\,\dot{e}_{11} + \lambda\,\dot{e}_{kk}) \qquad (\mathrm{VII})$$

Equating (vi) and (vii) we get

$$\frac{\mu\,(3\lambda + 2\mu)}{\lambda'\mu - \lambda\mu'}\,(2\,\mu'\,e_{11} + \lambda'\,e_{kk}) = \frac{\mu'\,(3\lambda' + 2\mu')}{\lambda\mu' - \lambda'\mu}\,(2\mu\,\dot{e}_{11} + \lambda\,\dot{e}_{kk})$$

$$\therefore\quad \left(\frac{2\mu'}{\lambda'\mu - \lambda\mu'}\right)(\mu\,e_{11}) + \frac{\lambda'\mu}{\lambda'\mu - \lambda\mu'}\,e_{kk} = \frac{\mu'}{\chi\,(\lambda\mu' - \lambda'\mu)}\,(2\mu\dot{e}_{11} + \lambda\,\dot{e}_{kk})$$

$$\therefore\quad \frac{\mu'}{\lambda'\mu - \lambda\mu'}\,(2\,\mu\,e_{11} + \lambda\,e_{kk}) + \left(\frac{\lambda'\mu}{\lambda'\mu - \lambda\mu'} - \frac{\lambda\mu'}{\lambda'\mu - \lambda\mu'}\right)e_{kk}$$

$$= \frac{\mu'}{\chi\,(\lambda\mu' - \lambda'\mu)}\,(2\,\mu\,\dot{e}_{11} + \lambda\,\dot{e}_{kk})$$

$$\therefore\qquad e_{kk} = \frac{\mu'}{\chi\,(\lambda\mu' - \lambda'\mu)}\,(2\mu\,\dot{e}_{11} + \lambda\,\dot{e}_{kk})$$

$$+\,\frac{\mu'}{\lambda\,\mu' - \lambda'\mu}\,(2\mu\,e_{11} + \lambda\,e_{kk}) \qquad (3')$$

From (18) and (19) we have

$$\frac{\lambda}{\lambda'} = \frac{\mu}{\mu'},\quad \chi = \frac{\mu}{\mu'},\quad c_1^2 = d^2\left(1 + \frac{\lambda}{2\mu}\right)$$

Hence (3′) becomes

$$\left(\frac{\mu'^2}{\mu}\,\frac{\partial}{\partial t} + \mu'\right)(2\,\mu\,e_{11} + \lambda\,e_{kk}) = 0 \qquad (25)$$

The substitution gives

$$\left(\frac{\mu'^2}{\mu}\frac{\partial}{\partial t}+\mu'\right)\left[2\mu\left(\frac{\partial^2\varnothing}{\partial x_1^2}+\frac{\partial^2\psi}{\partial x_1\,\partial x_3}\right)+\lambda\left(\frac{\partial^2\varnothing}{\partial x_1^2}+\frac{\partial^2\varnothing}{\partial x_3^2}\right)\right]=0$$

We have

$$\frac{\partial^2\varnothing}{\partial x_1^2}=\left(l^2-\frac{\rho d^2}{2\mu}\right)\mathrm{ST}_2\;,\quad \frac{\partial^2\varnothing}{\partial x_3^2}=-\,l^2\,\mathrm{ST}_2$$

$$\frac{\partial^2\psi}{\partial x_1\,\partial x_3}=-\,iq\;\left\{\sqrt{q^2-\frac{\rho\,c_1^2}{2\,\mu}2.}\;\right\}(\mathrm{RT}_1)$$

$\therefore$ For $\mathrm{B}=\mathrm{F}=0$, $x_1=0$, $x_3=0$, we get with $\mathrm{T}_1=\mathrm{T}_2$

$$\frac{\partial^2\varnothing}{\partial x_1^2}=\left(l^2-\frac{\rho\,d^2}{2\mu}\right)\mathrm{ET}_1\;,\quad \frac{\partial^2\varnothing}{\partial x_3^2}=-\,l^2\,\mathrm{ET}_1$$

$$\frac{\partial^2\psi}{\partial x_1\,\partial x_3}=-\,iq\,\sqrt{iq^2-\frac{\rho\,c_1^2}{\mu}}\;\mathrm{A}\;\mathrm{T}_1$$

$$\therefore\;\left(\frac{\mu'^2}{\mu}\frac{\partial}{\partial t}+\mu'\right)\left[2\mu\left\{\left(l^2-\frac{\rho\,d^2}{2\mu}\right)\mathrm{E}-iq\,\sqrt{q^2-\frac{\rho\,c_1^2}{\mu}}\,\mathrm{A}\right\}\right.$$
$$\left.+\,\lambda\left\{\left(l^2-\frac{\rho\,d^2}{2\mu}\right)-l^2\right\}\mathrm{E}\right]\mathrm{T}_1=0$$

$$\therefore\left(\frac{\mu'^2}{\mu}\frac{\partial}{\partial t}+\mu'\right)\left[\left\{-(\lambda+2\mu)\left(\frac{\rho\,c_1^2}{\lambda+2\mu}\right)+2\mu q^2\right\}\mathrm{E}-i2\mu q\sqrt{q^2-\frac{\rho c_1^2}{\mu}}\,\mathrm{A}\right]=0$$

$$\rightarrow\;\left\{(\lambda+2\mu)\left(\frac{\rho\,c_1^2}{\lambda+2\mu}\right)-2\mu\,q^2\right\}\mathrm{E}+2\mu\,iq\,\sqrt{q^2-\frac{\rho\,c_1^2}{\mu}}\,\mathrm{A}=0$$

$$\rightarrow\;(\rho\,c_1^2-2\mu\,q^2)\,\mathrm{E}+i\,2\mu q\,\sqrt{q^2-\frac{\rho\,c_1^2}{\mu}}\,\mathrm{A}=0 \tag{26}$$

We have

$$2\,iq\,\sqrt{q^2-\frac{\rho\,c_1^2}{\lambda+2\mu}}\,\mathrm{E}+\left\{2q^2-\frac{\rho\,c_1^2}{\mu}\right\}\mathrm{A}=0 \tag{24}$$

For non-trivial solutions to exist the determinant of (24) and (26) must vanish i. e.

$$\Delta=\begin{vmatrix}\rho\,c_1^2-2\mu\,q^2 & 2\mu\,iq\,\sqrt{q^2-\frac{\rho\,c_1^2}{\mu}}\\ 2\,iq\sqrt{q^2-\frac{\rho\,c_1^2}{\lambda+2\mu}} & 2\,q^2-\frac{\rho\,c_1^2}{\mu}\end{vmatrix}=0$$

$$\rightarrow\;4\left(1-\frac{c_1^2}{\alpha^2\,q^2}\right)^{\frac12}\left(1-\frac{c_1^2}{\beta^2\,q^2}\right)^{\frac12}=\left(2-\frac{c_1^2}{\beta^2\,q^2}\right)^2 \tag{27}$$

with

$$\alpha^2 \equiv \frac{\lambda + 2\mu}{\rho} \tag{28}$$

$$\beta^2 \equiv \frac{\mu}{\rho} \tag{29}$$

This equation (27) is of the same form as the frequency equation for Rayleigh Waves in elastic materials (Bullen, page 89). But here $\frac{C_1}{q}$ is, in general, not the speed of propagation of the waves. The procedure is, with given α and β to find first $\frac{C_1}{q}$ from (27) and then solve (20) for p. Let $p = s + ir$. Then s is the time damping coefficient and $\frac{r}{q}$ is the speed of propagation. From (27) we can see that p is, in general, a function of q, the wave number. Therefore, since here the speed of propagation depends on q, the viscous element in the Maxwell material leads to a dispersion. In order to find a specific value of p, a value of q must be chosen. After p is determined in this manner, the displacement functions u_1, and u_2 can be obtained from (11). When $\mu' \to \infty$ we have $\chi \to 0$ and it follows from (20) that $p = \pm i\, c_1$. From (3) we see that for $\mu' \to \infty$, the strain rates consist only of an elastic part. Hence our problem reduces to the elastic case. There will be no damping, and the speed of propagation does not depend on the wave length.

If χ is small compared to 1, we write $p = s + i(\nu_0 + \epsilon)$ where $\nu_0 = c_1$. We would expect ϵ to be small compared to ν_0. If higher order terms in ϵ are neglected from (20) we obtain the following.

$$\{s + i(\nu_0 + \epsilon)\}^3 + 2\chi\,\{s + i(\nu_0 + \epsilon)\}^2 + (c^2_1 + \chi^2)\,\{s + i(\nu_0 + \epsilon)\} + c^2_1\,\chi = 0$$

$$\therefore \quad s^3 + 3s^2\, i\,(\nu_0 + \epsilon) - 3s(\nu_0 + \epsilon)^2 - i(\nu_0 + \epsilon)^3$$
$$+ 2\chi\,\{s^2 + 2is(\nu_0 + \epsilon) - (\nu_0 + \epsilon)^2\}$$
$$+ (\nu^2_0 + \chi^2)\,\{s + i(\nu_0 + \epsilon)\} + \nu^2_0\,\chi = 0$$

$$\therefore \quad s^3 + i\,3s^2(\nu_0 + \epsilon) - 3s(\nu^2_0 + 2\nu_0\,\epsilon) - i(\nu^3_0 + 3\nu^2_0\,\epsilon)$$
$$+ 2\chi\,\{s^2 + 2i\,s(\nu_0 + \epsilon) - (\nu^2_0 + 2\nu_0\,\epsilon)\}$$
$$+ (\nu^2_0 + \chi^2)\, s + i(\nu^2_0 + \chi^2)\,(\nu_0 + \epsilon) + \nu^2_0\,\chi = 0$$

$$\therefore \quad [s^3 - 3s(\nu^2_0 + 2\nu_0\,\epsilon) + 2\chi s^2 - 2\chi(\nu^2_0 + 2\nu_0\,\epsilon) + (\nu^2_0 + \chi^2)\,s + \nu^2_0\chi)]$$
$$+ i\,[3s^2(\nu_0 + \epsilon) - (\nu^3_0 + 3\nu^2_0\,\epsilon) + 4\chi\, s(\nu_0 + \epsilon) + (\nu^2_0 + \chi^2)\,(\nu_0 + \epsilon)]$$
$$= 0$$

Equating the real and imaginary parts of the above equation we get, first, from the real part

$$s^3 - 3s\,\nu^2_0 - 6s\,\nu_0 \in + 2\chi\, s^2 - 2\chi\nu^2_0 - 4\chi\,\nu_0 \in + \nu^2_0\, s + \chi^2 s + \nu^2_0\,\chi = 0$$

$$\therefore \quad -4\chi\,\nu_0 \in = 2\nu^2_0\, s + \chi\,\nu^2_0 - 2\chi\, s^2 - s^3 + (6s\,\nu_0 \in - \chi^2 s) \qquad (31\,a)$$

$$\therefore \quad -(4\chi\,\nu_0 + 6s\,\nu_0) \in = 2\nu^2_0\, s + \chi\,\nu^2_0 - 2\chi\, s^2 - s^3 - \chi^2 s. \qquad (31)$$

From the imaginary part we get

$$3s^2\,\nu_0 + 3s^2 \in - \nu^3_0 - 3\nu^2_0 \in + 4\chi\, s\,\nu_0 + 4\chi\, s \in + \nu^3_0 + \chi^2\,\nu_0 + (\nu^2_0 + \chi^2) \in = 0$$

$$\therefore \quad (2\nu^2_0 - \chi^2 - 3s^2 - 4\chi\, s) \in = \chi^2\,\nu_0 + 4\chi\,\nu_0\, s + 3\nu_0\, s^2. \qquad (32)$$

Eliminating $\in$ from (31) and (32) we get

$$(2\nu_0^2 - \chi^2 - 3\,s^2 - 4\,\chi s)\left\{ - \frac{(2\nu_0^2 s + \chi\,\nu_0^2 - 2\,\chi\, s^2 - s^3 - \chi^2 s)}{(4\,\chi\,\nu_0 + 6\,s\,\nu_0)} \right\}$$

$$= (\chi^2\,\nu_0 + 4\chi\,\nu_0\, s + 3\nu_0\, s^2).$$

$$\rightarrow \left\{(2\nu^2_0 - \chi^2) - (3s^2 + 4\chi\, s)\right\}\left\{(2\nu^2_0\, s + \chi\,\nu^2_0 - 2\chi\, s^2 - s^3) - \chi^2 s\right\}$$
$$+ \left\{(4\chi\,\nu_0) + 6s\,\nu_0\right\}(\chi^2\,\nu_0 + 4\chi\,\nu_0\, s + 3\nu_0\, s^2) = 0$$

$$\therefore \quad [(2\nu^2_0 - \chi^2)(2\nu^2_0\, s + \chi\,\nu^2_0 - 2\chi\, s^2 - s^3) + 4\chi\,\nu_0\,(\chi^2\,\nu_0 + 4\chi\,\nu_0\, s + 3\nu_0\, s^2)]$$
$$- [(2\nu^2_0 - \chi^2)\,\chi^2 s + (3s^2 + 4\chi\, s)(2\nu^2_0\, s + \chi\,\nu^2_0 - 2\chi\, s^2 - s^3) - \chi^2 s\,(3s^2 + 4\chi\, s)$$
$$- 6s\,\nu_0\,(\chi^2\,\nu_0 + 4\chi\,\nu_0\, s + 3\nu_0\, s^2)] = 0$$

$$\therefore \quad [(3\chi^2 + 2\nu^2_0)\,\chi\,\nu^2_0 + (4\nu^2_0 + 14\chi^2)\,\nu^2_0\, s + (8\chi\,\nu^2_0 + 2\chi^3)\, s^2 - (2\nu^2_0 - \chi^2)\, s^3]$$
$$- [(-\chi^4)\, s - (4\chi^3 + 13\chi\,\nu^2_0)\, s^2 - (11\chi^2 + 12\nu^2_0)\, s^3 - 10\chi\, s^4 - 3s^5] = 0$$

$$\therefore \quad [(3\chi^2 + 2\nu^2_0)\,\chi\,\nu^2_0 + (4\nu^2_0 + 14\chi^2)\,\nu^2_0\, s + (8\chi\,\nu^2_0 + 2\chi^3)\, s^2 - (2\nu^2_0 - \chi^2)\, s^3]$$
$$+ [\chi^4 s + (4\chi^3 + 13\chi\,\nu^2_0)\, s^2 + (11\chi^2 + 12\nu^2_0)\, s^3 + 10\chi\, s^4 + 3s^5] = 0$$

$$\therefore \quad [(3\chi^2 + 2\nu^2_0)\,\chi\,\nu_0^2 + (4\nu^4_0 + 14\chi^2\,\nu^2_0 + \chi^4)\, s + (6\chi^3 + 21\chi\,\nu^2_0)\, s^2$$
$$+ (12\chi^2 + 10\,\nu^2_0)\, s^3 + 10\chi\, s^4 + 3s^5] = 0. \qquad (33)$$

As $\chi \rightarrow 0$ we know $s = 0$. It is found that for small χ the proper values of s as roots of (33) are the negative ones. i.e. viscosity effects will introduce attenuation of the waves.

Concluding Remarks

The results of the theory presented here on Rayleigh Waves in a Maxwell Body which are embodied in equations (20) and (29) clearly show that effects pertaining to period selectivity, attenuation and dispersion are obtained for a Maxwell Body which cannot, in principle, be accounted for by an elastic theory of Rayleigh Waves. This becomes analytically evident by comparing equations (20) and (29) with their counterparts for the elastic case as presented on page 89 of Reference 6. Also as we found in the case of Love waves, the effects of inelastic constitution in conjunction with layering should lead to significant, observable manifestation in seismic data, which in principle cannot be accounted for by an elastic theory.

We are in the process of carrying out extensive numerical calculations based on the theory of Rayleigh Waves in a Maxwell Body presented here.

We are also extending the present theory so to accommodate layering and will thus be in a position to make decisive comparisons with measurements and numerical results based on theory of Rayleigh Waves in a layered elastic body.

An Appreciation and Acknowledgement

The Senior Author expresses deepest appreciation to his most esteemed teacher Professor Beno Gutenberg, for his constant encouragement in poursuit of the new pathways in Geophysics which led to this work.

The Authors express their appreciation to Mr. Shrikand Desai for checking calculations and to the Fluid Mechanics Branch of the Office of Naval Research for making preparation of this paper possible.

BIBLIOGRAPHY

1. « Relaxation Phenomena and the Origin of Earthquakes » by Paul LIEBER, Ph. D. dissertation, California Institute of Technology, 1961.
2. Paul LIEBER, « On an Elastic-Plastic Model of the Earth's Crust and Upper Mantle », Transactions American Geophysical Union, December 1962, Volume 43, N° 4, p. 456.
3. Paul LIEBER, « A Theory of Love Waves for an Elastic-Plastic Model of the Earth's Crust ant Mantle », Transactions American Geophysical Union, December 1962, Volume 43, N° 4, pp. 428-429.
4. Paul LIEBER, « Further Consideration on an Elastic-Plastic Model of Earth's Crust and Upper Mantle », Transactions American Geophysical Union, March 1963, Volume 44, N° 1, p. 99.

5. Paul Lieber, « Concerning Surface Waves on a Multilayered Inelastic Earth », Transactions American Geophysical Union, March 1963, Volume 44, N° 1, p. 102.

6. « Introduction to the Theory of Seismology » by K. Bullen, Cambridge University Press, Second Edition, page 89.

TABLE OF SYMBOLS

$X_i \; (i = 1, 2, 3)$	rectangular Cartesian coordinates.
u_i	components of the displacement vector.
e_{ij}	components of the strain tensor.
σ_{ij}	components of the stress tensor.
λ, μ	Lame elastic constants.
λ', μ	Material constants of the viscous element.
ρ	density of the Maxwell material.
$\chi = \dfrac{(3\lambda + 2\mu)}{(3\lambda' + 2\mu')}$	
s	damping coefficient.
q	wave length
μ/q	wave velocity of propagation.
$p = s + i$	
$\nabla^2 = \dfrac{\partial^2}{\partial x_i \; \partial x_i}$	Laplace operator.

INVERSION OF SURFACE WAVE DISPERSION DATA

Charles ARCHAMBEAU and Don L. ANDERSON
(Seismological Laboratory, California Institute of Technology)

The principal goal of the study to be outlined here was to obtain a systematic and practical means of determining structural models of the earth from the observed dispersion of surface waves or from the free oscillation spectrum. This was accomplished through a perturbation scheme which has its basis in Rayleigh's Principle. That is, an initial test structure is assumed and then perturbed until its theoretical dispersion agress with the observed dispersion to within some preselected degree of accuracy. The problem is therefore to determine the necessary perturbations for rapid convergence of the theoretical spectrum to the observed spectrum.

The essential concepts of the perturbation method were stated and utilized by Rayleigh himself and recently restated by Jeffreys in a context similar to that of the present study. However, up to the present time the method has been employed to predict the effect on the vibrational frequencies due to a specified change in the parameters of the system, such as density and the elastic constants. The present problem is just the inverse of this, that is, to determine changes in the system parameters which give a specified change in the characteristic vibrational frequencies. The application of Rayleigh's Principle to this inverse problem was first suggested to us by Dr. Freeman Gilbert.

We have generalized the method to a form applicable to this inverse problem in a radially inhomogeneous, spherical earth and have programed the procedure for automatic computation of the required structure. In addition, we have formulated the method in a manner which shows, very clearly, the nature of the dependence of the dispersive properties on small changes in the structure parameters. From this formulation we find that this perturbation scheme, which is exact to first order and, therefore, representative of any first order theory, is not by itself sufficient to predict the required first order changes in a test structure. However, if mild supplementary conditions of constraint are introduced, then the perturbation scheme does yield corrections which in practice have given rapid convergence. Thus, constraints, based on knowledge of the structure derived from other sources, have been shown to be a necessary as well as desirable part of the method.

Once having obtained a structure giving the same vibrational spectrum as that observed, the question of uniqueness arises. In practice, only limited portions of the spectrum are observed and the spectral data will also have an associated error. In addition, the surface wave data represents an averaged dispersion over a laterally inhomogeneous earth. Under these conditions there is no question but that the derived structure is *not* unique. That is, there are other structures which will satisfy the data, which is necessarily limited in extent and accuracy, as well or very nearly as well. Further, depending on the conditions of the experiment, the model or models obtained can only represent an averaged structure for the earth, especially for the crust. Therefore, in view of the experimental limitations alone, it is only realistic to consider the structure obtained in the light of other independent evidence.

Thus, for example, travel time curves are being computed from structures obtained from dispersion data for comparison with the arrival times of body phases. In addition, as more and better data becomes available, especially with regard to the higher mode surface waves, the practical uniqueness of the method will improve considerably.

Fig. 1 shows of the essential features of the theory in a condensed and symbolic form. Throughout the next few figures H and H,

ABSTRACT FORMULATION

Defn. $(u, v) \equiv \int_{D_H} \cdots \int u \bar{v} \, dx_1 \cdots dx_k$

Variational Principle

$$\lambda_\ell = \frac{(Hu_\ell, u_\ell)}{(u_\ell, u_\ell)} = MIN \frac{(Hu, u)}{(u, u)}$$

$$(u, u_m) = 0, \quad m = 1, 2, \cdots, \ell - 1$$

Associated Euler-Lagrange Equation

$$H u_\ell = \lambda_\ell u_\ell$$

(Plus Boundary Conditions)

Approximate Variational Method

$$\lambda_\ell^N = \frac{\sum_{s=1}^{N} \{H_s u_\ell^s, u_\ell^s\}}{\sum_{s=1}^{N} \{u_\ell^s, u_\ell^s\}} = MIN \frac{\sum_{s=1}^{N} \{H_s u^s, u^s\}}{\sum_{s=1}^{N} \{u^s, u^s\}}$$

$$\{u^s, u_m^s\} = 0 \; ; \quad m = 1, 2, \cdots, \ell - 1$$

$$\lambda_\ell = \lim_{N \to \infty} \lambda_\ell^N$$

Associated Euler-Lagrange Eqs.

$$H_s u_\ell^s = \lambda_\ell u_\ell^s, \quad s = 1, 2, \cdots, N$$

(Plus Boundary Conditions on u_ℓ^s)

Defn. $\{u, v\} = \int_{D_{H_s}} \cdots \int u \bar{v} \, dx_1 \cdots dx_k$

Fig. 1

denote differential operators, the U' *s* and λ' *s* are the eigenfunctions and eigenvalues belonging to the operators H. The Euler-Lagrange equations are, in the present context, just the equations of motion for Love of Rayleigh waves or equivalently for the torsional or spheroidal oscillations of the earth.

The inner product of two functions is the indicated integral over the region in which the operator H is meaningful (i.e. the domain of H). In the present application this is the interior of our spherical earth model.

The variational principle indicated is fundamental to this theory; the first equality is an identity while the second equality is essentially a statement of Rayleigh's principle. Thus the eigenvalue is obtained by minimizing the indicated functional by varying U subject to the orthogonality condition indicated.

The approximate variational method is in fact the approach used in the present application and corresponds to the usual layered approximation of a radially inhomogeneous earth. Formally it may be obtained from the exact variational formulation by breaking the integrals up into a sum of integrals over short intervals in the radial direction. For sufficiently small intervals the integrand in the individual integrals can be approximated so that the coefficients of the differential operator are constants and the eigenfunctions are solutions of the indicated set of differential equations each appropriate for a layer. The boundary conditions connect the solutions U'_i in each layer so as to maintain continuity and satisfy the original boundary conditions for the exact variational method.

In the limit as the number of integration intervals (or layers) becomes large, the eigenvalue for this approximate theory will approach that of the exact theory.

The perturbation theory shown in Fig. 2 actually follows from the statement of Rayleigh's principle. However, it may be formulated and derived in greater generality in the manner indicated in these equations. Here we indicate how a perturbation affects one of the layer equations. The layer index is momentarily suppressed for clarity.

The unperturbed system corresponds to our test structure while the perturbed system corresponds to a structure giving the observed dispersion. The difference in the structures corresponds to a perturbation of the coefficients of the differential operator. Taking the perturbations in the λ' *s* and P_i' *s* to be small so that second order variations may be neglected, it is easy to show that (4) follows from these relationships.

<u>*Perturbation Theory*</u>

$$(1)\quad H u_\ell = \lambda_\ell u_\ell \quad (\textit{Unperturbed}), \qquad H \equiv \frac{d}{dx}\left({}^{(0)}P_1 \frac{d}{dx}\right) + {}^{(0)}P_2$$

$$(2)\quad \mathcal{H} U_\ell = \Lambda_\ell U_\ell \quad (\textit{Perturbed}), \qquad \mathcal{H} \equiv \frac{d}{dx}\left(P_1 \frac{d}{dx}\right) + P_2$$

where: $P_i - {}^{(0)}P_i = \delta P_i\,, \quad i = 1, 2$

$$(3)\quad \begin{cases} \Lambda_\ell - \lambda_\ell = \delta\lambda_\ell \\ \mathcal{H} = H + \sum_i H_i\,\delta P_i \\ U_\ell = u_\ell + \sum_i \left(\frac{\partial U_\ell}{\partial P_i}\right)\delta P_i + \left(\frac{\partial U_\ell}{\partial \Lambda}\right)_{\lambda_\ell}\delta\lambda_\ell + O(\delta P_i^2, \delta\lambda_\ell^2) \end{cases}$$

Thus $(\lambda_\ell + \delta\lambda_\ell)(U_\ell, U_\ell) = (\mathcal{H} U_\ell, U_\ell)$, *and from* (3) *using* (1);

$$(4)\quad \boxed{\sum_i (H_i u_\ell, u_\ell)\,\delta P_i = \delta\lambda_\ell\,(u_\ell, u_\ell) + O(\delta P_i^2, \delta\lambda_\ell^2)}$$

<u>*Partial Variations*</u>:

$$\left(\frac{\delta\lambda_\ell}{\delta P_1}\right)_{P_2} = \frac{(H_1 u_\ell, u_\ell)}{(u_\ell, u_\ell)}\;; \qquad \left(\frac{\delta\lambda_\ell}{\delta P_2}\right)_{P_1} = \frac{(H_2 u_\ell, u_\ell)}{(u_\ell, u_\ell)}$$

Fig. 2

It is convenient to express this result in a form analogous to partial derivatives. Thus, we consider the ratio of the variation in the eigenvalue to the variation or perturbation of one of the elastic parameters with all the other parameters held fixed.

For the layer or step approximation expressed in its full form we have indicated in figure 3 the two relations giving the unperturbed and perturbed eigenvalues. We now can show how the difference between these two eigenvalues depends on the differences between the elastic parameters in each layer. Thus proceeding in the same manner as in the previous figure we get the first order relationship indicated.

Again the result may be expressed in terms of the partial variations, where all but one of the layer parameters are held constant for each partial. These partials are expressed in terms of the known unperturbed eigenfunctions and the known perturbation operators, and may therefore be computed from the test structure.

An application of these ideas to the toroidal oscillations of the earth yields the relation show in figure 4. We shall use this mode of oscillation as an example of an application of the method.

The conditions on the rigidity and density functions indicated denote the layer approximation and a representation involving a continuous variation of the elastic properties which also may be

Fig. 3

Perturbation Theory (Step Approximation)

$$\lambda_\ell^N = \frac{\sum_{s=1}^{N}\{H_s u_\ell^s, u_\ell^s\}}{\sum_{s=1}^{N}\{u_\ell^s, u_\ell^s\}}, \quad \text{(unperturbed)}$$

$$\Lambda_\ell^N = \frac{\sum_{s=1}^{N}\{\mathcal{H}_s U_\ell^s, U_\ell^s\}}{\sum_{s=1}^{N}\{U_\ell^s, U_\ell^s\}}, \qquad \mathcal{H}_s = H_s + \sum_i H_i^S \delta P_i^S \quad \text{(Perturbed)}$$

$$\{\mathcal{H}_s U_\ell^s, U_\ell^s\} = \Lambda_\ell^N \{U_\ell^s, U_\ell^s\}$$

$$\{H_s u_\ell^s, u_\ell^s\} = \lambda_\ell^N \{u_\ell^s, u_\ell^s\}$$

From the result (4):

$$\Lambda_\ell^N = \lambda_\ell^N + \delta\lambda_\ell^N = \sum_{s=1}^{N}\left[\frac{\{H_s u_\ell^s, u_\ell^s\}}{\sum_{s=1}^{N}\{u_\ell^s, u_\ell^s\}} + \frac{\sum_i\{H_i^S u_\ell^s, u_\ell^s\}\,\delta P_i^S}{\sum_{s=1}^{N}\{u_\ell^s, u_\ell^s\}}\right]$$

$$\therefore \boxed{\delta\lambda_\ell^N = \sum_{s=1}^{N}\left[\frac{\sum_i\{H_i^S u_\ell^s, u_\ell^s\}\,\delta P_i^S}{\sum_{s=1}^{N}\{u_\ell^s, u_\ell^s\}}\right]}$$

Partial Variations:

$$\boxed{\left(\frac{\delta\lambda_\ell^N}{\delta P_i^S}\right)_{P_j^r} = \frac{\{H_i^S u_\ell^s, u_\ell^s\}}{\sum_{s=1}^{N}\{u_\ell^s, u_\ell^s\}} \;;\quad P_j^r \text{ fixed for } r = 1, 2, \cdots S-1, S+1, \cdots N}$$

Toroidal Oscillations, Love waves

Rayleighs Principle

$${}_n\omega_\ell^2 \sum_{s=1}^{N}\int_{r_s}^{r_{s+1}} \rho(r)\left[{}_nW_\ell^{(s)}(r)\right]^2 r^2 dr =$$

$$\sum_{s=1}^{N}\int_{r_s}^{r_{s+1}} \mu(r)\left[\left(\frac{d_nW_\ell^{(s)}}{dr} - \frac{{}_nW_\ell^{(s)}}{r}\right)^2 + (\ell-1)(\ell+2)\left(\frac{{}_nW_\ell}{r}\right)^2\right] r^2 dr$$

$$\left.\begin{matrix}\mu(r) = \mu_s \\ \rho(r) = \rho_s\end{matrix}\right\} r_s \le r \le r_{s+1} \quad \underline{\text{or}} \quad \begin{matrix}\mu(r) = \sum_{j=0}^{K_1} \alpha_j r^j \\ \rho(r) = \sum_{j=0}^{K_2} \beta_j r^j\end{matrix}$$

Associated Euler-Lagrange Equations

$$\mu_s \frac{d^2{}_nW_\ell^{(s)}}{dr^2} + \frac{2\mu_s}{r}\frac{d_nW_\ell^{(s)}}{dr} + \mu_s\left[\frac{{}_n\omega_\ell^2}{\beta_n^2} - \frac{\ell(\ell+1)}{r^2}\right]{}_nW_\ell^{(s)} = 0, \quad S = 1, 2, \cdots, N$$

(Plus Bondary Conditions)

$${}_nW_\ell^{(s)} = {}_nA_\ell^{(s)} j_\ell({}_nk_\ell^{(s)} r) + {}_nB_\ell^{(s)} n_\ell({}_nk_\ell^{(s)} r) \;;\; {}_nk_\ell^s = \frac{{}_n\omega_\ell}{\beta_s}, \quad \beta_s = [\mu_s/\rho_s]^{1/2}$$

Fig. 4

used. Use of the latter structure representation involves some further complications which we shall not discuss, but is included here to indicate an alternate approach which is used and which is generally superior to the layer approximation.

The associated equations of motion in the individual layers are as indicated and yield solutions in terms of Bessel functions.

This formulation is actually somewhat awkward for numerical calculation. Figure 5 shows an alternate approximate form of the equation of motion which is simple and highly accurate.

Alternate Form (Toroidal Oscillations and Love Waves)

$$\mu_s \frac{d^2 W_s}{dr^2} + \frac{2\mu_s}{r}\frac{dW_s}{dr} + \mu_s\left[\frac{\omega^2}{\beta_s^2} - \frac{(ka)^2}{r^2}\right] W_s = 0 \ ; \quad W_s \equiv {}_nW_\ell^{(s)}, \ (ka)^2 \equiv \ell(\ell-1)$$

(Anderson's flat earth approximation)

$$N_s \frac{d^2 V_s}{dz^2} + L_s\left[\frac{\omega^2}{\beta_s'^2} - k^2\right] V_s = 0 \ ; \quad V_s = (a-z) W_s$$

where : $N_s \equiv \left(\frac{a - z_s'}{a}\right)\mu_s \ , \quad L_s \equiv \mu_s$ (Anisotropic)

$$\beta_s' = \left(\frac{a}{a - z_s'}\right)\beta_s$$

valid when : $h_s = (z_{s+1} - z_s) << a$

$$\left(\frac{a-z}{a}\right)_s^2 \simeq \left(\frac{a - z_s'}{a}\right)^2, \quad z_s' = z_s + h_s/2$$

solution :

$$V_s = A_s \sin k\gamma_s z + B_s \cos k\gamma_s z \ , \quad \gamma_s = \left(\frac{a}{a - z_s'}\right)\left[\left(\frac{c}{\beta_s'}\right)^2 - 1\right]^{1/2}$$

Fig. 5

By introducing the parameters and new variables indicated we can transform the equation for the toroidal oscillations into an equation wich has the form of an equation for Love waves in a flat layered anisotropic half-space. Thus we can actually consider simultaneously the toroidal oscillations of a sphere or Love wave propagation in a half-space. The approximation is valid when the layer thicknesses are small compared to the earth's radius (a). The solutions are seen to have a very simple form.

Using the previous approximate equation of motion we find that Rayleigh's principle takes the simple form indicated (Fig. 6). Under (a) we have indicated the relationship for the layered approximation and under (b) that for a polynomial approximation for the elastic parameters. In both cases the integrals may be evaluated analyti-

Alternate Rayleigh Principle (Toroidal Oscillations)

$$\omega^2 \sum_{s=1}^{N} \int_{z_s}^{z_{s+1}} \rho(z)\, V_s^2(z)\, dz = \sum_{s=1}^{N} \int_{z_s}^{z_{s+1}} \mu(z) \left[\left(\frac{N_s}{L_s}\right)\left(\frac{dV_s}{dz}\right)^2 + k^2 V_s^2\right] dz$$

$$\text{(a)} \quad \omega^2 \sum_{s=1}^{N} \rho_s I_0^s = k^2 \sum_{s=1}^{N} \mu_s I_0^s + \sum_{s=1}^{N} \mu_s I_1^s$$

$$I_0^s = \int_{z_s}^{z_{s+1}} V_s^2(z)\, dz \;; \quad I_1^s = \left(\frac{N_s}{L_s}\right) \int_{z_s}^{z_{s+1}} \left(\frac{dV_s}{dz}\right)^2 dz$$

(Structure Approximated by Step Functions)

$$\text{(b)} \quad \omega^2 \sum_{j=1}^{k_1} \alpha_j J_0^j = k^2 \sum_{j=1}^{k_2} \beta_j J_0^j + \sum_{j=1}^{k_2} \beta_j J_1^j$$

$$J_0^j = \sum_{s=1}^{N} \int_{z_s}^{z_{s+1}} z^j\, V_s^2(z)\, dz \;; \quad J_1^j = \sum_{s=1}^{N} \left(\frac{N_s}{L_s}\right) \int_{z_s}^{z_{s+1}} z^j \left(\frac{dV_s}{dz}\right)^2 dz$$

(Structure Approximated by Polynomials)

Fig. 6

cally due to the simplicity of the eigenfunctions V_s shown on the previous figure.

The results of the perturbation theory can be applied and we easily obtain the variational partials of interest. Further, the phase and group velocity are defined as indicated (Fig. 7) and can be

Variational Partials

u = Group Velocity = $\frac{d\omega}{dk}$ $\quad V_r$ = P.E. of r^{th} layer $\quad \mathcal{T}$ = Total K.E.

c = Phase Velocity = ω/k $\quad T_r$ = K.E. of r^{th} layer $\quad E$ = Total Energy = $2\mathcal{T}$

$$u = \left(\frac{\delta\omega}{\delta k}\right)_{\mu,\rho} = \frac{1}{c}\left(\frac{\sum_{s=1}^{N} \mu_s I_0^s}{\sum_{s=1}^{N} \rho_s I_0^s}\right)$$

(a) Layered Structure Approximation ($k = k_0$ = constant)

$$\frac{\rho_r}{c}\left(\frac{\delta c}{\delta \rho_r}\right)_{\mu} = \frac{\rho_r}{\omega}\left(\frac{\delta\omega}{\delta\rho_r}\right)_{\mu} = -\frac{1}{2}\left[\frac{\rho_r I_0^r}{\sum_{s=1}^{N} \rho_s I_0^s}\right] = -\left(\frac{T_r}{E}\right)$$

$$\frac{\mu_r}{c}\left(\frac{\delta c}{\delta \mu_r}\right)_{\rho} = \frac{\mu_r}{\omega}\left(\frac{\delta\omega}{\delta\mu_r}\right)_{\rho} = \frac{1}{2}\left[\frac{\mu_r (k_0^2 I_0^r + I_1^r)}{\omega^2 \sum_{s=1}^{N} \rho_s I_0^s}\right] = \left(\frac{V_r}{E}\right)$$

$$\delta c = \sum_{r=1}^{N} \left[\left(\frac{\delta c}{\delta \rho_r}\right) \delta\rho_r + \left(\frac{\delta c}{\delta \mu_r}\right) \delta\mu_r\right]$$

$$\boxed{E\left(\frac{\delta\omega}{\omega}\right) = E\left(\frac{\delta c}{c}\right) = \sum_{r=1}^{N} \left[V_r\left(\frac{\delta\mu_r}{\mu_r}\right) - T_r\left(\frac{\delta\rho_r}{\rho_r}\right)\right]}$$

$$\boxed{E\left(\frac{\delta\omega}{\omega}\right) = E\left(\frac{\delta c}{c}\right) = \sum_{r=1}^{N} \left[(V_r - T_r)\frac{\delta\mu_r}{\mu_r} + 2T_r \frac{\delta\beta_r}{\beta_r}\right]}$$

Note: $\sum_{r=1}^{N} V_r = \sum_{r=1}^{N} T_r = \frac{E}{2}$; $\quad \sum_{r=1}^{N} \frac{V_r}{\mu_r} \neq \sum_{r=1}^{N} \frac{T_r}{\rho_r}$ in general

Fig. 7

related by a variation of the wave number k and frequency ω holding the elastic parameters constant. The result is as shown and was originally obtained by Meissner.

By defining the potential and kinetic energies for each layer of the medium we are able to show that the partial variations of interest may be expressed in terms of the kinetic or potential energy of the layer divided by the total energy of the system in the manner indicated.

Then using the first order relationship between the variations in the phase velocity or frequency and the variations in the elastic parameters, we obtain the final perturbation formulas for the toroidal oscillations or Love waves. Clearly the coefficients of the variations in the elastic parameters on the right are related by the condition noted and this relationship is important to the question of inversion, since these relationships will be used to solve for the variations in the elastic parameters in terms of δc and the energies at different frequencies.

Figure 8 indicates the perturbation formulas for the polynomial approximation as well. In this case the partial variations involving

<u>Variational</u> <u>Partials</u> (continued)

(b) POLYNOMIAL Approximation ($k = k_0 =$ constant)

$$\frac{1}{c}\left(\frac{\delta c}{\delta \alpha_i}\right)_\beta = \frac{1}{\omega}\left(\frac{\delta \omega}{\delta \alpha_i}\right)_\beta = -\frac{J_0^i}{2\sum_{j=1}^{k_1} \alpha_j J_0^j}$$

$$\frac{1}{c}\left(\frac{\delta c}{\delta \beta_i}\right)_\alpha = \frac{1}{\omega}\left(\frac{\delta \omega}{\delta \beta_i}\right)_\alpha = \frac{k_0^2 J_0^i + J_1^i}{2\omega^2 \sum_{j=1}^{k_1} \alpha_j J_0^j}$$

$$\delta c = \sum_{i=1}^{k} \left[\left(\frac{\delta c}{\delta \alpha_i}\right)_\beta \delta \alpha_i + \left(\frac{\delta c}{\delta \beta_i}\right)_\alpha \delta \beta_i\right] \; ; \quad k = \mathrm{Max.}[k_1, k_2] \ll N$$

Note: $\sum_{i=1}^{k} \alpha_i \left(\frac{\delta c}{\delta \alpha_i}\right)_\beta = -\sum_{i=1}^{k} \beta_i \left(\frac{\delta c}{\delta \beta_i}\right)_\alpha \; ; \; \sum_{i=1}^{k} \left(\frac{\delta c}{\delta \alpha_i}\right)_\beta \doteq \sum_{i=1}^{k} \left(\frac{\delta c}{\delta \beta_i}\right)_\alpha$

<u>FORMAL</u> <u>INVERSION</u>

$\omega_s =$ Discrete set of frequencies, $s = 1, 2, \ldots M \geq \binom{2N}{2k}$

$$E(\omega_s)\left[\frac{\delta c(\omega_s)}{c(\omega_s)}\right] = b_s$$

$$\frac{V_r(\omega_s)}{\mu_r} = a_{sr}$$

$$-\frac{T_r(\omega_s)}{\rho_r} = a_{s,r+N}$$

$$\delta \mu_r = x_r$$

$$\delta \rho_r = x_{r+N}$$

MATRIX EQUATION

$$\boxed{\begin{aligned} A_1 x &= b \\ x &= (A_1^T A_1)^{-1} A_1^T b \end{aligned}}$$

(Best solved by Relaxation or Iterated)

Fig. 8

the polynomial coefficients cannot be connected to the energies of the system so directly as they were for the layered case. However,

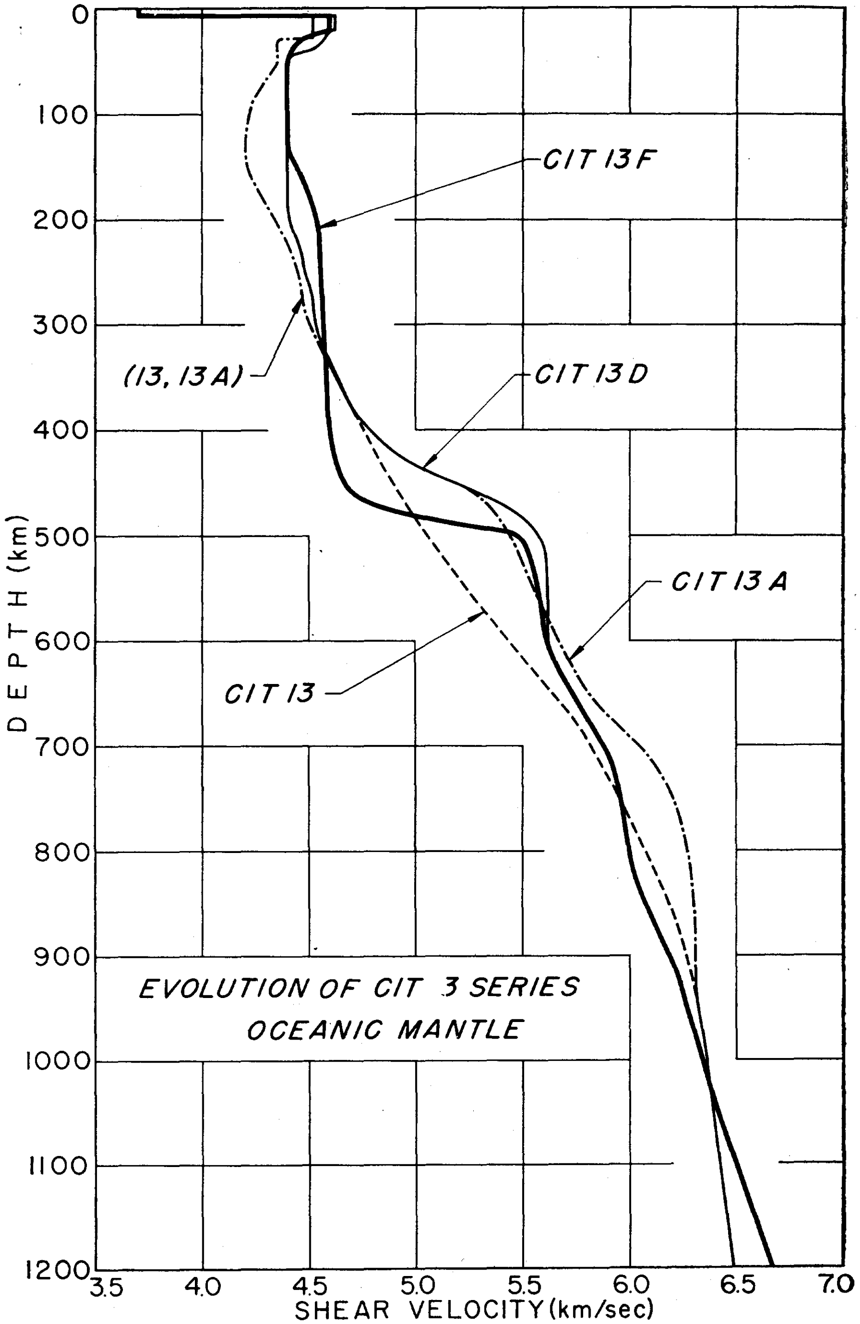
0
100
200
300
400
500
600
700
800
900
1000
1100
1200
DEPTH (km)
3.5
4.0
4.5
5.0
5.5
6.0
6.5
7.0
SHEAR VELOCITY (km/sec)
CIT 13F
(13, 13A)
CIT 13D
CIT 13A
CIT 13
EVOLUTION OF CIT 3 SERIES
OCEANIC MANTLE

Fig. 9

the partials can be shown to be related in a fashion similar to those for the layered approximation.

Now we can generate a set of perturbation equations corresponding to a set of observations at M distinct frequencies ω_s. This set of equations may obviously be expressed as a matrix equation of the form indicated for the layered approximation. The matrices A, b and x are defined as indicated and in this case we wish to obtain the required perturbations of the elastic parameters. Therefore, we must consider the inverse of the matrix A. Due to the relationship between the matrix elements of A, which is, in this case, that the sum of the layer potential energies is equal to the sum of the layer kinetic energies, we find that the matrix A is singular. Therefore, in order to achieve a solution for the x' s, constraints are introduced so as to limit at least one of the layer parameters to have zero variation. In practice we have generally limited the rigidity in one or more crustal layers to be fixed. Under such constraints we denote the new conditioned A matrix by A_1, and it is easy to show that the inverse of A_1 exists. Therefore, the inversion may be accomplished in the least squares sense indicated or by simple relaxation or iteration methods. A similar situation holds for the method when the polynomial approximation is used.

Fig. 9 and 10 show various stages in the evolution of an earth structure and the resulting dispersion compared to longperiod Love wave data.

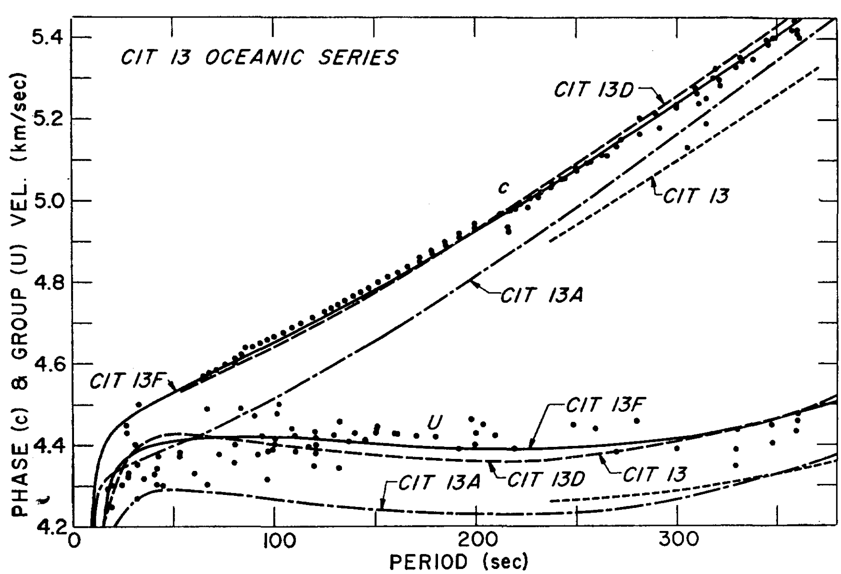

Fig 10

THE DETERMINATION OF THE ENERGY OF EARTHQUAKES WITH AN ACCOUNT OF THE FREQUENCY SPECTRUM OF SEISMIC VIBRATIONS

by N. K. KARAPETIAN

An attempt is made in the present study to determine the energy of volumetric seismic waves emitted from the earthquake site, making use of our previously suggested method of determining the earthquakes with an account of the frequency spectrum of seismic vibrations [1]. The vibrations of the ground are represented by Fourier's integral [2], with the aim of obtaining frequency spectrum with nonperiodic seismic waves :

$$f(t) = \frac{1}{2\pi} \int_{-\infty}^{+\infty} S(\omega)\, e^{i\omega t}\, d\omega \tag{1}$$

The function $f(t)$ describes in our case the law of vibration of the ground when the seismic waves traverse during a finite time. The main part of the complex spectrum of this function is contained within the frequencies $(0, \omega)$. Consequently, the endless limits of integrating can be substituted by finite values, that is, in order to effect the integration from the very beginning of the vibrating process to its dying away and within the frequencies from 0 to ω :

$$f(t) = \frac{1}{2\pi} \int_{0}^{\omega} S(\omega)\, e^{i\omega t}\, d\omega \tag{2}$$

The spectral density of the complex amplitude $S(\omega)$ can be represented as follows :

$$S(\omega) = \frac{\Phi(\omega)}{u(\omega)}\, e^{i[\varphi(\omega) - \varphi_1(\omega)]} \tag{3}$$

where $\varphi(\omega)$ is the initial stage; $\varphi_1(\omega)$ is the frequency characteristic of the device; $u(\omega)$ stands for the magnifying of the device.

The modulus $\varphi(\omega)$ of the complex spectrum $S(\omega)$ forms the amplitude spectrum of the function, $f(t)$, while the argument $\varphi(\omega)$ represents the phase spectrum of the same function.

These spectra can be expressed by Fourier's coefficient :

$$\mathcal{A}(\omega) = \int_0^t f(t) \cos \omega t\, dt \quad , \qquad \mathcal{B}(\omega) = \int_0^t f(t) \sin \omega t\, dt \tag{4}$$

in the following way

$$\Phi(\omega) = \sqrt{\mathcal{A}^2(\omega) + \mathcal{B}^2(\omega)}$$

$$\varphi(\omega) = \text{arc tg} \frac{\mathcal{B}(\omega)}{\mathcal{A}(\omega)} \pm n\,\mathcal{F} \qquad (6)$$

Tabulating the values of the functions $f(t)$ according to the time with certain rather small intervals of time, amplitude and phase spectra are obtained with the help of electronic computers in conformity with the above-given formulas.

Such spectra make it possible to solve a number of seismological problems with great reliability.

One of the most complicated problems in modern seismology is the determination of the total energy of elastic seismic waves. The energy of the volumetric waves radiated from the centre may be estimated by the well-known formula [3, 4] :

$$E = 2\pi R^2 \rho c \frac{\sin \Delta \ \sin e_0}{f(e, \alpha) \cos e \frac{d\,e}{d\,\Delta}} e^{k\Delta} \int_0^{T} v^2 \, dt \qquad (7)$$

where R is the radius of the Earth; ρ is the density of the rocks of the site where the seismic stations are installed; c is the velocity of the dissemination of the waves; e is the corner of the egress from the centre; e_0 is the corner of emergence to the surface of the Earth; Δ is the epicentric distance; k is the index of the damping; $f(e, d)$ is the function including the irregular radiation of energy depending upon the mechanism of the centre; T is the duration of the earthquake and v is the instantaneous vibration velocity of the particles of the ground in the emerging seismic waves.

The value of the integral $y = \int_0^{T} v^2 dt$ in the formula (7) is proportional to the energy density.

If we have an amplitude spectrum determined in the abovementioned way we can compute the integral y with great accuracy, and therefore determine the energy of elastic seismic waves. To achieve this aim the method of determining energy known from the theory of the spectra [5] is adopted; namely, by using Rayleigh's theorem according to which

$$\int_{-\infty}^{+\infty} f^2(t)\, dt = \frac{1}{\pi} \int_0^{\infty} \Phi_1^2(\omega)\, d\omega \qquad (10)$$

Here $\varphi_1(\omega)$ is the modulus of the spectrum of the function $f(t)$. Therefore, $\varphi_1^2(\omega)$ represents the spectral density of the energy.

In determining the energy of the seismic waves the function $f(t)$ is the velocity of vibration of the ground particles.

In this way to determine the value of y proportional to the energy density it is necessary to compute the integral

$$\frac{1}{\pi}\int_0^\infty \Phi_1^2(\omega)\, d\omega = \int_0 v^2\, dt \tag{11}$$

In the formula (11) $\varphi_1(\omega)$ is the modulus of the velocity spectrum.

It is well known that the complex spectrum of the derivative is obtained from the complex spectrum of the function multiplied by the circular frequency ω.

Therefore, the integral for the determination of the value proportional to the energy density will assume the following form :

$$y = \frac{1}{\pi}\int_0^\infty \omega^2\, \Phi^2(\omega)\, d\omega \tag{12}$$

The value is determined for various component vibrations either by an analytic computation of the integral y with the help of computers or by a graphic measurement of the area involved between the velocity spectrum, the axis of the abscess and the ordinates corresponding to the beginning and the end of the spectrum. The total energy density is determined along all the components of the emerging waves, with a due account of the influence of the earth's surface. To determine the total energy of the volumetric seismic waves it is necessary to include the value of the total energy density in the formula (7).

When the above-given method is applied to the determination of the earthquake energy one can receive at the same time the energetic spectrum of the earthquake; namely, the curve of energy determination of the seismic waves by frequency. We can take, for instance, the determination of y, the values of proportional energy density of the seismic waves in the case of three blasts. The explosions were conducted at a site consisting of basalt. The registration of the vibration of the ground was made by the electrodynamic seismographs of VEGIK located in the pit-wells at the layer of unweathered basalt (*fig.* 1).

The registration, made by the horizontal seismograph W-E, of the displacement of the ground is analysed for the first blast with a charge of 400 grms: of explosive. Registrations, made by a vertical seismograph, of the displacement of the ground are analysed

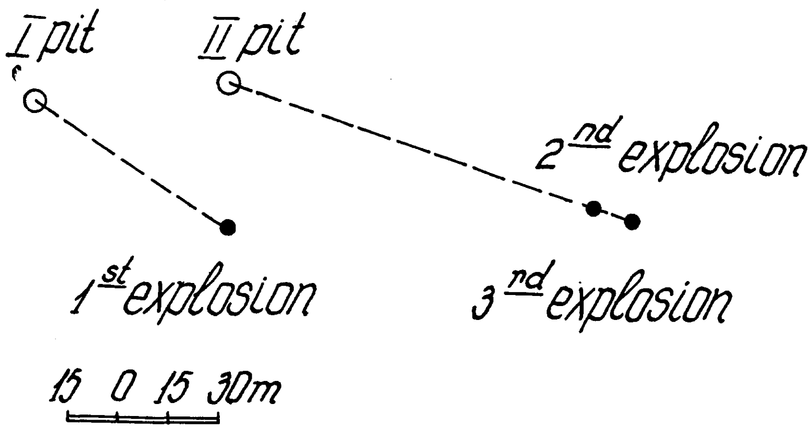

FIG. 1.

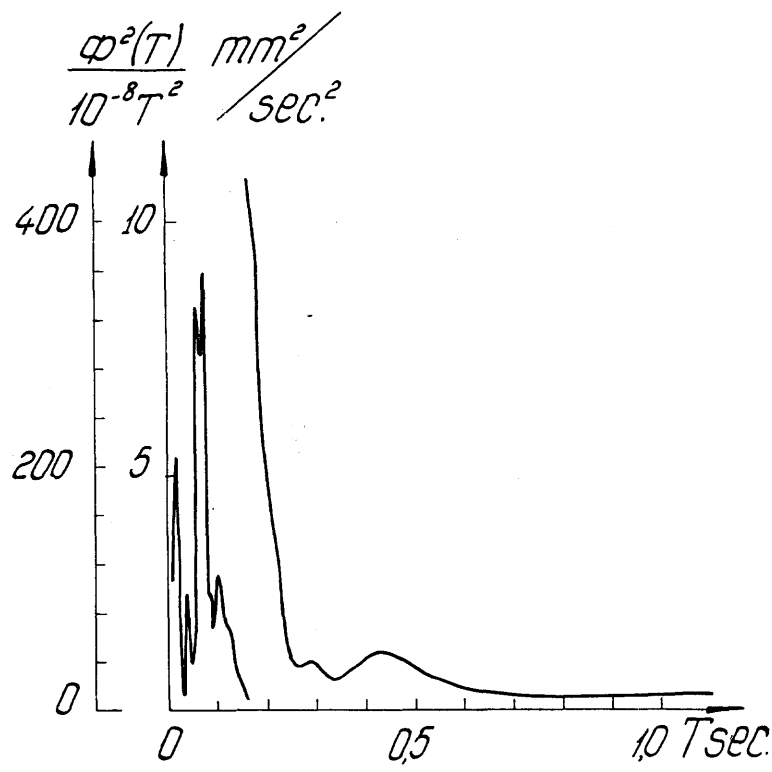

FIG. 2.

for the second and the third blasts with charges of 15 kgs. and 100 kgs. of explosive respectively. In determining the spectrum a division of the waves was not effected in view of the small epicentric distance and the comparative uniformity of the medium (the epicentre of the blast and the seismograph are located in the basalt); and all of the recording was analysed as a whole.

In order to obtain amplitude and phase spectra the analysed recordings were magnified about ten times and the values of the function $f(t)$ were accordingly measured; that is, the displacement of the ground in terms of time, beginning with zero until the vibrations die down, once every 0.005 seconds. These values are tabulated with the help of which $\Phi(\omega)$ and $\varphi(\omega)$ values are obtained for every curve at the computing centre of the Armenian Academy of Sciences for periods of 0.005 sec. every 0.005 sec. up to one second and in every 0.01 sec. beginning with one second.

Energetic spectra are calculated and drawn, based on the values $\Phi(\omega)$. The obtained spectra are in fact velocity spectra. However, in view of the fact that the velocity spectrum practically differs from the energetic only by a constant factor the spectra drawn may also be called energetic.

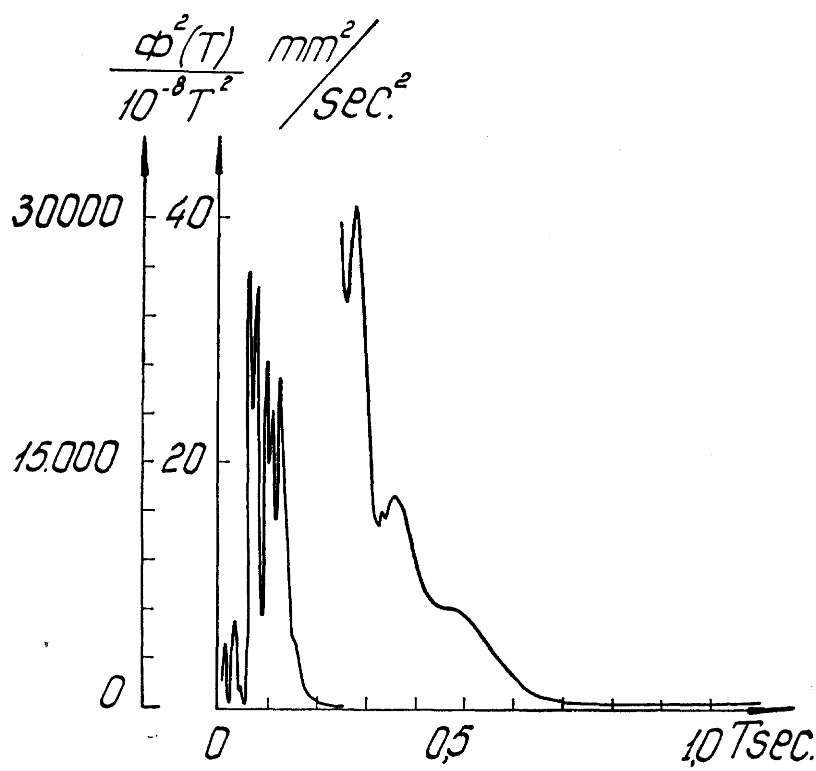

Fig. 3.

Figure 2 illustrates the energetic spectrum of the first blast, fig. 3 — of the second and fig. 4 — of the third.

Considering the energetic spectra drawn it can be noted that in the case of an increase of the quality of the charge of the explosive the range of the periods relating to the maximum values of energy also increases.

The value proportional to the density of the energy y was calculated graphically. For the first explosion it turned out to equal $y_1 = 4{,}19.10^{-7}$ cm²/sec, for the second $y_2 = 5{,}61.10^{-5}$ cm²/sec and for the third $y_3 = 2{,}60.10^{-4}$ cm²/sec.

The suggested method of determining the seismic energy is convenient inasmuch as the frequency spectrum in use can be successfully applied also to the solution of a number of seismological problems. And conversely, in solving a number of seismological problems without an additional waste of time, the energy of the earthquake can also be calculated.

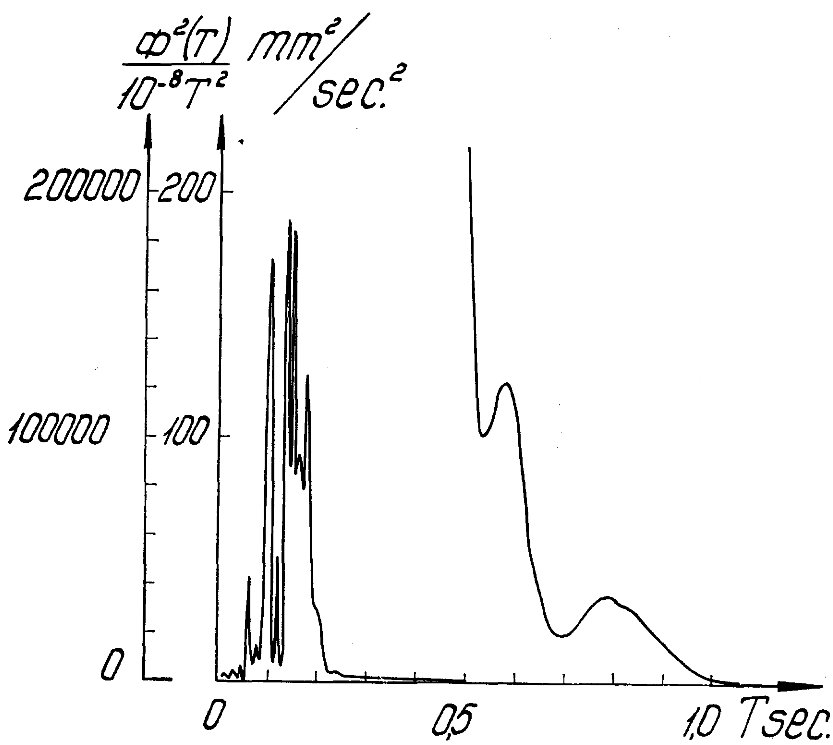

FIG. 4.

REFERENCE LIST

[1] KARAPETIAN (N. K.). The Method of Determining the Earthquake Energy with an Account of the Frequency Spectrum of Seismic Vibrations, DAN, ARM. SSR, in print.
[2] KARAPETIAN (N. K.). The Method of Determining the Spectrum with an Account of the Nonperiodicity of Seismic Vibrations. DAN, ARM. SSR, 1962, vol. XXXIV, No 2.
[3] SAVARENSKY (E. F.), KONDORSKAYA (N. V.), BELOTELOV (V. L.). On the Determination of the Energy of Elastic Waves formed by the Earthquake. *Izvestia an USSR,* geophysical series, 1960, No 5.
[4] BELOTOV (V. L.), SAVARENSKY (E. F.), FEOFILAKOV (V. D.). The Determination of Earthquake Energy on the 15th of Nov. 1959. *Izvestia Aknauk,* geophysical series, 1960, No 11.
[5] KHARKEVICH (A. A.). *Spectra and Analysis,* Moscow, 1957.

LOW-VELOCITY SURFACE WAVES GIVING MAXIMUM AMPLITUDES TO SEISMOGRAMS

by TAKASHI KIZAWA

Meteorological Research Institute, Tokyo, Japan

The magnitude and energy of near earthquakes have hitherto been estimated, in most cases, from the maximum amplitudes as seen in the seismograms of those earthquakes, assuming that the maximum amplitudes of near earthquakes are due to the bodily S-waves.

However, the present author has found some examples which seem to indicate that this assumption is not always adequate. It is suggested that there are some kinds of low-velocity surface waves which display maximum amplitudes in some seismograms of near earthquakes that have been observed at certain localities; examples will be shown in the following [22, 29]. We must, therefore, be well aware of this fact in the estimation of magnitude and energy of near earthquakes. Evidence of such waves has been found time and again in a number of earthquake swarms and aftershock groups of shallow origin. It has thus been revealed that such kinds of M-phases are observed very clearly even at very short epicentral distances ranging from some ten or twenty kilometers up to two hundred kilometers. It has also been demonstrated that the velocity of such M-phases varies with locality or wave path, and with the focal depth of the earthquake. The velocities of these waves are low, within a range of 0.2 km/sec to 1.9 km/sec, and therefore these phases form solitary groups with predominant amplitudes considerably later than those of the S-phases. It is not seldom that the amplitudes of these later phases overwhelm those of the S-phases, as is indicated in the seismograms shown here. [see Figs. 2-13] From the well-known theory of dispersion of surface waves [7, 18] it may naturally be presumed that these M-phases belong to certain kinds of Airy phases [8, 10] which are related to the surface waves along the sedimentary layers near the earth's surface in the region concerned.

Since this presumption should not be ignored in all cases, and since such a geological structure may be found in other parts of the world, the appearance of these low-velocity surface waves which give maximum amplitudes to seismograms may also be expected in other countries of the world.

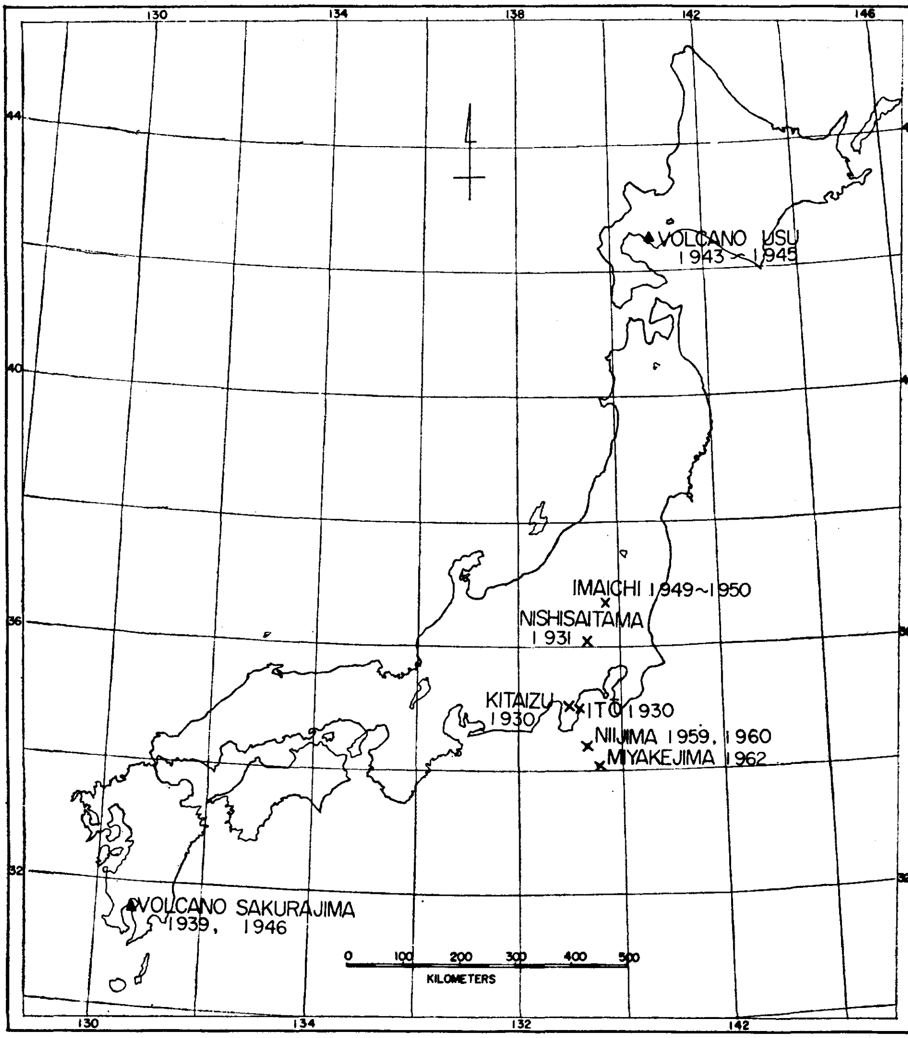

FIG. 1 : Map of Japan, showing distribution of epicenters of earthquake swarms in which M-phases were recognized.

We have already mentioned the necessity of precautions to be taken in estimating the magnitude and energy of near earthquakes. From the practical point of view we cannot overlook the usefulness of these remarkable M-phases in the prompt determination of epicentral region and hypocentral depth of earthquakes, as well as in the studies of crustal structure and other problems. This is because the particular seismogram types characterized by these M-phases are nothing but a manifestation of effects of the previously mentioned factors and the distance between epicentral region and observing station.

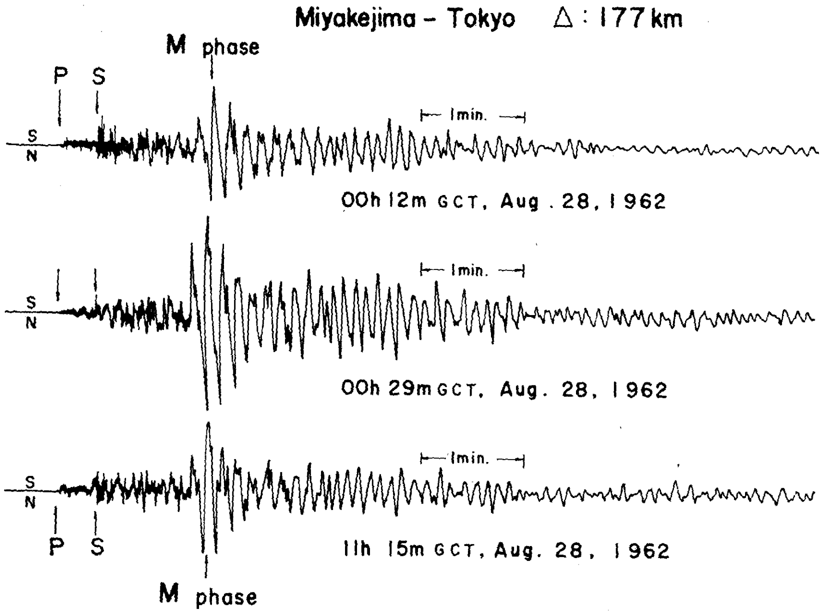

FIG. 2 : Examples of seismograms showing M-phases which appeared in the Miyakejima earthquake swarm (1962) as recorded in Tokyo.

Examination of these M-phases, which consist not only of Rayleigh-type waves but also of Love-type waves (as observed in some places of the Kanto Plain and in the vicinity of the Sakurajima Volcano), will give us a clue to the study of particular crustal structures such as low-velocity layers, etc. Most of the examples shown here seem to be ascribable to the effect of liquid coupling along the submarine paths, but there are some other cases in which no submarine paths are involved. It is thus suggested that the existence of low-velocity sedimentary layers near the surface is also effective in the generation of these low-velocity M-phases. Brief descriptions of the examples will now follow.

APPEARANCE OF LOW-VELOCITY M-PHASES

i) Historically speaking, in the early thirties of this century, MATSUZAWA [19] and FUKUTOMI found conspicuous wave groups of almost the same category as those we have dealt with in the seismograms of the earthquake swarms originating in the south-western part of the Kanto Plain and around the Spa of Itô in 1930 and 1931. The amplitudes of these waves were not always the largest on the seismograms, but they constituted two outstanding wave groups which were propagated with velocities $V_1 = 1.9$ km/sec and $V_2 = 1.1$ km/sec, respectively. They were observed at stations of epicentral distances from 50 to 130 kilometers.

ii) Usu earthquake swarm

Several years ago (1955-1956), the writer found two remarkable wave groups were found in the study of the earthquake swarm which accompanied the volcanic activity of Mt. Usu in 1943-1945, and he classified such waves as were classified 3rd and 4th phases [26, 29]. At the Mori Meteorological Station, 54 km distant from the volcano, these phases were observed in a later portion of the seismograms. The greater part of the wave path from Mt. Usu to the town of Mori runs under the sea, and the velocity of the earlier M-phase was $V_M = 0.6$ km/sec, while that of the later one was $V = 0.2$ km/sec. The dominant periods of these phases were around 2 seconds. The earthquakes of this swarm continued for about two years from 1943 to 1945. More than two thousands earthquakes belonging to this swarm displayed, without exception, these two remarkable wave groups of maximum amplitudes at similar portions of the seismograms as observed at the Mori Meteorological Station. But, a contrasting phenomenon was observed at the Sapporo Meteorological Observatory, 69 km in epicentral distance, where no particular low-velocity M-phases were observed in the seismograms of the same swarm. Such a difference in the seismogram types observed at Mori and Sapporo is very interesting. This difference may be attributable to the difference in geological structures along the paths of seismic waves from Usu to Mori and to Sapporo. A somewhat detailed study of this point has already been reported (*Fig.* 3 à 7).

iii) Sakurajima earthquake swarms

The activity of the Sakurajima Volcano is almost invariably accompanied by a swarm of earthquakes. Such earthquakes have been observed at the Kagoshima Meteorological Station, which is about 10 kilometers from the center of the volcano. In all the seismograms of the earthquakes which took place in 1910, 1939 and 1946, the present writer found two remarkable M-phases similar to those mentioned previously. The velocities, calculated on an assumption that these earthquakes originated at the center of the volcano, turned out to be $V_M = 0.4$ km/sec and $V = 0.2$ km/sec. The wave path from the origin to the observing station crosses the

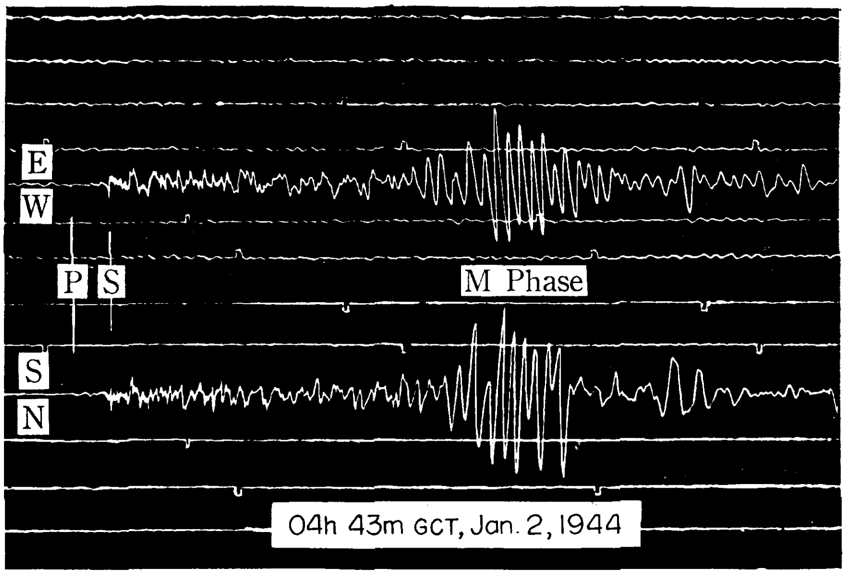

FIG. 3 : Examples of M-phases of the pre-eruption stage as observed Mori station.

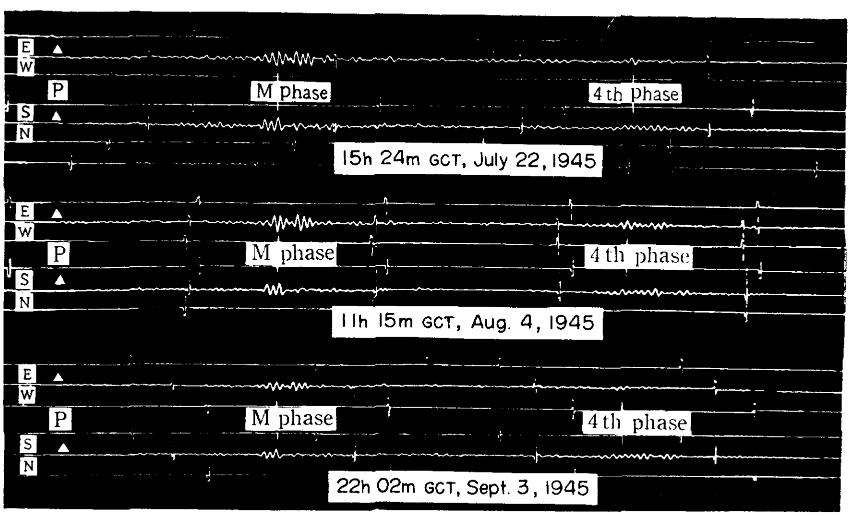

FIG. 4 : Seismograms of Mori showing the post-eruption earthquakes, and the M-phases (3rd phases) and the 4th phases.

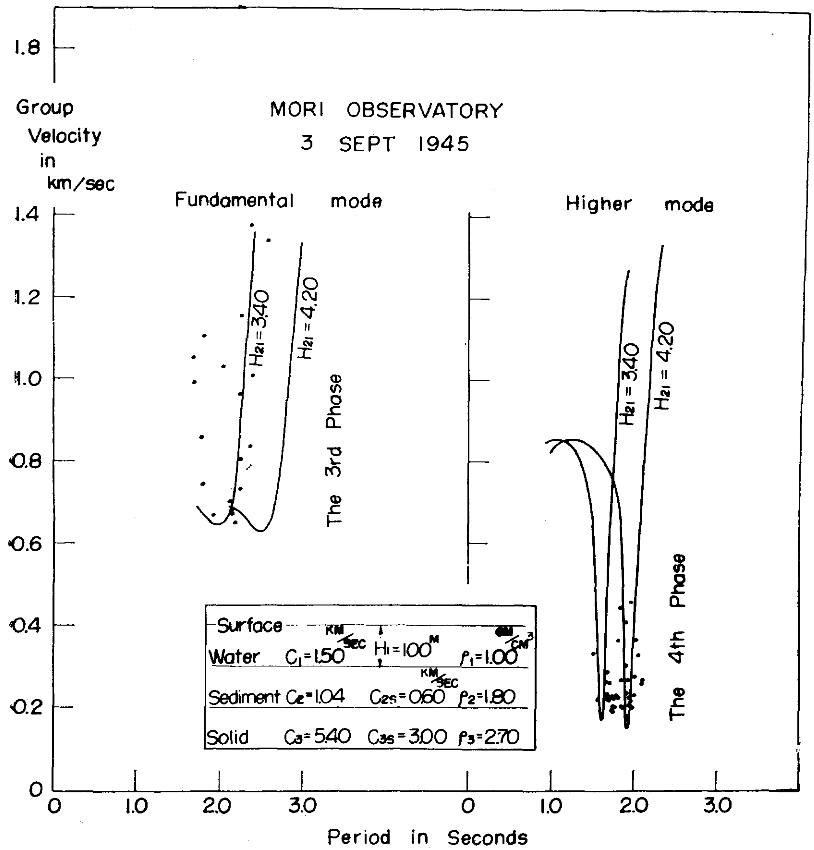

FIG. 5 : Usu-Mori. Agreement of experimental data with theoretical curves. Observed group velocity of M(3rd) and 4th phases compared with the theoretical Rayleigh waves dispersion.

Bay of Kagoshima, and the resemblance of the circumstances to those of the case *ii*) at the Mori Meteorological Station should be particularly noted (*Fig.* 8).

iv) Itô earthquake swarm

Seismograms of the Itô earthquake swarm of 1930, as observed at Tokyo, Yokohama and Tomisaki [29], were also examined by the present writer. Some earthquakes belonging to this swarm were previously studied by MATUZAWA and FUKUTOMI as mentioned already (in case *i*), although the seismograms used in their study were recorded by the seismographs at the Earthquake Research Institute of the University of Tokyo, whereas the data used by the writer are records at the local stations of the Japan Meteorological Agency. Notwithstanding the difference in the type of seismo-

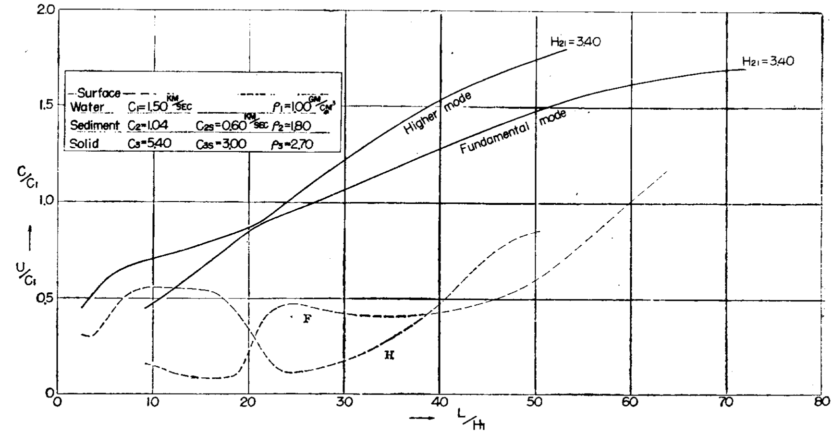

FIG. 6 : The theoretical dispersion curves, explaining very well the M-phase (3rd phase) and 4th phase which were observed in the Usu-Mori path. They indicate that when the velocity of compressional waves of the sedimentary second layer in solid case is smaller than that of the first layer, two remarkable group velocities, splendidly explaining the 3rd and 4th phases, would make their appearance [27, 28].

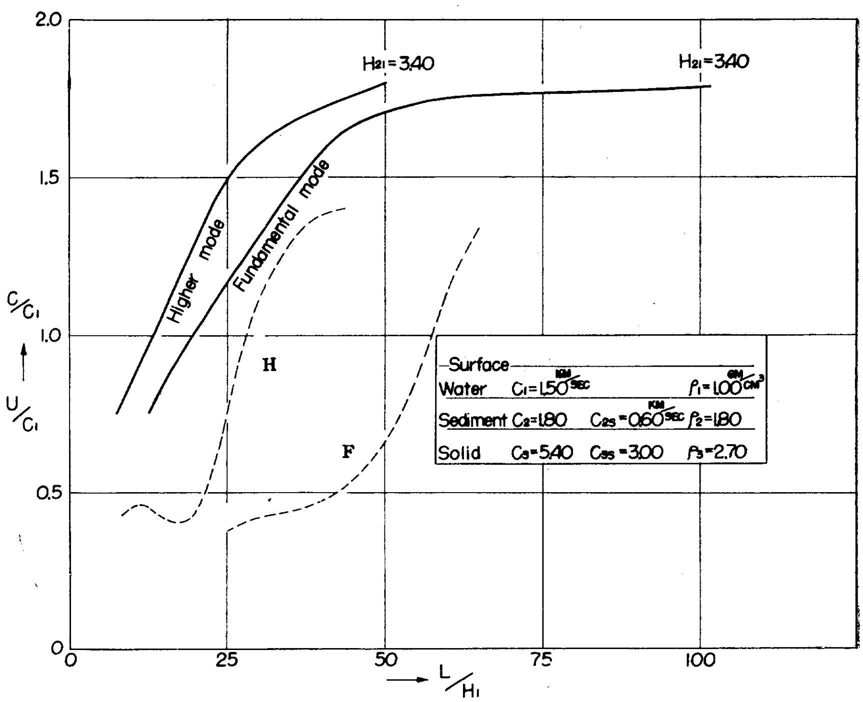

FIG. 7 : When the velocity of compressional waves of the second layer is larger than that of the first, while other constants remain unchanged, the two remarkable velocities as you have seen just now would not appear [27, 28].

graphs, similar characteristic M-phases were observed in all the seismograms of this earthquake swarm which lasted for about six months, observed at the three stations, Tokyo ($\Delta = 97$ km),

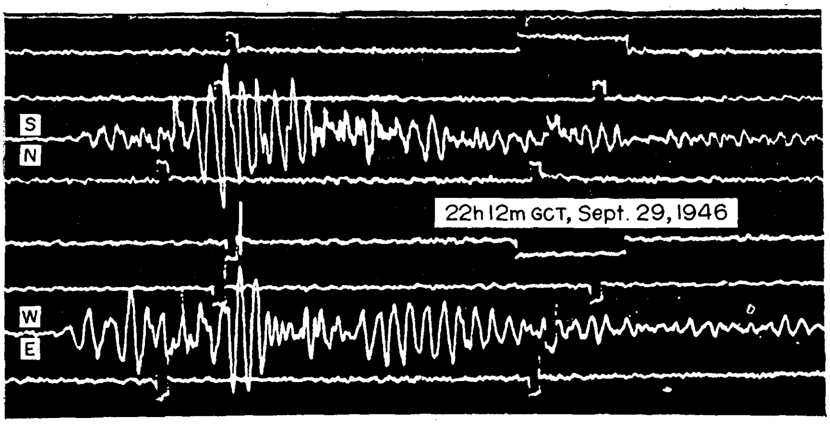

FIG. 8 : Seismograms at Kagoshima ($\Delta = 10$ km).

Yokohama ($\Delta = 69$ km) and Tomisaki ($\Delta = 67$ km). The velocity of propagation of the M-phase was found to be $V_M = 1.1$ km/sec, irrespective of the station's location (*Fig.* 9).

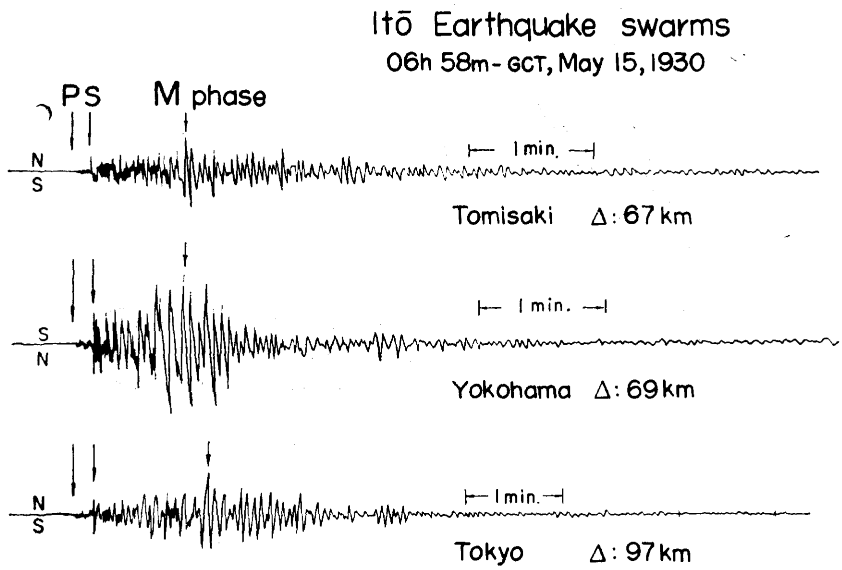

FIG. 9 : Seismograms at Tokyo, Tomisaki and Yokohama, showing M-phases which appeared in the Itô earthquake swarm (1930). These observatories use the Wiechert type seismograph.

v_1) Miyakejima earthquake swarms

v_2) Miyakejima and Niijima earthquake swarms

A wave group exactly similar to that of case *iv*) was seen in each of the seismograms at Tokyo, Yokohama and Tomisaki stations, in the case of the Miyakejima earthquake swarms of 1962. The epicentral distance of these stations being 177 km, 147 km and 94 km respectively. The same was true in the seismograms recorded in Tokyo, in relation to the earthquake swarms occuring near Niijima Island in 1957 and 1960. The velocity of these M-phases was $V_M = 1.1$ km/sec in both Miyakejima and Niijima swarms, and the dominant period of the same phases was about 6 to 7 seconds [*Fig.* 10 (Miyakejima), *Fig.* 11 (Niijima)].

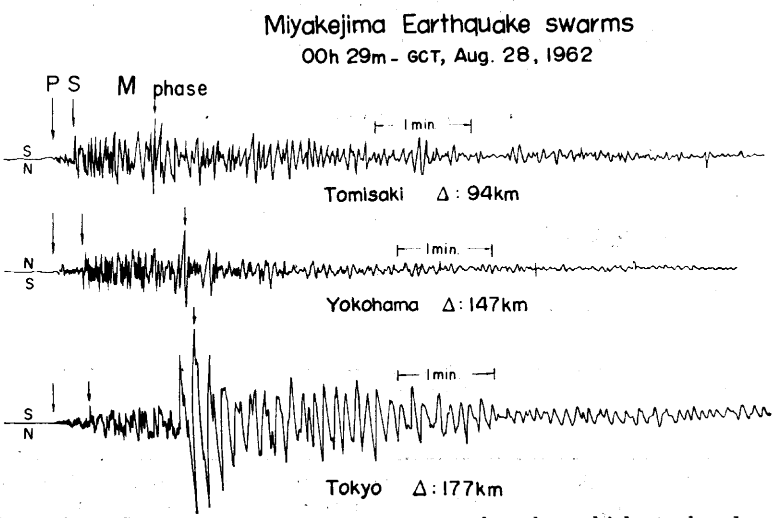

FIG. 10 : Seismograms recording the earthquake which took place on Miyakejima showing occurrence of M-phases. As you see, occurence of the M-phase is very distinct in many places.

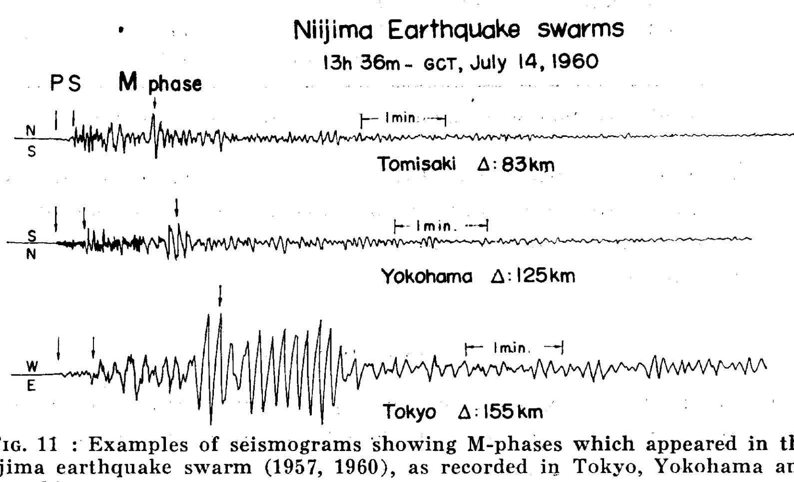

FIG. 11 : Examples of seismograms showing M-phases which appeared in the Niijima earthquake swarm (1957, 1960), as recorded in Tokyo, Yokohama and Tomisaki.

vi) Examples of low-velocity M-phases propagated along the land paths

From the previous examples we perceive that in shallow earthquakes similar characteristic low-velocity M-phases are observed when the wave-paths traverse this particular district, even though the epicentral regions are somewhat different. It is noted also that the greater part of the paths which gave rise to the low-velocity M-phases is covered by sea-water, although this is not an absolutely necessary condition to cause this phenomenon, as was already noted in case *i*). Examples of such low-velocity surface waves, manifesting the largest amplitudes in seismograms in spite of their land paths of propagation, will now be given (*Fig.* 12).

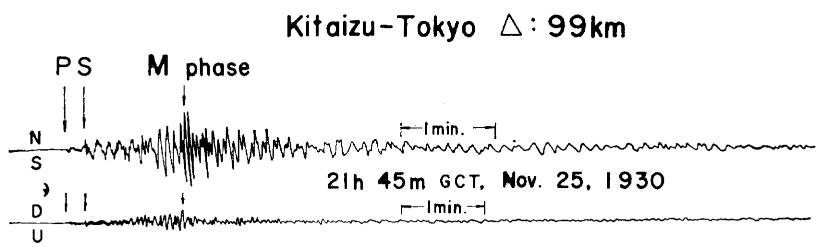

FIG. 12 : Seismogram showing M-phase which appeared in the Kitaizu earthquake swarm (1930) as recorded in Tokyo.

	Earthquake group	Year	Observing station	Epicentral distance	Velocity V_M km/sec
a	Northern Izu	1930	Tokyo	99	1.2
b	Western Saitama	1931	Tokyo	60	1.1
c	Imaichi	1949-50	Tokyo	114	0.5
			Yokohama	142	(1.1*)

* Remarkable surface-wave group whose amplitude was not the largest.

Since Tokyo is situated at the center of the Kanto Plain where diluvial and alluvial formations are prevalent, the effect of these sedimentary layers on the appearence of these particular wave groups cannot be disregarded.

CONCLUDING REMARKS

From the foregoing examples we have realized that even in short epicentral distances, from 10 to 200 kilometers, the largest amplitudes in the seimograms of shallow earthquakes are not always

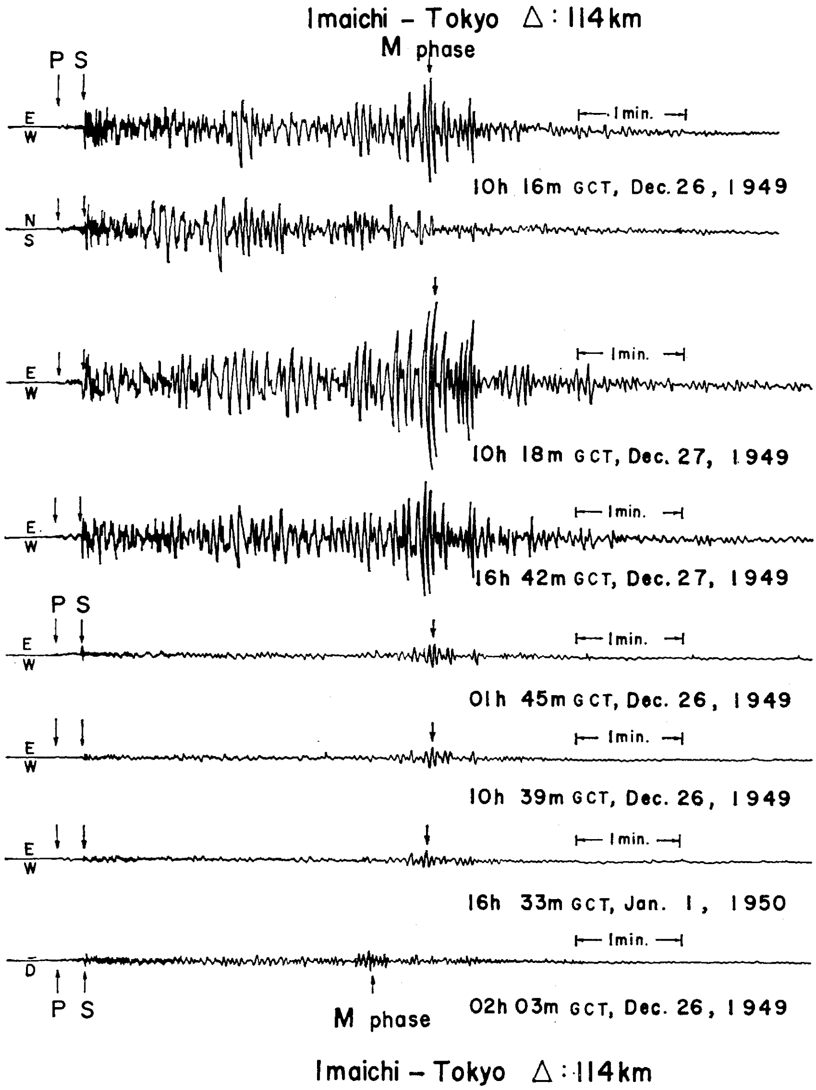

FIG. 13 : Seismogram showing M-phase which appeared in the Imaichi earthquake swarm (1949), as recorded in Tokyo.

Thus, the occurence of M-phases was distinctly observed at the earthquake observatories of Tokyo ($\Delta = 114$ km), Yokohama ($\Delta = 142$ km) and Tomisaki ($\Delta = 200$ km).

On the other hand, it is noticeable that M-phases did not appear in the seismograms of such observatories as Maebashi, Nagano, Nagoya and Shizuoka. To reach these observatories, the seismic waves have to take a mountainous path.

The paths to Tokyo, Yokohama, Tomisaki and Choshi ,in which M-phases were recognized, run through the Kanto Plain, as the figure indicates. It is interesting that the difference in the direction of these paths is related to the difference in the geological condition of the ground. The mountainous region of the Kanto district is composed chiefly of Paleozoic formations and metamorphic rocks, whereas the Kanto Plain is composed of alluvial (Recent) and diluvial (Pleistocene) beds covering the Tertiary basement.

Particularly, the Imaichi-Tokyo, -Yokohama and -Tomisaki paths lie in the Kanto tectonic basin where the Tertiary beds are downwarped deeply into the basin. This area was once below the sea.

due to S-waves, and in some cases they must be assigned to the surface wave groups whose velocities are as low as 0.2 to 1.2 km/sec or so. We must, therefore, take due precaution in the calculation of magnitude and energy of near earthquakes if we have to deal with M-phases of the present category.

Although it is not yet the time for a full explanation of the waves we have been concerned with, we have found that the so-called low-velocity sedimentary layer subjacent to the sea-water plays an important role in the generation of these waves observed at Mori in case ii). Thus, we may possibly assign similar conditions to the cases i) to v) in which submarine wave paths are involved. Such M-phases could be considered as surface waves due to the so-called liquid coupling.

However, we have also recognized that similar low-velocity M-phases are present in the earthquake motions propagated through land paths across the Kanto Plain where diluvial and alluvial formations prevail. Whether or not the existence of a low-velocity layer is a necessary condition for the occurence of such M-phases is an important question (*Fig.* 13).

It is, therefore, necessary to study this question theoretically from various angles. It is also necessary to collect, accumulate and assess the data related to the appearance of the M-phase as well as to make a detailed analysis of the materials already obtained.

At present the writer can only point out the new evidence of these interesting M-phases, and its important bearing on other problems in this field of science. The writer ardently hopes that the study of these waves, through collaboration of seismologists throughout the world, will lead to a rapid advance in knowledge and will give important clues to solve many problems of seismology and geology.

Acknowledgements. — On concluding this report, my heartiest gratitude is expressed to Dr. Hiroshi Kawasumi, Professor of the University of Tokyo and Director of the Earthquake Research Institute, for his constant guidance and valuable advice. My thanks are also extend to Misses E. Minemoto and R. Fusejima for their kind co-operation.

REFERENCES

Magnitude

[1] RICHTER (C. F.). An Instrumental Magnitude Scale, B.S.S.A., *25* (1935), 1-32.

[2] KAWASUMI (H.). Intensity and Magnitude of Shallow Earthquakes., Pub. Bur. Centr. Seism. Int., Serie A. Travaux Scientifiques, *19* (1956), 99-114.

Energy

[3] KAWASUMI (H.). Study on the Propagation of Seismic Waves (2nd Paper). Amplitude of Seismic Waves with Structure of the Earth's Crust and Mechanism of their Origin (continued), B.E.R.I., *12* (1934), 660-705.

[4] SAGISAKA (K.). On the Energy of Earthquake, Geophy. Mag., *26* (1954), 53-82.

Magnitude and Energy

[5] GUTENBERG (B.) and RICHTER (C. F.). Earthquake Magnitude, Intensity, Energy and Acceleration (2nd Paper), B.S.S.A., *46* (1956), 105-145.

[6] TSUBOI (C.). On the Magnitude of Earthquakes, Jour. Seism. Soc. Japan, II *10* (1957), 6-23.

Airy phase and Rayleigh waves of comparatively short periods

[7] STONELEY (R.). « The Effect of the Ocean on Rayleigh Waves », *Mon. Not. Roy. Astron. Soc., Geophys. Suppl., 1* (1926), 349.

[8] PEKERIS (C. L.). « Theory of Propagation of Explosive Sound in Shallow Water », *Geol. Soc. Amer., Memoir, 27* (1948), 1-116.

[9] PRESS (F.) and EWING (M.). « Low-speed Layer in Water-covered Areas », *Geophysics, 13* (1948), 404.

[10] PRESS (F.), EWING (M.) and TOLSTOY (I.). « The Airy Phase of Shallow-focus Submarine Earthquakes », *Bull. Seis. Soc. Amer., 40* (1950), 111-148.

[11] PRESS (F.) and EWING (M.). « Propagation of Explosive Sound in a Liquid Layer Overlying a Semi-infinite Elastic Solid », *Geophysics, 15* (1950), 426.

[12] EWING (M.) and PRESS (F.). « Crustal Structure and Surface Wave Dispersion », *Bull. Seism. Soc. Amer., 40* (1950), 271.

[13] JARDETZKY (W. S.) and PRESS (F.). « Crustal Structure and Surface Wave Dispersion, Part III : Theoretical Dispersion Curves for Suboceanic Rayleigh Waves », *Bull. Seism. Soc. Amer., 43* (1953), 137.

[14] TOLSTOY (I.). « Dispersive Properties of a Fluid Layer Overlying a Semi-infinite Elastic Solid », *Bull. Seism. Soc. Amer., 44* (1954), 493.

[15] PEKERIS (C. L.) and LONGMAN (I. M.) « Ray Theory Solution of the Problem of Propagation of Explosive Sound in a Layered Liquid », *Jour. Acoust. Soc. Amer., 30* (1958), 323-328.

[16] SATÔ (Y.) and YAMAGUCHI (R.). Velocity Equation of the Love Waves Propagated in Multilatered Media, *Jour. Seism. Soc. Japan, 21* (1959), 61-67.

[17] PEKERIS (C. L.), LONGMAN (I. M.) and LIPSON (H.). Application of Ray Theory to the Problem of Long-range Propagation of Explosive Sound in a Layered Liquid, *B.S.S.A., 49* (1959), 247-250.

[18] EVISON (F. F.), INGHAM (C. E.), ORR (R. H.) and LE FORT (J. H.). « Thickness of the Earth's Crust in Antarctica and the Surrounding Oceans », *Geophys. Jour., 3* (1960), 289.

[19] MATUZAWA (T.) und FUKUTOMI (T.). Zwei merkwürdige Wellengruppen bei einigen Erdbeben in Kwantô und die dritte Mitteilung über den vorlaufenden Teil der Erdbebenbewegungen, B.E.R.I., *10* (1932), 499-516.
[20] KIZAWA (T.). Investigation of the Great Earthquake in Chile of January 25, 1939, Quart. Jour. Seism., *11* (1941), 435-468.
[21] KIZAWA (T.). Volcanic Tremor and Tilting of Ground, Quart. Jour. Seism., *15* (1951), 18-34.
[22] KIZAWA (T.). Geophysical Phenomena in Relation to Volcanic Activity (I), Jour. Met. Res., *3* (1951), 249-260.
[23] KIZAWA (T.). Geophysical Phenomena in Relation to Volcanic Activity (II), Jour. Met. Res., *3* (1951), 277-291.
[24] KIZAWA (T.). Geophysical Phenomena Accompanied by Volcanic Activities, Geophys. Mag., *23* (1952), 389-397.
[25] KIZAWA (T.). A Study of Earthquakes in Relation to Volcanic Activity (I), Pap. Met. Geophys., *8* (1957), 150-169.
[26] KIZAWA (T.). A Study of Earthquakes in Relation to Volcanic Activity (II), Pap. Met. Geophys., *9* (1959), 204-239.
[27] KIZAWA (T.). Some New Phases Observed in a Study of Earthquake Swarms Relating to Volcanic Activity (I), Geophys. Mag., *29* (1960), 477-498.
[28] KIZAWA (T.) and YAMAGUCHI (R.). Some New Phases Observed in a Study of Earthquake Swarms Relating to Volcanic Activity (II), Geophys. Mag., *30* (1960), 93-129.
[29] KIZAWA (T.). A Study of Earthquakes in Relation to Volcanic Activity (III), Pap. Met. Geophys., *11* (1960), 30-96.

A SHORT-PERIOD SURFACE WAVES DISPERSION IN THE DIFFERENT REGIONS OF EUROPE-ASIA CONTINENT

by V. M. ARHANGELSKAYA

During the last time the interest for the surface waves study have been considerably increased. Besides a well studied Love and Rayleigh's waves of the main tone on the far earthquakes seismograms it is possible often to mark short-period surface waves, previous to the waves of the main tone [1]. So at near eartquakes surface waves are marked, previous to the main Rayleigh waves [2].

Let us consider some results of these waves experimental investigation, which had been obtained by us during the last time.

The investigations of the waves for far earthquakes with epicentral distances which are equal to 2000 km and more showed, that at continental ways of distribution 5 individual waves groups are observed, which have enough lenticular arrivals on all the three displacement components. Every group has a definite distribution velocity and the range of vibrations periods. The first group (Rx_1) has the most velocity $\sim$ 4,0 km/sec and the fifth group (Rx_5) has the least velocity $\sim$ 3,3 km/sec.

Fig. 1 serves as the example of short-period waves record. For each of these 5 waves groups, on the base of the observations

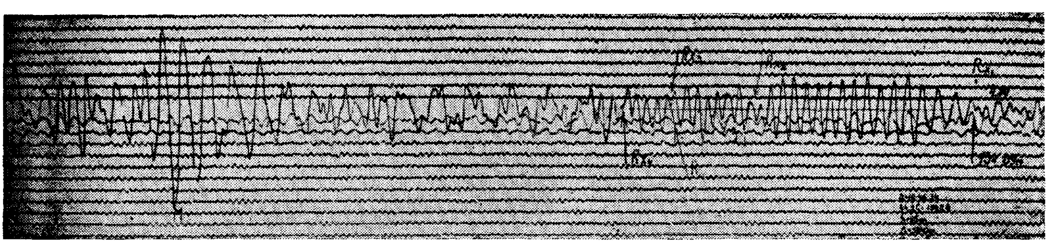

FIG. 1. — The earthquake 16.XII.1939 with the record of waves Rx_1, Rx_2, Rx_3, Rx_4. " Sverdlovsk " station $\Delta = 5840$ km.

great number (more than 200 earthquakes have been studied) the experimental travel-time curves of these waves apparent arrivals have been constructed.

The investigation of the particles movement character at these waves passing proves that these waves, named by us as Rxi are the surface ones, of Rayleigh's type. The first group waves are the first obertone of Rayleigh's wave, the wave M_2. It has a normal dispersion.

The comparison of earthquakes records with different focus depth (the foci of studied earthquakes had a depth from 0 to 130 km) showed, that the relation of displacements in all 5 waves groups to the main tone displacement is increasing with focus depth. This dependence is shown on fig. 2.

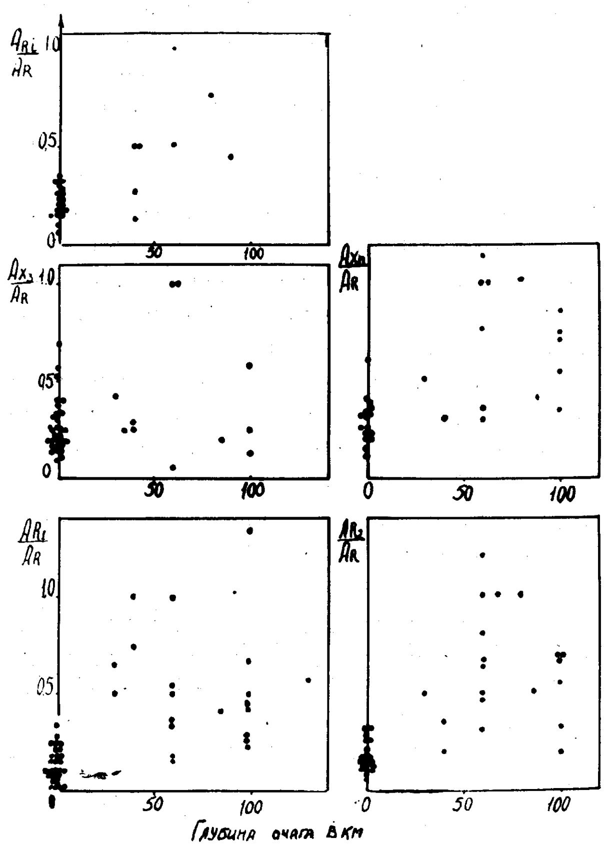

FIG. 2. — The graphs of maximum displacements relation dependence in each group of waves (A_{Rxi}) to a maximum displacement value in Rayleigh wave (A_R) from earthquake focus.

Such a behaviour at least for the first obertone, is quite regular one. For example, for 1st obertone of Love's waves, of T = 10 sec*, period, at layer thickness which is 30 km, the displacements am-

---

* V. I. KEILIS-BOROK, A. L. LEVSHIN'S and oth. verbal communication on the conference of IGY in February of 1963.

plitude variation with depth is : at H = 60 km, A = 1/3 A_0 at H = 100 km — 1/10 A_0. For the main tone at T = 14 the amplitude of displacement is at H = 60 km, A = 1/30 A_0 at H = 100 km, A = 1/100 A_0, where H — is the focus depth in km, but A_0 — displacements amplitude at H = 0 km. On the surface A_0 of obertone is 3 times less than A_0 of the main tone.

For Rayleigh's waves this dependence becomes apparent more intensively.

Noting such a picture and for the other groups of waves (see *fig.* 2) it is possible to suppose, that such a behaviour to some extent may serve as the base for the conclusion, that subsequent groups are the high obertones.

For dispersional properties study of the wave Rx_1 (M_2) with the aim of their use for the crustal study, the records of the stations "Sverdlovsk" and the Middle Asia stations of earthquakes, which had taken place in the regions of : Kamchatka, Japan, China, the Middle Asia and the Persian gulf have been investigated. All the sections of these waves distribution are passing only along the Asia continent.

The dispersion, observed for each section is compared with theoretical curves, which are : 1) Haskell's [3], calculated for two-layered model of the structure :

$$H = 30 \text{ and } 35 \text{ km};\ H_2 = \infty;\ v_{S1} = 3{,}43;\ v_{S2} = 4{,}70 \text{ km/sec} :$$
$$\rho_1 = 2{,}7,\ \rho_2 = 3{,}0 \text{ g/cm}^3;$$

2) Dorman's [4] for three cases of the structure : 8012, 8073

and 8089 at $v_{p1} = 5{,}95$; $v_{p2} = 6{,}4$; $v_{p3} = 7{,}9$ km/sec; $v_{S1} = 3{,}44$; $v_{S2} = 3{,}70$; $v_{S3} = 4{,}56$ km/sec and H = 35, 40, 45, 50 km and

3) Bolt and Butcher's [5] for 11 models of two-layered crustal structure.

The group velocities values are given on fig. 3. They have been found by us for M_2 in dependence on the period for earthquakes : Kamchatka, the Kuril islands and the North Japan (*fig.* 3 *a, b, c*) and fort the earthquakes of Alpine Thibet and the Himalayas (*fig.* 3 *d*).

As it is seen from fig. 3, the dispersion of the waves M_2 founded for the earthquakes groups 1, 2, 3 is in a good correspondence with each other and coincides enough well with the theoretical curves 1 (the case 8089, P (the case 8012) [3], with the curves of the case A, B, C, [4] at the layer thickness H = 35-40 km (of the structure $v_{p1} = 5{,}8$; $v_{p2} = 7{,}9$ km/sec; $v_{s1} = 3{,}44$; $v_{s2} = 4{,}7$ km/sec;

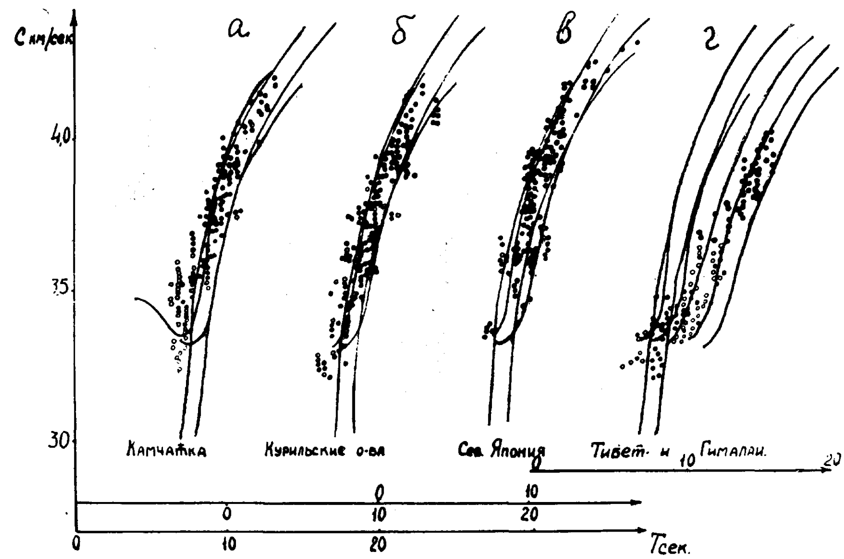

FIG. 3. — The group velocities dependence on the wave period for the earthquakes 1, 2, 3 groups (Kamchatka, the Kuril islands, the North Japan regions) and 4 groups (the regions of Mountainous Thibet and the spurs of the Himalaya mountain basin).
1 : M_2 waves; — 2 : Rx_2, Rx_3, Rx_4, Rx_5 waves.

$\frac{\rho_1}{\rho_2} = 1{,}236$; H = 35-40 km) and with Haskel's curves 2 at H = 30-35 km. Such a coincidence makes it possible to value quite confidently the average thickness of the earth crust on the directions as 35 km ± 5 km, that is proved with the data, having been obtained by the main tone waves dispersion [6].

The dispersional data comparison for the earthquakes of the group 4 (*fig.* 3 *d*) with theoretical curves shows considerably the great average thickness of the earth crust on this direction. The waves distributing from the earthquakes of this group to Sverdlovsk, are passing from the South to the North, through the thick mountain systems of the Himalayas, Thibeth, Tien-Shan. The general average thickness of the earth crust on this direction is already 50 km ± 5 km.

The obtained values of the earth crust thickness are in quite good agreement with the deep seismic sounding data, having been obtained for some regions of the Middle Asia [7, 8, 9, 10].

Let us consider now the results of surface wave investigation at near earthquakes.

Still in 1953 [2] on the near earthquakes records we had found a new long-period wave, arriving just (after 1,5-2 sec) after the transverse wave P arrival. The wave was marked on the records of many seismic stations, equiped with apparatus of D. P. Kirnos. The geological conditions of the sections of this wave passing had been different ones. It is noted, that this wave is much more intensive than P waves, but less intensive, than usual surface waves. The movement of the earth surface particles at these waves passing is in a vertical plane, orientated to epicenter, the particles move along elliptical orbits.

On the base of the properties revealed the supposition have been made, that this wave is the surface one of Rayleigh's type, connected with the earth crust upper layers. The possibility of its use for azimuth determination to the epicenter of earthquake have been revealed.

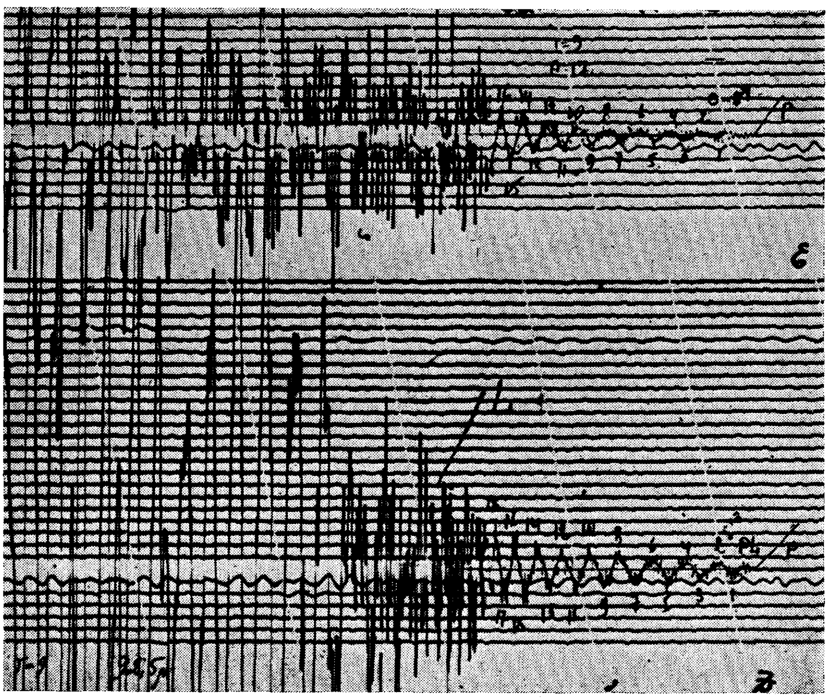

FIG. 4. — The earthquake 14.XI.56, with the record of PL waves and usual Rayleigh waves. The Ashkabad station.
$\Delta = 1120$ km; $\varphi = 37°0$ C; $\lambda = 71°0$ B; H $= 80$ km.

During the last time this wave records also of 40 earthquakes, registered by the Middle Asia stations have been investigated.

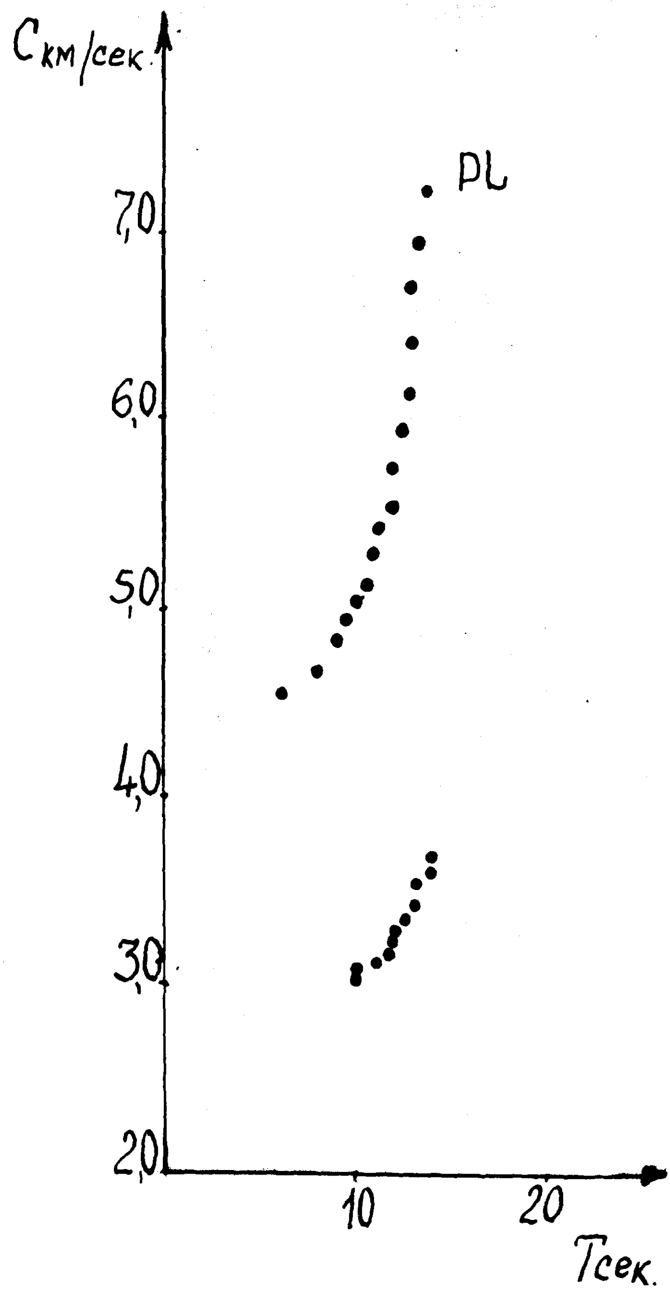

FIG. 5. — Group velocities dependence on a period in PL and R waves for earthquake on 14.XI.56.

Epicentral distances varied from 90 to 2290 km. It is ascertained, that this wave arrives just after P wave arrival and vibrations continue till the moment of transverse waves and Rayleigh's usual surface waves appearance. It is wonderfully, that this wave, alike surface waves shows a normal dispersion, the same ranges of periods variation in both waves are marked. We consider, that it is the wave PL [11].

The next seismogram (*fig.* 4) serves as obvious example of legible (accurate) record of this wave PL with obviously expressed dispersion. It is the record of the Ashkhabad station, the earthquake 14.XI.56 in Hindukush ($\varphi = 37°0$; $\lambda = 71°0$ B; $\Delta = 1120$; H = 80 km).

On the next graph (*fig.* 5) the data about the dispersion observed for this earthquake in the wave PL and the usual surface wave are presented. The comparison shows almost the same ranges of periods variations.

Almost for all the studied earthquakes by the wave PL records the azimuth to epicenter is determined. The azimuth is determined quite synonimously and confidently, while it is often impossible to mark the arrivals of the wave P.

The revealed properties of this wave, alike in the record character of the waves both types, the presence of the observed dispersion prove the conclusion, which have been made by us before, that this wave is connected with the same media (guide), in which Rayleigh usual surface wave is propagating.

LITERATURE

[1] ARHANGELSKAYA (V. M.). « Rayleigh short-period surface seismic waves investigation. » Izv. AN SSSR, ser. geophys., 1961, n° 8.

[2] ARHANGELSKAYA (V. M.). « About the use of a new type wave in azimuth determination of near earthquake epicenter. » Izv. AN Turkmenskoi SSR, 1954 d, n° 5.

[3] HASKELL (N. A.). « The dispersion of surface waves on multilayered media. » Bull. Seism. Soc. Amer., 43, n° 1, 1953.

[4] OLIVER (J.), DORMAN (J.), SUTTON (C.). « The second shear mode of continental Rayleigh waves ». Bull. Seism. Soc., vol. 49, n° 4, 1959.

[5] BOLT (B. A.), BUTCHER (J. C.). « Rayleigh wave dispersion for a single layer on an elastic half space. » Australian Journal of Physics, vol. 13, n° 3, 1960.

[6] SHECHKOV (B. N.). « The crustal structure in Eurasia according to the surface waves dispersion. » Izv. AN SSSR, ser. geophys., n° 5, 1961.

[7] KOSMINSKAYA (I. P.), MIHOTA (G. G.), SHUMINA (Ju. V.). « The crustal structure in Pamir-Altai zone according to the deep seismic sounding data. » Izv. AN SSSR, ser. geophys., n° 10, 1958.

[8] GAMBURZEV (G. A.), VEIZMAN (L. S.), DAVIDOVA (N. I.), SHUMINA (Ju. V.). « The deep seismic sounding of the earth crust on the North Tien-Shan. » Bull. of the Soviet on seismology, n° 3, 1957.
[9] GAMBURZEV (G. A.), VEIZMAN (L. S.). The crustal structure peculiarity in the North Tien-Shan region according to GSS and their comparison with geology, seismology and gravimetry data. » Bull. of the Soviet on seismology, n° 3, 1957.
[10] GODIN (Ju. N.), VOLVOVSKY (B. S.), VOLVOVSKY (I. S.). « The earth crust seismic investigations in the region of intermontane Fergana basin. DAN SSSR, vol. 133, n° 6, 1960.
[11] OLIVER (J.), MAJOR (M.). « Leaking modes and the PZ phase. » Bull. Seism. Soc. Amer., vol. 50, n° 2, 1960.

SULLA CANALIZZAZIONE DELL'ENERGIA SISMICA

di PIETRO CALOI

1. — Nel 1953, per la prima volta, si parlò di onde canalizzate; e fu nell'annuncio da me dato all'Accademia dei Lincei dell'esistenza di onde longitudinali e trasversali guidate dall'astenosfera (1) : onde da me indicate con P_A ed S_A e per le quali Gutenberg — che subito ne confermò l'esistenza e l'interpretazione — propose i simboli P_a e S_a, cambiando da maiuscola in minuscola la lettera *a*, iniziale di « astenosfera ».

E' noto che, nell'interpretazione mia e di Gutenberg, la condizione fisica atta a consentire la propagazione di tali onde é costituita dall'esistenza di una vasta zona a flessione di velocità (« low velocity layer ») al di sotto della crosta terrestre, alla quale da molti é stato dato il nome di « astenosfera ». Di tale zona Gutenberg fece oggetto dei suoi studi in diverse epoche della sua laboriosissima vita, a partire dal 1926. L'ultimo precedette di poco la sua morte (avvenuta, com'é noto, il 5.I.1960). In esso (2), a pag. 351, vengono riportati i valori delle velocità delle onde longitudinali e trasversali — di 10 in 10 km — per profondità crescenti da 40 a 400 km.

Secondo Gutenberg, il minimo di velocità per le onde longitudinali (7,8 km-sec; altre volte aveva indicato 7,85-7,9 km/sec), dovrebbe riscontrarsi ad una profondità di 80-100 km, mentre il minimo di velocità per le onde trasversali (4,40 km/sec) si avrebbe alla profondità di 150 km ca.

Di quest'ordine quindi (7,9; 4,4 km/sec) dovranno risultare le velocità *reali* delle onde P_a, S_a rispettivamente; e tali, infatti, furono i valori medi da me trovati per la velocità di queste onde nel primo lavoro sull'argomento (1).

Senonchè, successivamente, furono calcolati, da quanti si occuparono di queste onde, valori più elevati per le loro rispettive velocità; a cominciare da Ewing e Press, che, indipendentemente da Caloi, ebbero ad interessarsi delle stesse onde nel 1954.

Naturalmente, non starò a riportare i risultati ottenuti dai diversi ricercatori. Mi limiterò ad uno dei più accurati di tali studi, quello di *Magnitsky e Khorosheva* (3), concernente gli esempi di onde P_a ed S_a tratti dallo studio di 9 terremoti, registrati da stazioni sismiche russe, per distanze epicentrali comprese fra 22° e 150°. Ai due studiosi russi, le dromocrone per le onde P_a ed S_a risultarono rette di equazioni

$$t^m = 0{,}9558 + 0{,}2205\ \Delta^\circ \qquad P_a$$
$$t^m = 0{,}3780 + 0{,}4180\ \Delta^\circ \qquad S_a$$

Da queste si traggono, per le P_a ed S_a rispettivamente, le velocità 8,3 e 4,47 km/sec.

Del resto, è questo il valore medio ottenuto per la velocità di tali onde, anche nello studio di registrazioni relative ad un singolo terremoto. Esisterebbe quindi una sensibile differenza fra i valori ottenuti da Gutenberg — con metodi relativi alla propagazione delle onde spaziali — per i minimi di velocità nell'astenosfera, e quelli forniti dallo studio delle onde canalizzate.

Ma le velocità tratte direttamente dalle curve dei tempi d'arrivo delle onde P_a ed S_a sono davvero le velocità *reali*? E' facile provare che esse sono, in realtà, velocità apparenti. Indicando infatti con r_a il raggio dell'astenosfera (nella sua parte caratterizzata dal minimo di velocità) e con v_a la velocità reale di propagazione sulla circonferanza di tale raggio, se t sono i tempi ottenuti in superficie per la propagazione delle onde longitudinali (o trasversali) guidate dall' astenosfera (tempi forniti dalle relative dromocrone), si ottiene [4] — essendo Δ la distanza epicentrale in arco —

$$\frac{\partial t}{\partial \Delta} = \frac{r_a}{r_o} \frac{1}{v_a},$$

dove r_o è il raggio medio della Terra. La velocità data dalle dromocrone (rette) è

$$V_a = \frac{d\Delta}{dt},$$

ne segue

$$v_a = \frac{r_a}{r_v} Va \qquad (1)$$

Le dromocrone danno V_a (velocità apparente); noto tale valore, la [1] permette di ottenere la velocità reale v_a.

Ebbene, applicando la [1] ai valori delle velocità — velocità V_a — ottenute de Magnitsky e Khorosheva, si ottiene per il minimo delle velocità delle onde canalizzate longitudinali alla profondità di 100 km

$$v_a(P_a) = 8{,}17 \text{ km/sec};$$

per il minimo delle stesse velocità a 150 km di profondità

$$v_a(P_a) = 8{,}1 \text{ km/sec}.$$

Calcolando il vero valore della velocità delle onde canalizzate trasversali alla profondità di 150 km, si ottiene — sulla base della velocità apparente, ottenuta dai due ricercatori russi —

$$v_a(S_a) = 4{,}365 \text{ km/sec.}$$

La velocità delle P_a data ultimamente da Gutenberg è leggermente inferiore a quella sopra riportata. Va però notato che, in precedenti lavori, Gutenberg assegna al minimo di velocità per le onde longitudinali nell'astenosfera un valore medio di 7,9 km/sec. Va ancora osservato che — in corrispondenza delle profondità riportate — I. Lehmann [5] calcola per la velocità delle onde longitudinali il valore 8,12 km/sec. L'accordo, quindi, non potrebbe essere migliore. Per le S_a poi, possiamo parlare di coincidenza.

Applichiamo la [1] ad un altro caso. Il terremoto dell'Egitto del 12.IX.1955, avvenuto a 32°24′25″ N, 29°52′40″E, ad una profondità di 25 km ca. (secondo i dati, non ancora pubblicati, ottenuti da L. Marcelli), ha fornito nette registrazioni di onde P_a, S_a. Le velocità apparenti, dedotte dalle dromocrone, portarono ai valori $V_a(P_a) = 8{,}08$ km/sec, $V_a(S_a) = 4{,}54$ km/sec. L'applicazione della [1] dà, per i valori reali,

alla profondità di 100 km	$v_a(P_a) = 7{,}95$ km/sec
— — — 150 km	$v_a(P_a) = 7{,}90$
— — — —	$v_a(S_a) = 4{,}43.$

In conclusione, la [1] permette di ottenere la *reale* velocità di propagazione delle onde canalizzate P_a, S_a, che — nei casi considerati — coincide con i valori minimi delle velocità di propagazione delle onde longitudinali e trasversali, ottenuti con metodi diretti (per le stesse profondità) da Gutenberg e dalla Lehmann.

In ciò si deve vedere una ulteriore testimonianza sulla reale esistenza delle onde canalizzate P_a, S_a e sull'esattezza del meccanismo di propogazione di tali onde, da me proposto — per la prima volta — nel 1953.

2. — A mio avviso, non si è data ancora tutta l'attenzione che merita al fenomeno della canalizzazione o guida dell'energia sismica. Tale fenomeno giuoca un ruolo di primaria importanza nell'acquisizione delle conoscenze sulle caratteristiche fisico-chimiche del mantello superiore, le quali potranno essere raggiunte solo dopo uno studio accurato di esso, che assume proporzioni ben più estese di quanto finora non si è portati a credere. Questa, ad ogni modo, è la mia convinzione.

A parità di altre condizioni, la canalizzazione interessa essenzialmente le stratificazioni della crosta terreste o l'astenosfera, a seconda che il terremoto ha origine nella crosta o a profondità dell'ordine di qualche centinaio di km. Nel caso di terremoti a profondità intermedia, di sufficiente intensità, tutta la parte superiore del mantello, dall'astenosfera alle stratificazioni superficiali delle crosta, diventa sede di canalizzazione.

Valgano gli esempi che seguono.

E' già stato provato da Ewing, Press, Bath, Gutenberg, ... che le stratificazioni superficiali della crosta terrestre conducono onde trasversali (L_g, L_R, ...), sebbene il loro meccanismo di propagazione sia variamente interpretato (riflessioni multiple o onde superficiali di nodalità elevata secondo Ewing, Press, Oliver, ...; canalizzazione in zone a flessione di velocità secondo Gutenberg, Bath, ...). Questi tipi d'onde, di periodo piuttosto breve, non sembrano propagarsi a grandi distanze. In questa breve esposizione mi riferirò, quasi esclusivamente, ad onde aventi periodo alquanto elevato (da 10 sec ca. in su).

Quello che quì mi preme di documentare è che tale fenomeno non si limita all'astenosfera. Vedasi l'esempio fornito dalle registrazioni, provocate in sismografi con periodo medio (p. es. i Galitzin I.N.G. di Roma), dal terremoto della dorsale sommersa dell'Oceano Atlantico del 24.IV.1947 (*fig.* 1). Da esso appare chiaro che, oltre che dalle P_a, l'onda S è preceduta da altre fasi, che non possono essere attribuite a riflessioni multiple, bensì a parte dell'energia sismica catturata e propagata dai canali della crosta terrestre.

Nel caso specifico, poichè il terremoto è di origine atlantica, tale canalizzazione, inizialmente limitata all'astenosfera, è da ritenere abbia successivamente interessato la zona dello zoccolo continentale, per estendersi quindi alle tre stratificazioni continentali.

Ma dove il fenomeno di canalizzazione assume proporzioni rilevanti è per terremoti originanti verso i 100 km di profondità. Una testimonianza di interesse eccezionale è fornita, a questo riguardo, dal terremoto del 25.VII.1960. Vedasi il sismogramma riprodotto nella fig. 2; esso è stato registrato da un pendolo a lungo periodo (90 sec ca.), funzionante — ancora in fase sperimentale — presso la nuova stazione sismica de L'Aquila. Il terremoto in questione — cui corrispondono i seguenti dati caratteristici : $\varphi = 54°$ N, $\lambda = 159°$ E, H = 11.12.00, h = 100 km ca., M = 7 (Pasadena, Roma) — ha avuto una profondità di circa 100 km : si noti il lungo seguito, senza soluzione di continuità, di onde canalizzate dall'astenosfera e dalle stratificazioni della crosta terrestre, sia longitudinali che trasversali. Il sismogramma può essere diviso in quattro parti distinte : onde longitudinali e spaziali, dirette e riflesse, a breve periodo (1ª) ; onde

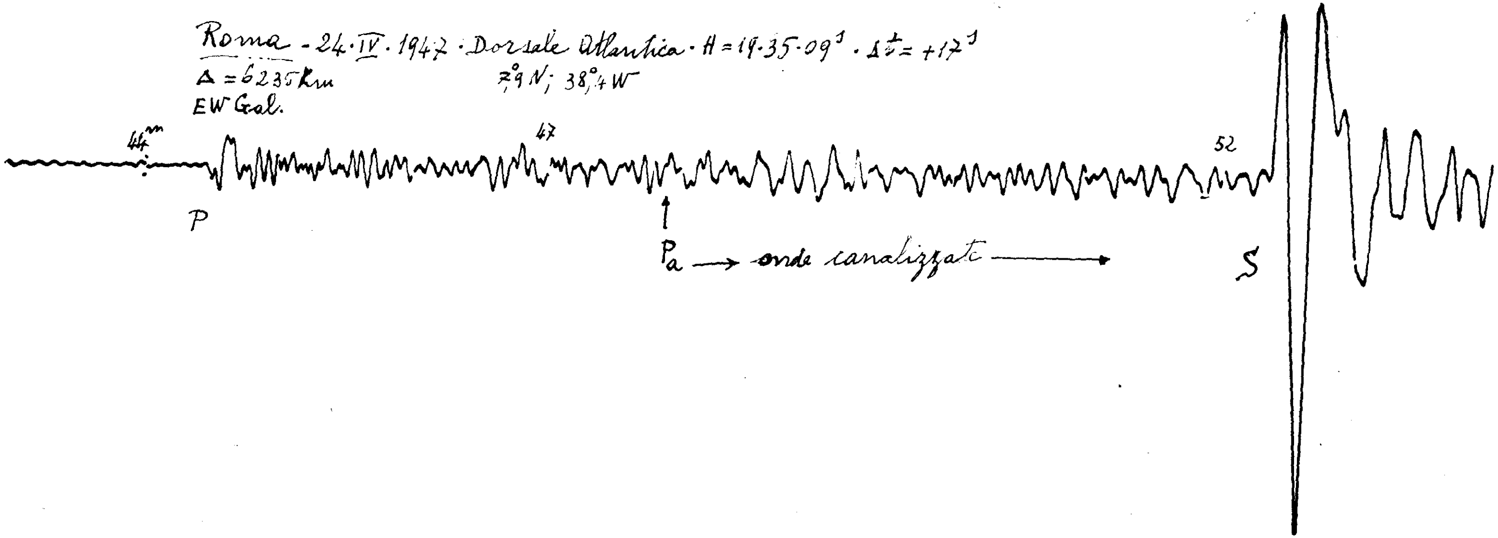

FIG. 1. — Onde canalizzate su tragitto misto, atlantico-continentale.

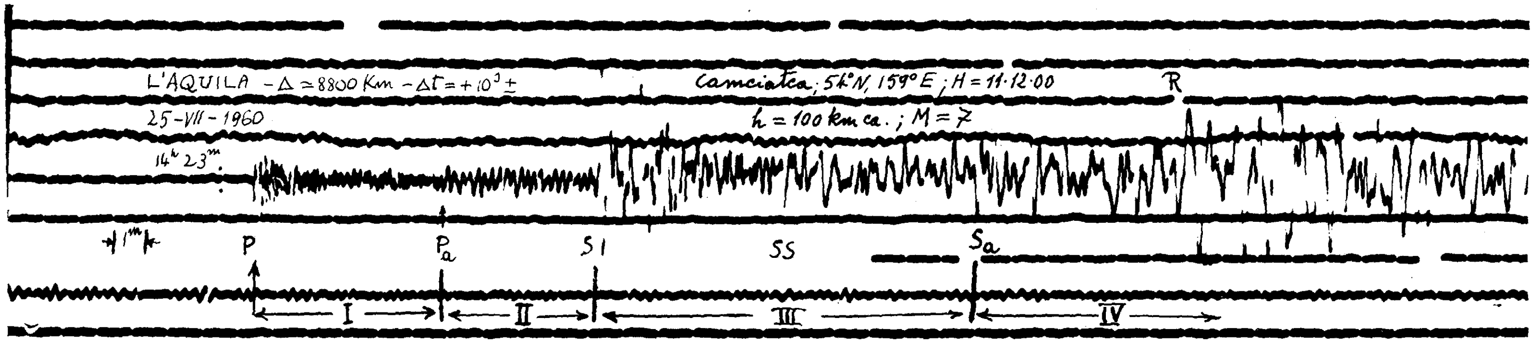

FIG. 2. — Chiaro esempio di canalizzazione astenosfera - crosta terrestre. I zona : onde longitudinali dirette e riflesse; II zona : onde canalizzate; III zona : onde trasversali dirette e riflesse; IV zona : onde canalizzate trasversali (oltre ad onde L e R).

canalizzate dall'astenosfera e dalla crosta terrestre, a periodo nettamente più lungo (2^a); onde trasversali spaziali dirette e riflesse (3^a) ed onde trasversali canalizzate (4^a). Queste ultime vanno ritenute le analoghe traversali delle onde canalizzate longitudinali della parte 2^a (salvo le onde di Love, che vengono registrate fra esse).

3. — Nel caso di terremoti profondi (con ipocentro ad oltre 350 km dalla superficie esterna, secondo la suddivisione di Gutenberg) esiste la possibilità di canalizzazione? In caso positivo, quali zone interessa?

Ho studiato, con questo scopo, il forte terremoto profondo del Mar del Giappone, avvenuto nel punto 40°,0 N, 129°,7 E l'8.X.1960, con il tempo origine H = 05.53.01,1, ad una profondità di h = 600 km ca., secondo l'U.S.C.G.S. La sua magnitudo è stata valutata, da Pasadena, fra 6,5 e 6,75.

In possesso di una cinquantina di sismogrammi — limitando, per ora, l'esame alle onde S_a — ho notato, specialmente fra le registrazioni di sismografi a medio e a lungo periodo, cospicui esempi di onde canalizzate trasversali. Risolta la relativa dromocrona con il metodo dei minimi quadrati, ho ottenuto

$$V_a(S_a) = 4{,}615 \text{ km/sec},$$

da cui, in forza della [1],

$$v_a(S_a) = 4{,}41 \text{ km/sec}.$$

Si tratta quindi di onde canalizzate dall'astenosfera.

Sono queste fra le fasi più appariscenti dei sismogrammi da me consultati (*fig.* 3); anzi, in molti casi, la S_a risulta la fase di maggior

Roma, 8-X-1960 $\Delta = 8\,864$ km Mar del Giappone, H = 05.53.01,1 (USCGS)
$\Delta t = -2^s{,}7$ EW Galitzin $h = 600$ *km* M = 61/2

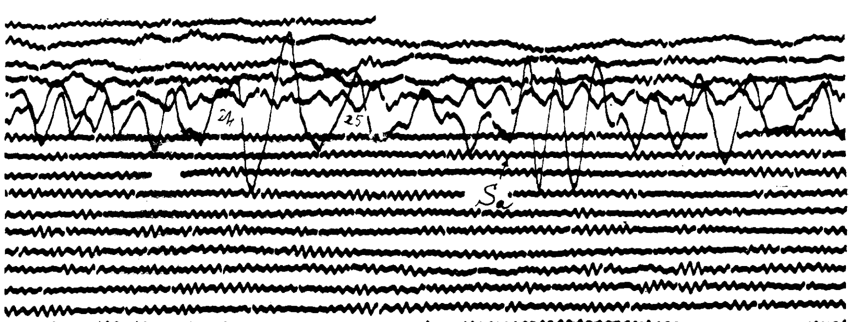

FIG. 3. — La canalizzazione dell'astenosfera, provocata dal basso (terremoto di grande profondità).

spicco di tutto un sismogramma. Ciò sta a provare che, *non solo è possibile la canalizzazione dal basso, ma che essa è altresì capace di convogliare una forte aliquota dell'energia sismica nell'astenosfera.*

E' sempre molto accentuata la componente verticale delle S_a.

Nel terremoto studiato, non sono risultati apprezzabili esempi di canalizzazione da parte della crosta terrestre.

Concludendo, la canalizzazione si presenta come un fenomeno generale, che giuoca un ruolo notevole nella propagazione dell'energia sismica. Esso può interessare le stratificazioni della crosta terrestre e l'astenosfera. Presenta la sua massima efficacia in corrispondenza di forti terremoti con origine nell'astenosfera, nel senso che può interessare contemporaneamente, oltre all'astenosfera stessa, anche i canali della crosta.

Nel caso di terremoti profondi, la canalizzazione assume particolare spicco nella sola astenosfera.

BIBLIOGRAFIA

[1] Caloi (P.). *Onde longitudinali e trasversali guidate dall'astenosfera.* Rend. Accademia Naz. dei Lincei, serie VIII, vol. XV, fasc. 6, 1953.

[2] Gutenberg (B.). *Wave Velocities below the Mohorovicic Discontinuity.* Geophys. Jour. of the R. Astron. Soc., vol. 2, n. 4, 1959.

[3] Magnitsky e Khorosheva. *The waveguide in the mantle of the Earth and its probable physical nature.* « Annali di Geofisica », 1961.

[4] Caloi (P.). *Lezioni di Sismologia.* Università di Roma, 1960.

[5] Lehmann (I.). *Velocities of longitudinal Waves in the upper part of the Earth's Mantle.* « Annales de Géophysique », t. 15, pp. 93-118, 1959.

THE UPPER MANTLE VELOCITY SECTION IN A TRANSITIVE ZONE FROM THE ASIA CONTINENT TO THE PACIFIC OCEAN

by R. S. TARAKANOV

At the analysis of the Kuril-Kamchatka zone earthquakes data the anomalously little travel times of longitudinal waves were marked in comparison with Wadaty and Jeffreys travel time curves. The analogous results were got at experimental travel time curves construction. Wadaty's travel time curve and the average experimental one for the foci depth of 30 and 80 km are given for a comparison on fig. 1. The differences in travel times increase with epicenter distances increase and reach at $\Delta = 1.500\text{-}2.000$ km 4 - 6 sec. These differences can not be explained only by differences

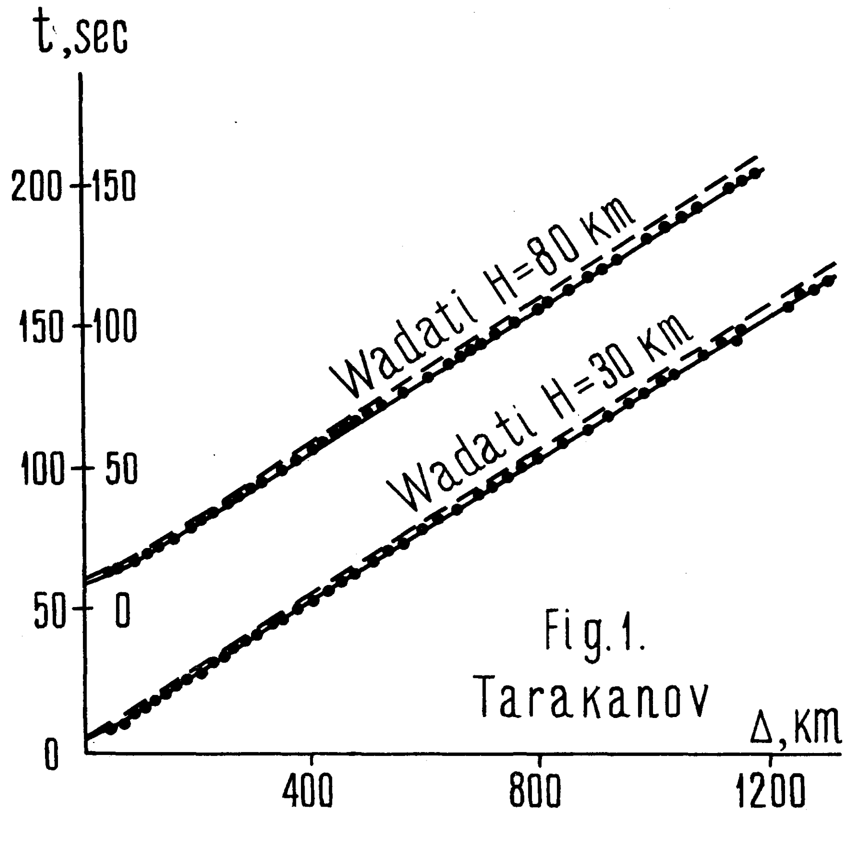

Fig. 1.
Tarakanov

in the crustal structure. It is possible, that the upper mantle in an transitive zone from the Asia continent to the Pacific ocean is characterized with high velocities of longitudinal waves in comparison with the velocities, obtained by Jeffreys and Wadaty.

We constructed the upper mantle velocity section on the base of the average empirical travel time curves of longitudinal waves for the foci depth of 0, 30, 60, 80 and 120 km.

For average travel time curves construction the more qualitative observations at 70 earthquakes for the period of 1953-1961, representing about of 2 000 travel times experimental meanings were used.

The earthquakes epicenters and the seismic stations, the observations of which were used for travel time curves construction, are located approximately on the South Kamchatka — the Central Japan profile (*fig.* 2). At an average travel time curve construction the stations and epicenters location secures almost an even accommodation of observations to the distances of 1 000 - 2 000 km. The average travel time curve was approximated by linear and hyperbolic sections. In both cases the travel times experimental values were averaged on the separate sections of the travel time curve by the least square method. The mean square error of experimental travel time curves is $\pm$ 1,5 sec.

The main earthquakes parameters were determined by methods, origin independent on a travel time curve. The mean error in individual parameters determination is : of epicenter $\pm$ 10 - 20 km; origin time $\pm$ 0,5 - 1 sec. The use of regional stations network on the South Kuril islands increases the exactness of earthquakes parameters determination. According to these stations data waves arrival moments are determined with accuracy of $\pm$ 0,1 - 0,2 sec.

At the velocity section construction by average experimental time curves we went out of the supposition, that longitudinal wave velocity increases with a depth according to the linear regularity :

$Vh = Vo(1 + \beta h)$, where Vh — the wave velocity on the depth h from the Earth crust bottom, β — the wave velocity variation coefficient with the depth, Vo — the velocity on the Earth crust boundary. Its mean value is determined by the South-Kuril earthquakes travel time curve and is equal to 7,8 km/sec.

In the case of linear increase of wave velocity with a depth the seismic rays represent arcs of circles.

Every ray is characterized with parameters : V max and h max.

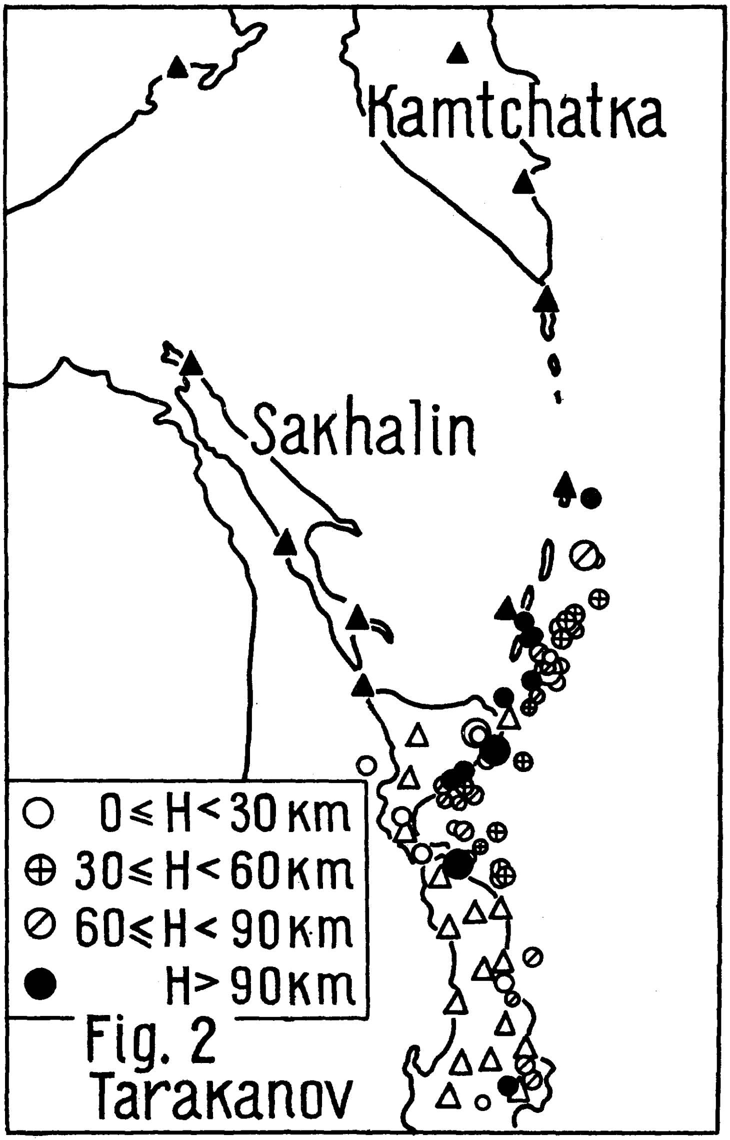

Fig. 2
Tarakanov

The derivatives were determined by us with linear sections of average travel time curves by the least square method.

We determined the coordinates V max and h max for 59 points, which are in the limits of three hundreds km layer of the mantle. With the help of these points complex, by the least squares method the average linear velocity section ($\beta = 6 \cdot 10^{-4}$ km^{-1}), is constructed, which is given on fig. 3 as the continuous line. The determination accuracy of V max for different points of a section is shown by the signs. The constructed velocity section is compared with the graphs according to Jeffreys, Gutenberg and Wadaty. Limits of possible velocities sections, obtained on an electronic computer are also given on fig. 3. For these sections the calculated travel time curve coin-

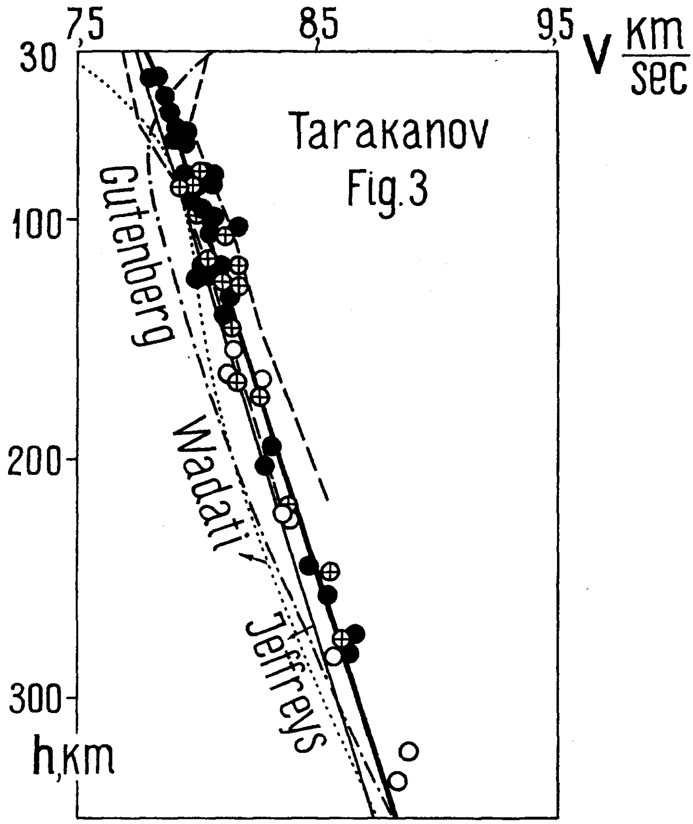

cides (with the accuracy of ± 1,5 sec) with average experimental travel time curve. From the velocity sections comparison it is seen that the upper mantle in an transitive zone from the Asia continent to the Pacific ocean is characterized with great velocities of longitudinal waves in comparison with velocities, determined by Jeffreys, Gutenberg and Wadaty.

The comparison of theoretical travel time curves, calculated at different parameters values V*o*, *d* and *β*, with experimental travel time curve for surface earthquakes is also carried out. Their best coincidance is obtained at : $V_0 = 7{,}8$ km/sec; $d = 30$ km and $\beta = 6.10^{-4}$ km^{-1}.

It is possible to notice on fig. 3 the dissymetrical points location in relation of the average section. In the depths interval of 80 - 120 and 250 km, they, in main, deviate to the right; on the depths of 130-250 km — to the left. The points deviation will decrease if we average the velocity section separate places. Hereto, the points deviations to the right correspond to the high velocity gradient in comparison with an average one, to the left — to low one.

Let us mark, that the velocity gradients variation is observed also in the velocity sections, given for a comparison. The velocity gradient increase in the interval of the depth of 80 - 120 km is given by the line of possible velocity sections. According to Gutenberg and Wadaty the velocity gradient decrease is marked in the depths interval of 100 - 200 km, the increase for the depths, which are greater than 220 km.

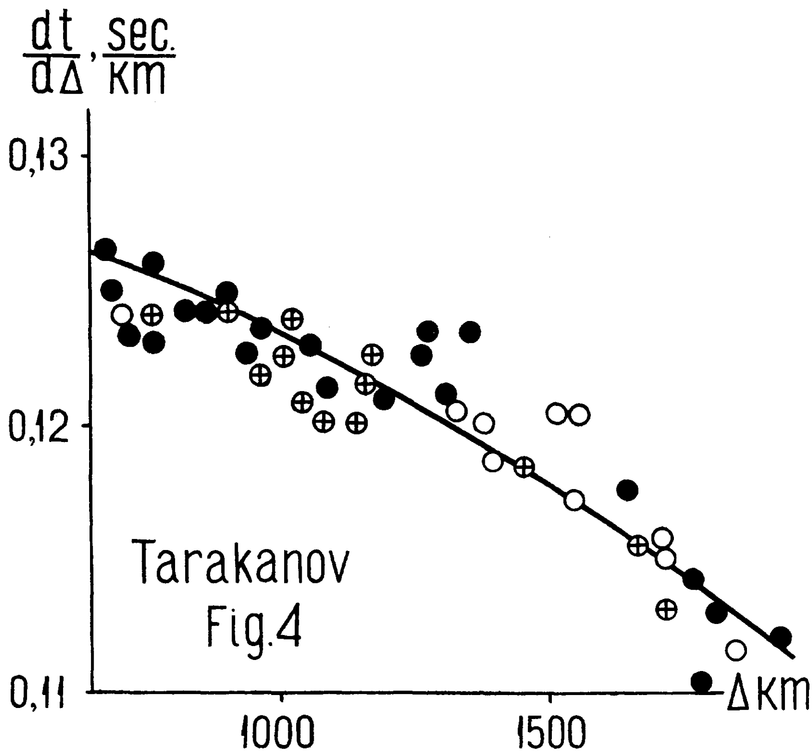

Apparently, the velocity section for a considering zone as well as according to Gutenberg and Wadaty is not linear one. The variation of a velocity gradient in the marked depths intervals, probably is explained by the upper mantle structure pecularities.

The fact of regular systematic deviations from an average section, which can be taken as a working hypothesis for a velocity section construction during another supposition about a velocity variation with a depth, is of interest.

In this connection we give the graph of travel time curve derivative variation in dependence on epicentral distance (*fig.* 4). On this graph the curve corresponds to a linear increase of waves velocity with a depth at $\beta = 6.10^{-4}$ km^{-1}. On epicentral distances of 1 200 - 1 700 km (H = 130-250 km) the points systematically deviate from a curve to the side of travel time curve derivative high values. The observing effect of systematic high values of travel time curves derivative is connected by us with a low velocity layer presence in the interval of depths, which are 130-250 km.

On the base of the average velocity section the travel time curves of longitudinal waves ($0 \leqslant H \leqslant 150$ km, $0 \leqslant \Delta \leqslant 2\,000$ km) are calculated. They have been approbated during 1962 and are used at present at the Far East zone earthquake data analysis. They satisfy better to the Far East conditions, than Wadaty and Jeffreys travel time curves.

SEISMIC REFRACTION STUDIES ON THE NOVA SCOTIAN SHELF

by D. L. BARRETT*, M. BERRY**, J. E. BLANCHARD*, M. J. KEEN* and R. E. McALLISTER*

1. Introduction

Crustal seismic refraction studies are being made along the Atlantic Coast of Nova Scotia. The studies are of interest from a regional point of view, because of the presence of the Appalachian mountain system and the boundary between the oceanic and the continental crusts. This paper is a report of the first continental crustal thickness obtained in Eastern Canada with a reversed seismic refraction profile.

2. Methods

(1) *The profile*

Recording sites were established at Port Hebert near Liverpool, Nova Scotia and at Cole Harbour, near Canso, Nova Scotia and charges were fired at sea every 15 km between the sites. The profile and location of recording sites can be seen in figure 1.

(2) *Instrumentation*

The site at Port Hebert was equipped with a Texas Instruments very low frequency system which was used with six vertical motion and two horizontal motion geophones with resonant frequency two cycles per second. The site at Cole Harbour was equipped with Southwestern Industrial Electronics Vela Uniform refraction system, used with similar geophones. The systems were calibrated and the method used will be described in another paper.

Communications between the ship and the shore stations were maintained using Kaar radio tranceivers. Absolute time was maintained at all stations using a broadcast time signal (Dominion Observatory, Ottawa or Washington) by Westrex chronometers. Distances were obtained from the ship's position, found by using "Decca".

(3) *Results*

In this report the crust has been considered to be made up of layers with sharp discontinuities in physical properties between the

* Institute of Oceanography and Department of Physics, Dalhousie University Halifax.

** Institute of Earth Sciences, University of Toronto.

Canadian contribution to the Upper Mantle Project, n° 41.

layers. The results are shown in the travel time plots, figure 2. It is possible to draw straight lines corresponding to P_1, S_1 (the major

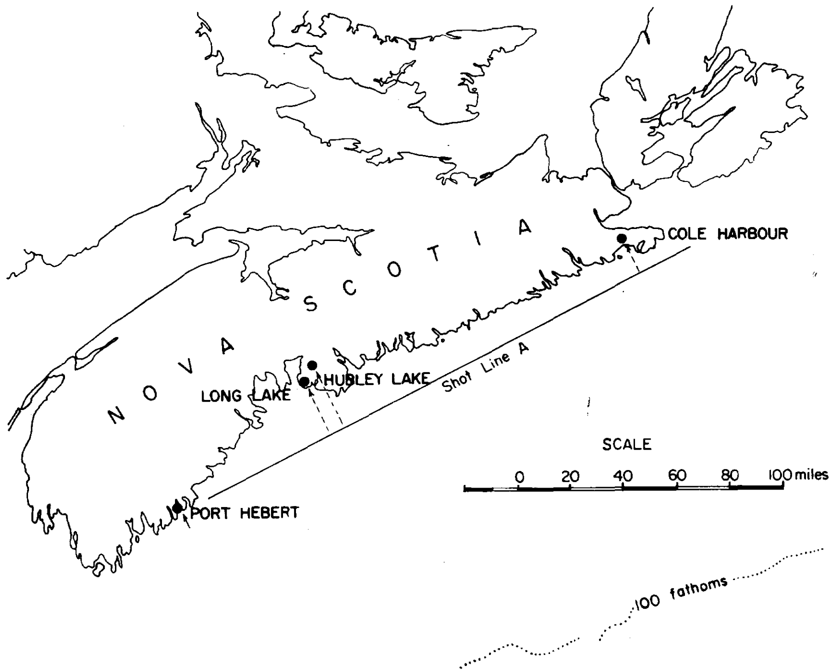

1. The location of the recording sites.

crustal layer), P_n, S_n (the upper part of the mantle) and P_o, S_o (the thin surface layer). The travel times of P_o, S_o were confirmed by studies of near surface velocity information at the recording sites.

The apparent velocities and time intercepts are given in Table 1. Models based on the travel time information were used to calculate the travel times for possible reflections, and these are also shown on figure 2.

(4) *Conclusions*

The model finally adopted is shown in Table 2. No model with a layer in which the compressional wave velocity is between 6.1 and 8.1 km sec^{-1} is necessary to satisfy the observations. Phases have been observed at distances greater than that corresponding to the critical angle which could be reflections of P and S from the Mohorovicic discontinuity. Evidence for reflections at distances less than this is slight.

(*a*)

(*b*)

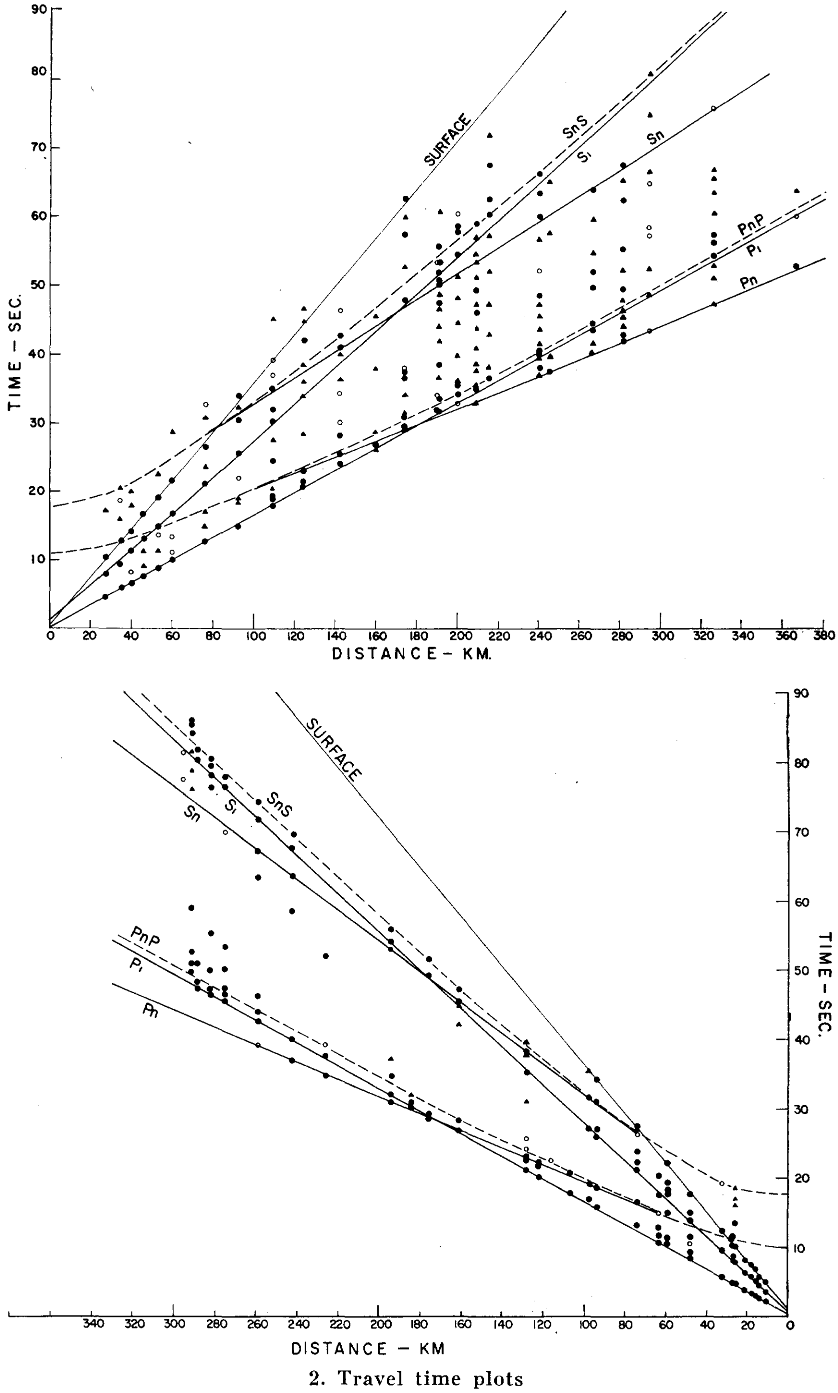

2. Travel time plots
(*a*) Port Hebert
(*b*) Cole Harbour.
The quality of arrivals is indicated thus :
● good
◢ fair
○ poor

(5) *Acknowledgements*

We are grateful to many Canadian Government agencies and to the officers and crew of C.N.A.V. Sackville; without their help this work would not have been possible. This work is supported by the National Research Council and the Defence Research Board of Canada.

TABLE 1

APPARENT VELOCITIES AND TIME INTERCEPTS

	Port Hebert		*Cole Harbour*	
	V (km/sec)	T (sec)	V (km/sec)	T (sec)
P_o	5.72	0.00	5.26	0.00
P_t	6.10	0.27	6.10	0.40
P_n	8.13	7.48	8.09	0.94
S_o	3.53	0.00	3.22	0.00
S_t	3.74	0.85	3.62	0.48
S_n	—	—	4.53	9.93

TABLE 2

Final Model

(*a*) THICKNESSES (km)

	Port Hebert	*Cole Harbour*
1. Surface layer..........................	2.8	2.1
2. Major crustal layer....................	33.5	30.5
TOTAL..........................	36.3	32.6

(*b*) TRUE VELOCITIES (km/sec)

	Port Hebert		*Cole Harbour*	
	P	S	P	S
1. Surface layer...................	5.72	3.53	5.26	3.22
2. Major crustal layer.............	6.10	3.68	6.10	3.68
3. Mantle......................	8.11	—	8.11	4.53

ORIGINE PROFONDE DES SÉISMES SUPERFICIELS ET DES ÉRUPTIONS VOLCANIQUES

par C. BLOT

Office de la Recherche scientifique et technique d'Outre-Mer,
Institut Français d'Océanie, Nouméa

RÉSUMÉ (1)

L'étude détaillée de la séismicité de la région des Nouvelles-Hébrides en particulier, et du Sud-Ouest Pacifique en général, a fait ressortir une corrélation entre les foyers profonds et intermédiaires, les séismes superficiels et les éruptions volcaniques.

Les délais entre « séismes » profonds et les phénomènes superficiels (tremblements de terre et éruptions des volcans) de l'ordre de plusieurs mois (et années) sont fonctions :
— de la profondeur des « séismes précurseurs »,
— de leur magnitude,
— de leur distance aux séismes superficiels et volcans.

Les lois trouvées pour la région du Sud-Ouest Pacifique, semblent vérifiées pour les autres régions du globe où existent des foyers profonds ou intermédiaires, Amérique, Japon, Indonésie, Indou-Koush, ...

Les séismes de très grande magnitude sont précédés par des séismes profonds de magnitude supérieure à 7, ou par plusieurs séismes profonds de magnitude moindre.

Signes utilisés dans les schémas

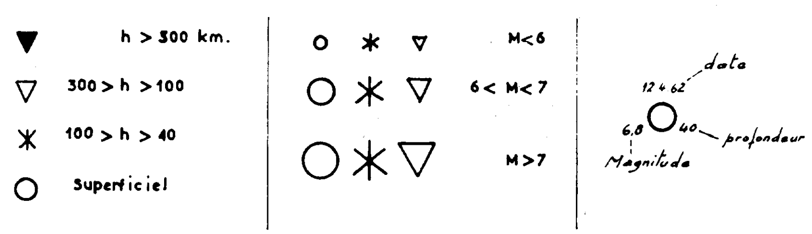

Introduction

L'étude de la séismicité et de l'activité volcanique dans l'Archipel des Nouvelles-Hébrides nous avait conduits à signaler une relation de temps entre des séismes intermédiaires se produisant au voisinage d'un volcan et les éruptions de celui-ci [*1] (voir liste des références).

(1) See the Abstract, p. 121.

Les conclusions de ce travail étaient les suivantes :

— tous les séismes intermédiaires de magnitude voisine de 7 ont été suivis d'éruptions violentes; les éruptions modérées ont été précédées de séismes de magnitude comprise entre 5 1/2 et 6 3/4.

— l'intervalle de temps séismes intermédiaires - éruptions dépend pour un même volcan de la profondeur du foyer séismique (120 à 250 km).

— la vitesse d'ascension du phénomène magmatique dépend du type du volcan et du caractère de ses éruptions. Elle varie de 1/2 à 2 km par jour.

Les recherches poursuivies depuis m'ont permis de mettre en évidence les faits suivants :

— existence de ces séismes intermédiaires antérieurs à chacune des éruptions récentes de divers volcans.

— origine plus profonde encore de ces séismes intermédiaires et des éruption volcaniques.

— production de séismes superficiels à partir de cette même origine profonde.

Les quelques cas présentés (il n'est pas possible dans le cadre de cet exposé de parler de tous les très nombreux exemples trouvés) illustreront les divers aspects du phénomène :

- ascension linéaire avec la succession des foyers séismiques à 600, 250, 100, 50 (± 50) km de profondeur aboutissant à une éruption volcanique,
- répétition dans le temps
  - à partir de même foyer avec production d'éruption volcanique et de séismes superficiels,
  - à partir de foyers profonds dont la situation géographique est différente,
- diffusion dans l'espace
  - suivant un plan de faille orogénique,
  - avec une divergence conique,
- interférences des phénomènes ascendants avec convergence à partir de foyers différents donnant de violents séismes ou de grandes éruptions volcaniques.

Structure de la région des Nouvelles-Hébrides

Les Nouvelles-Hébrides sont dans le Sud-Ouest Pacifique un Archipel de quelques 80 îles et îlots, faisant partie du groupe des îles Mélanésiennes et formant avec les îles Santa-Cruz un tronçon de l'arc des Salomonides reliant les îles de la Sonde, de Nouvelle-

Guinée, des Salomons à la Nouvelle-Zélande en passant par les îles Fidji, Tonga et Kermadec.

Les îles des Santa-Cruz et Nouvelles-Hébrides sont réparties sur une bande étroite de direction nord-nord-ouest à sud-sud-est, entre la ligne andésitique circum-pacifique et le géosynclinal Papou dont les îles Loyauté et la Nouvelle-Calédonie sont les terres émergées.

Cette région a le caractère d'un arc étroit actif du type circum-pacifique tourné vers le sud-ouest, en direction opposée du bassin du Pacifique. Les fosses océaniques sont adjacentes aux îles de ce côté.

Presque tous les séismes sont localisés sur une étroite bande confondue avec la guirlande d'îles des Santa-Cruz et Nouvelles-Hébrides. L'axe de cette bande, et en particulier la ligne des volcans actifs, a une direction nord 22° ouest. Les foyers séismiques superficiels se répartissent sous les fosses océaniques profondes, les foyers intermédiaires (h = 100 - 250 km) sous les îles.

Les foyers séismiques profonds (h = 550 ± 100 km), très rarement détectés avant 1959, plus fréquemment déterminés depuis la création de plusieurs stations séismologiques dans cette région, se groupent généralement au nord-est de l'archipel Néo-Hébridais (par 13° 1/2 S — 170° 1/2 E ± 1° 1/2).

Les séismes se répartissent ainsi sur un plan triangulaire incliné de 55° par rapport à la surface terrestre dont le sommet serait dans cet essaim de foyers profonds et la base l'axe des fosses océaniques à l'ouest de l'archipel.

Signalons l'existence d'un séisme profond extraordinaire, celui du 14 mars 1959 (h = 500 km) déterminé par 18° S et 166° E. Un tel foyer, situé en dehors des grandes structures orogéniques classiques n'est pas exceptionnel. En Nouvelle-Zélande, le 23 mars 1960, deux séismes à 610 km de profondeur ont été localisés par 39° S et 175° E, c'est-à-dire en dehors de la structure profonde normale de cette région.

Séismicité et volcanisme des Nouvelles-Hébrides

Le tableau I donne les caractéristiques des séismes précurseurs des éruptions du volcan Ambrym, de décembre 1950, septembre 1962 et avril 1963.

Tableau I

Séismes précurseurs des éruptions du Volcan AMBRYM

1					2					3				
Date	° S	° E	M	h	Date	° S	° E	M	h	Date	° S	° E	M	h
1949					*1961*					*1961*				
18/7	13,0	171,5	6,5	600	12/2	13,1	171,8	(6)	598	28/8	12,7	169,6	5,5	660
					5/12	16,4	168,0	6,5	205	*1962*				
										1/9	15,9	168,2		244
1950					*1962*									
21/7	16,1	168,3	6,5	150	12/3	16,1	168,2		170	11/11	15,9	167,8		155
										1963				
10/9	15,5	167	7,1	100	18/3	16,5	168,2		150	20/1	15,4	167,7	5,5	107
					28/9	16,7	167,5		50	12/3	15,5	168	4,5	
										15/4	16,6	167,8		
6/12		*Éruption*			28/9		*Éruption*			15/4		*Éruption*		
2/12	18,5	167,5	8,1	60						12/5	17,3	167,6		53
					6/10	17,4	167,7	6,5	33	1/7	17,4	167,6	5,5	33

La translation des foyers séismiques dans l'espace et le temps est illustrée par les graphiques de la figure 1.

Les 3 séismes profonds de juillet 1949, février 1961 et août 1961 localisés dans le même secteur ont précédé de 16 mois 1/2 dans le

NOUVELLES - HEBRIDES - Volcan AMBRYM

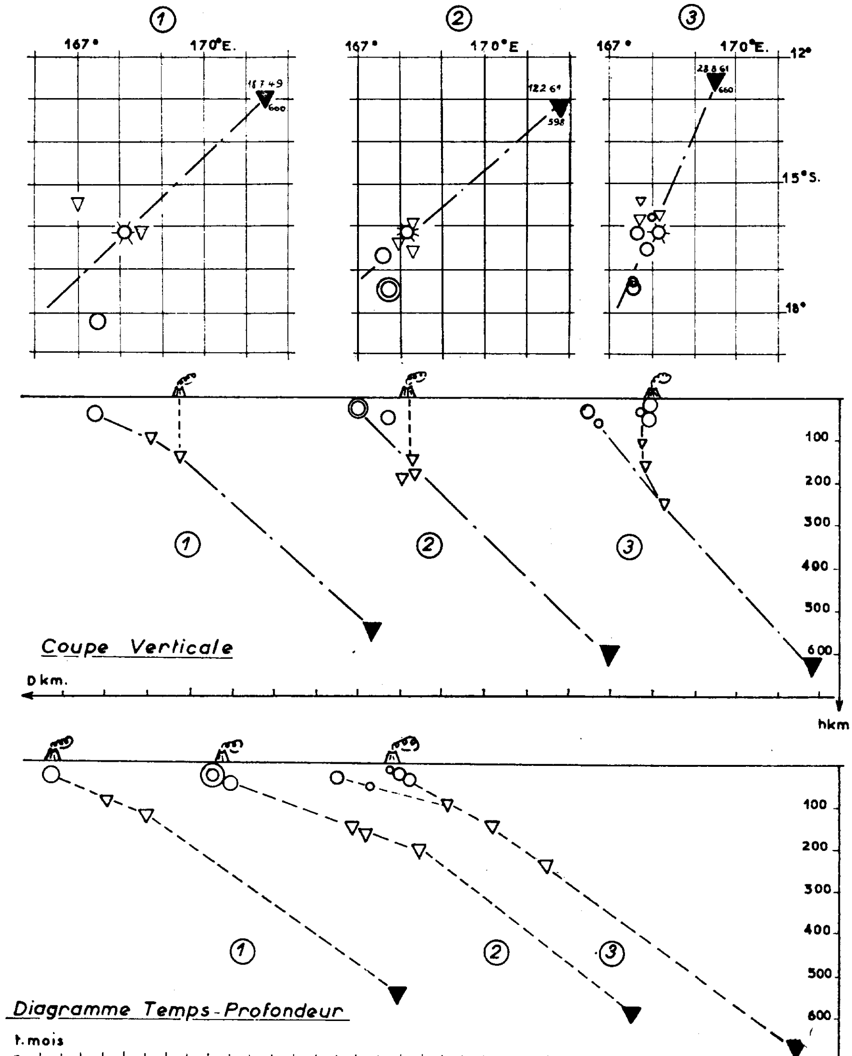

Figure 1

premier cas, de 19 mois 1/2 dans les deux autres cas, les éruptions du volcan.

Des séismes superficiels ont eu lieu en même temps ou peu après celles-ci. Les éruptions ont été modérées, les tremblements de terre ont été très violents dans le premier cas, moyens dans les deux autres. Le séisme profond de juillet 1949 est de magnitude supérieure à celle des séismes de février et août 1961, ce qui expliquerait le délai plus court d'ascension du phénomène.

Le tableau II présente le cas des 3 éruptions du volcan Lopevi, observés depuis 40 ans : novembre 1939, juillet 1960 et juillet 1963.

TABLEAU II

Séismes précurseurs des éruptions du Volcan LOPEVI

1					2					3				
Date	° S	° E	M	h	Date	° S	° E	M	h	Date	° S	° E	M	h
1938					*1959*					*1962*				
18/11	13	168	6,5	360	14/3	18	166	?	500	11/5	14,3	170.4	(6)	623
1939					*1960*					*1963*				
12/8	16,5	168,5	7,2	180	8/3	16,5	168,5	7,5	250	10/3	16,0	168,4	5,5	283
1/11	*Éruption*				10/7	*Éruption*				7/7	*Éruption*			

La figure 2 donne les représentations graphiques de ces cas.

Nous avions indiqué la différence entre le dynamisme et les types d'éruptions de ce volcan et de son voisin Ambrym, ainsi que la vitesse plus grande d'ascension du phénomène magmatique à partir du foyer séismique intermédiaire précurseur [*1].

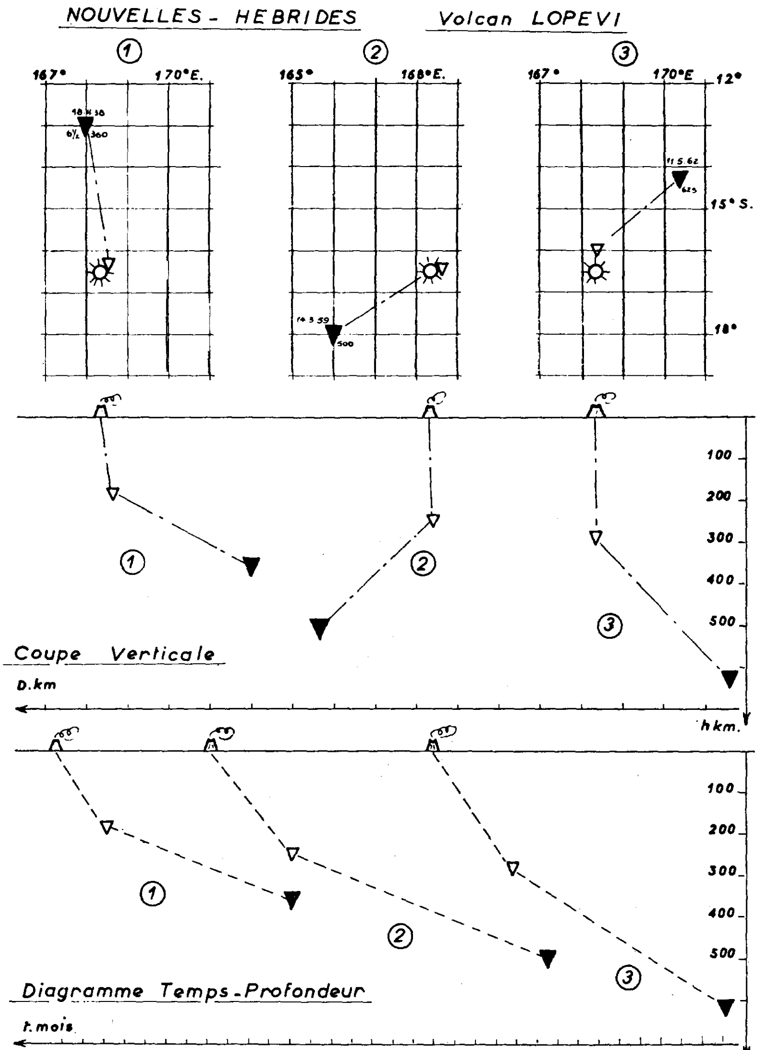

Figure 2

Les foyers des séismes profonds précurseurs sont dans des positions différentes pour chacun des 3 cas et par rapport à ceux précédant les éruptions d'Ambrym.

La très violente et très particulière éruption du 10 juillet 1960 [*2 et *3] aurait été précédée par le séisme du 14 mars 1959 (h = 500 km) situé par 18° S et 166° E, c'est-à-dire à l'inverse des foyers profonds habituels. Lors de cette éruption une fracture avec plusieurs cratères s'est ouverte sur le flanc sud-ouest du Lopévi

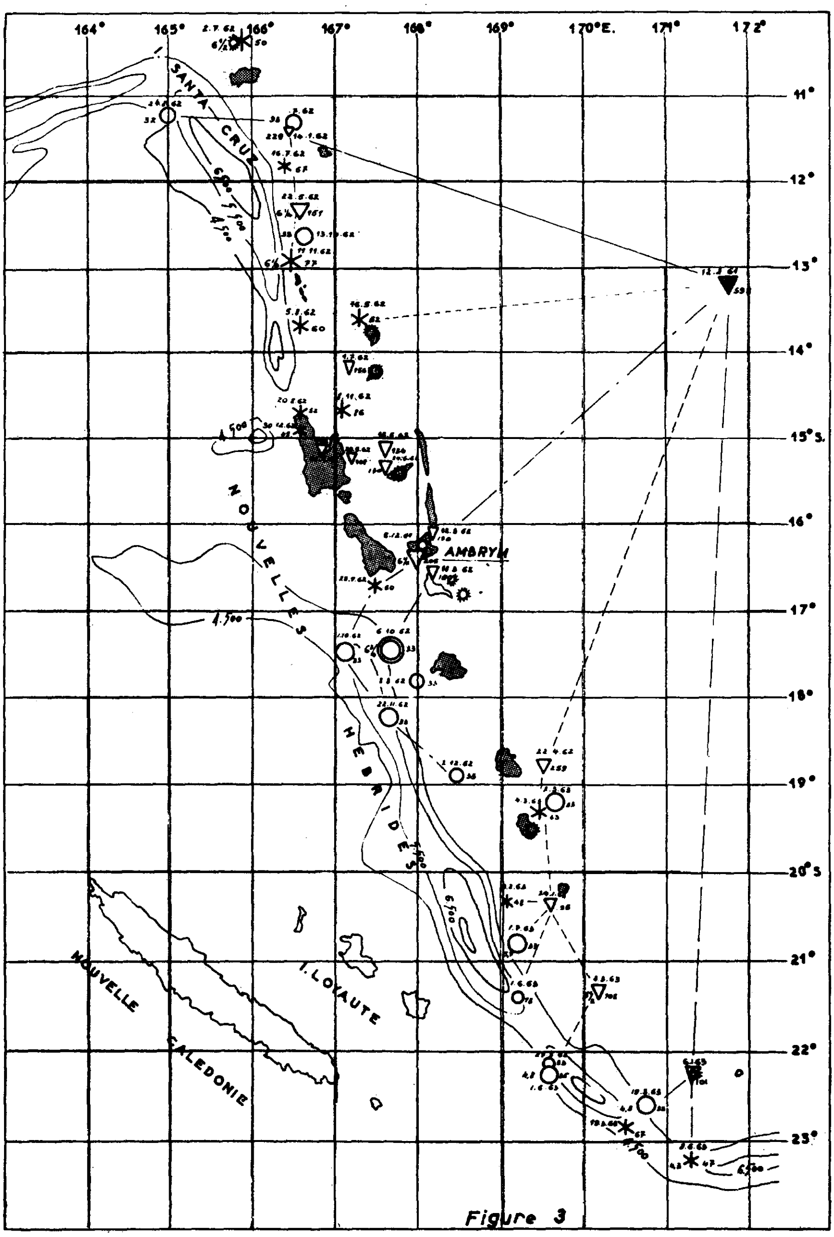

Figure 3

(dans la direction du foyer profond) alors que pour les autres cas les phénomènes éruptifs se sont produits au sommet et sur le flanc nord-est. D'autre part cette éruption avait précédée quelques jours et heures auparavant par des séismes superficiels au voisinage de l'île Lopévi.

La progression des séismes ne se fait pas uniquement dans une seule direction mais en éventail. La figure 3 illustre un cas où des séismes intermédiaires et superficiels survenus en 1962 et 1963 dans l'archipel des Nouvelles-Hébrides, ont eu pour origine le foyer profond du 12 février 1961.

Le diagramme de la figure 4 montre la répartition dans le temps des séismes pointés sur la carte précédente en fonction de leur profondeur. Des traits différents relient les principales séquences. On voit que les délais de progression des séismes dépendent de leurs distances au séisme profond initial, les séismes dans le nord puis le sud de l'archipel arrivant après les séismes du centre.

Tous les principaux séismes survenus aux Nouvelles-Hébrides durant ces dernières années ont pu être ainsi rattachés dans les mêmes conditions aux quelques séismes profonds survenus dans cette région.

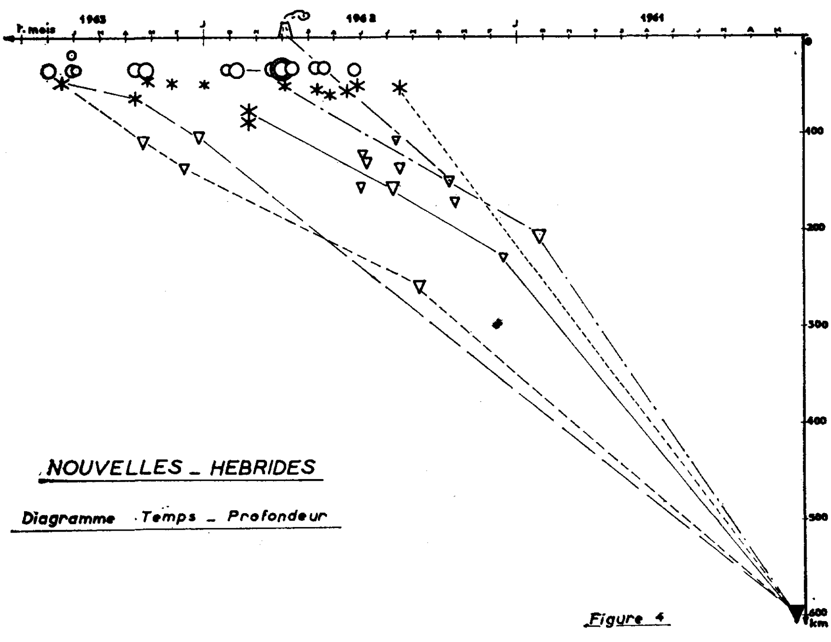

Figure 4

Séismicité de la région des Fidji - Tonga - Kermadec

Cette région est bien connue pour sa très grande activité séismique en profondeur. Il a pu être constaté que, 18 mois à 2 ans après les séismes profonds de forte magnitude situés à l'ouest des Tonga, avaient toujours eu lieu des séismes superficiels importants aux Fidji, Samoa, Tonga, Kermadec.

La carte de la figure 5 montre un exemple, parmi les autres cas, de l'importante séismicité de cette région durant les années 1949-50-

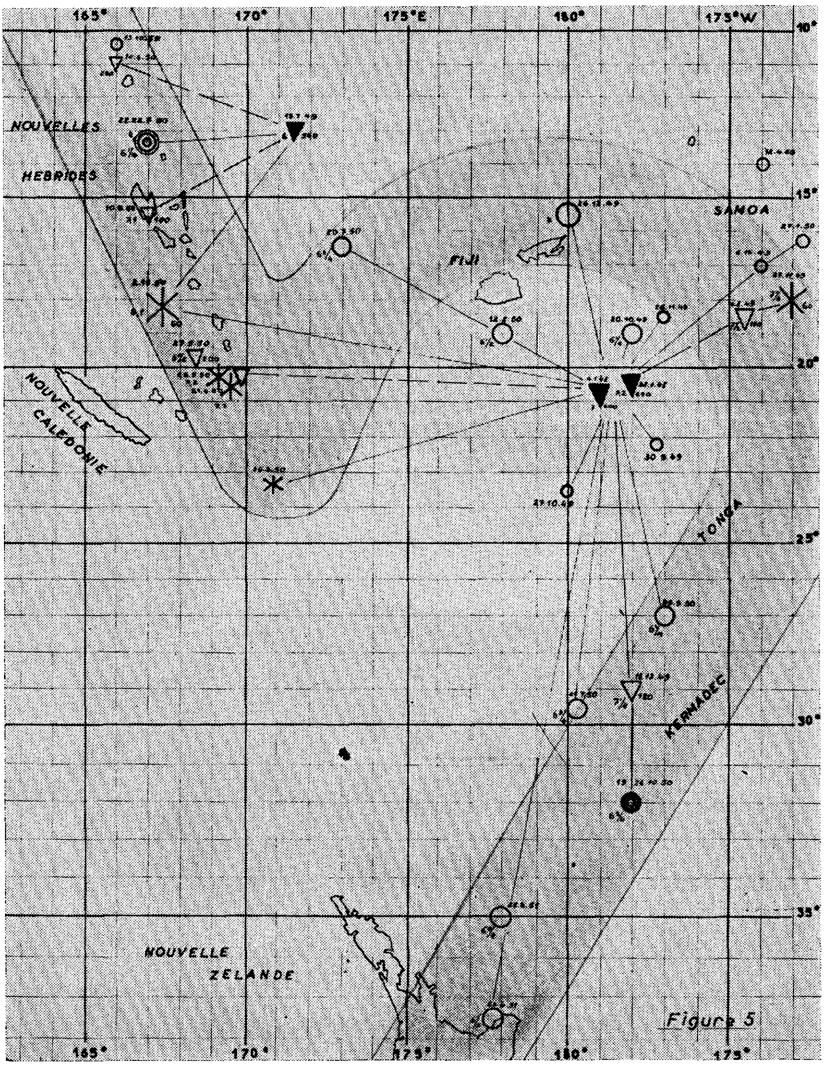

FIG. 5.

51 qui aurait eu pour origine les deux séismes profonds (h = 600 et 630 km) de magnitude 7 et 7,2 survenus en janvier 1948.

On remarquera la répartition conique des foyers séismiques dans l'espace et le temps conforme à la structure particulière de cette région.

Sur le diagramme de la figure 6 ont été pointés les différents séismes figurant sur la carte précédente en fonction de leurs dates et de leurs distances à l'épicentre des deux séismes profonds de janvier 1948.

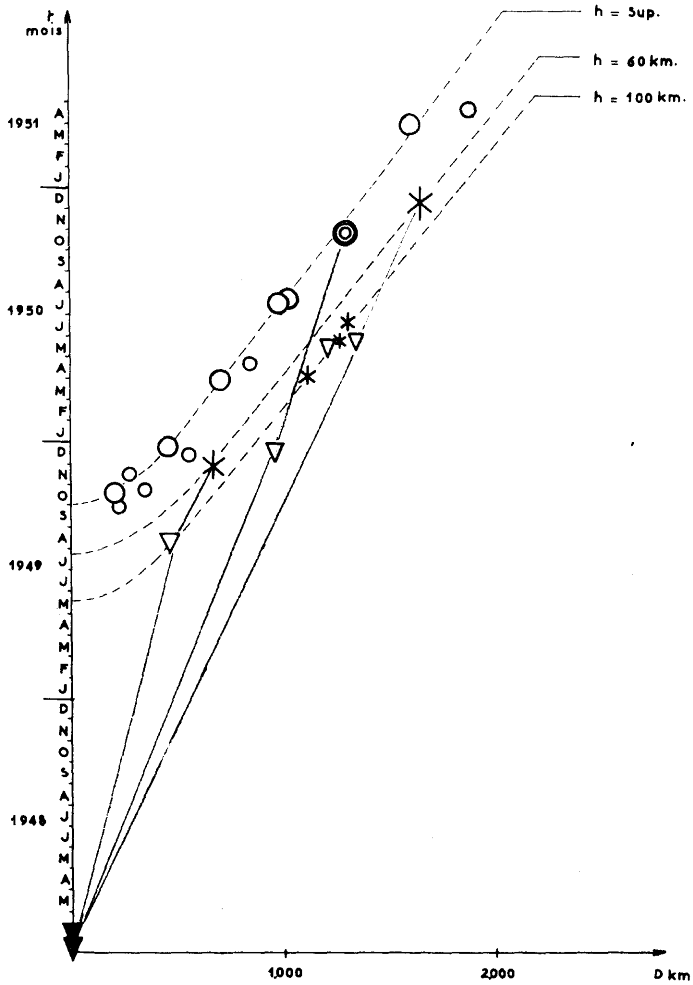

SUD – OUEST PACIFIQUE . 1948 – 1951

Diagramme Temps Distances

Figure 6

Ces séismes se répartissent sur des hodochrones différentes suivant les profondeurs des foyers.

On remarque ainsi que le séisme du 2 décembre 1950 situé à l'ouest de l'archipel des Nouvelles-Hébrides (séisme de magnitude 8,1 suivi durant tout le mois de décembre d'une multitude de répliques) est aligné avec les séismes des régions Fidji, Tonga, Kermadec de la même époque et issus des foyers profonds de janvier 1948.

L'importance de ce séisme peut être expliqué par la convergence des effets du séisme profond du 18 juillet 1949 (dont il a été question précédemment) au nord-est de l'archipel Néo-Hébridais et de ceux des séismes profonds de la région des Tonga en janvier 1948.

On a vu que le délai entre les séismes de juillet 1949 et décembre 1950 était de 16 mois 1/2, la distance entre les épicentres étant de 800 km. Le délai moyen entre les séismes de janvier 1948 et ce même séisme de décembre 1950 est de 34 mois 1/2 pour une distance entre les épicentres de 1 600 km. Dans ces deux cas la vitesse de propagation du phénomène ascendant est du même ordre de grandeur, ce qui justifierait l'hypothèse avancée.

On remarquera d'autre part que les séismes survenus en 1951 dans le nord de la Nouvelle-Zélande peuvent être rattachés aux séismes profonds de janvier 1948 au large des Tonga. Des analogies semblables ont été également observées entre les séismes de Nouvelle-Zélande et la séismicité des Tonga - Kermadec, antérieurement et postérieurement au cas présenté.

Autres exemples

J'ai pu retrouver pour les autres régions séismiques du globe et en particulier pour les zones circum-pacifiques de même structure de nombreux cas identiques.

Au Japon

Les 3 séismes de magnitude supérieure à 6 1/2 survenus en *1962* sur les côtes est du Honshu et d'Hokkaïdo :

	h m s	° ′	° ′		
12 avril	00 52 39	37 58 N	142 49 E	h = 40	M = 6,8
23 avril	05 58 12	42 12	143 55	60	7
30 avril	02 26 21	38 44	141 08	0	6,5

et les 2 violentes éruptions des volcans Tokachidake (29 juin) et Miyakejima (24 août) de cette même année, ont eu pour origine, en *1960*, le foyer profond situé sous la mer du Japon.

	h m s	°	°		
8 octobre	05 53 04	40 N	130 E	h = 610	M = 6 1/2

Les figures 7 et 8 montrent la similitude de cet exemple avec le cas présenté pour les Nouvelles-Hébrides (*fig.* 3 et 4).

Le très violent séisme (Magnitude 8,5) survenu le 2 mars 1933 au large de la côte nord-est du Honshu peut être interprété comme

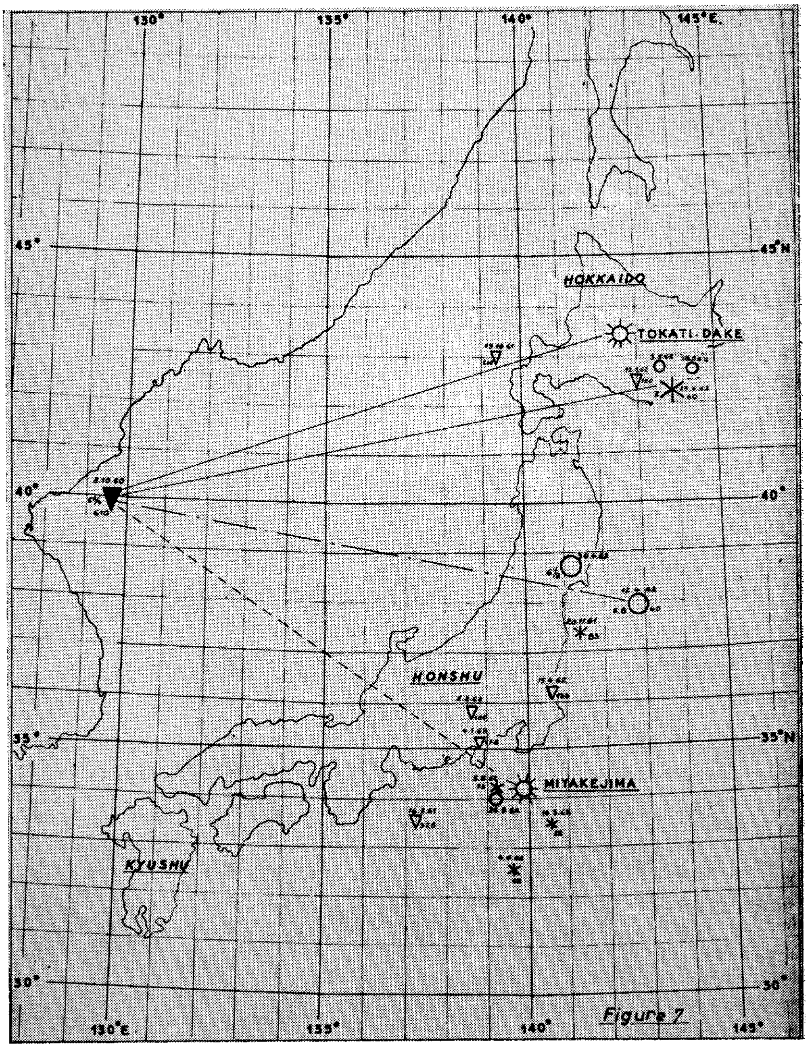

FIG. 7.

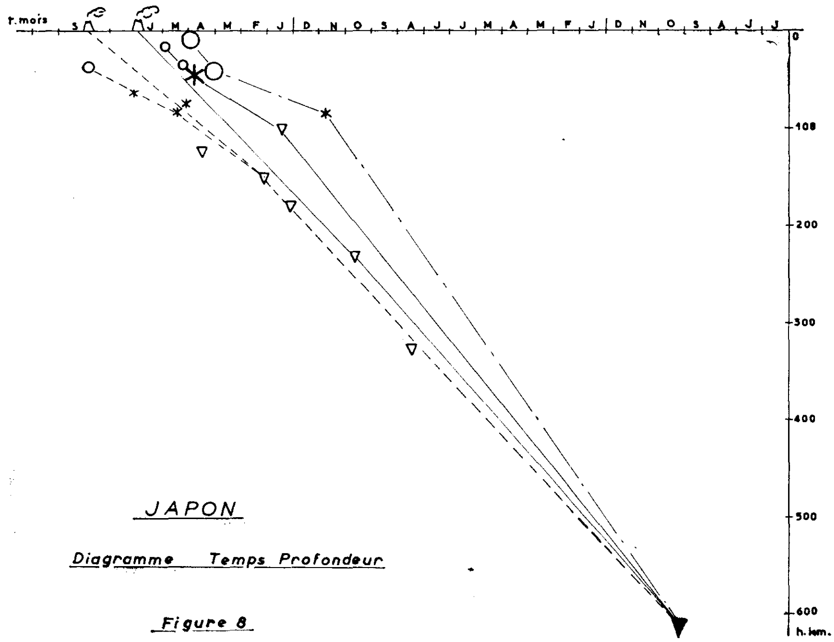

JAPON

Diagramme Temps Profondeur

Figure 8

la résultante de plusieurs séismes profonds répartis en 1931 et 32 de part et d'autre de la région ébranlée (voir la *fig.* 9).

Un diagramme temps-profondeur-distance montre que tous ces foyers s'alignent sur une même courbe analogue à celles précédemment décrites.

En Indonésie

L'éruption du volcan Gamalama dans l'archipel d'Halmahera au 25 décembre 1962 (la dernière éruption datant du 8 septembre 1938), serait due à l'existence de plusieurs séismes profonds survenus de janvier à juillet 1961 et qui auraient d'autre part provoqué un séisme de magnitude 7 en avril 1963 à quelque distance de ce volcan.

L'éruption du volcan Agung (8°3 S — 115°5 E) dans l'île de Bali a été précédée le 15 juillet 1961 par un séisme profond (h = 565 km) situé à proximité (6°8 S — 116°9 E) soit 20 mois auparavant, c'est-à-dire dans les mêmes délais trouvés. (Il n'y a pas d'autres séismes profonds dans cette région pendant les années précédant l'éruption).

En Europe

E. Peterschmitt avait signalé en 1956 [*4] « que la séismicité de la Mer Tyrrhénienne et de ses environs peut être rapprochée de

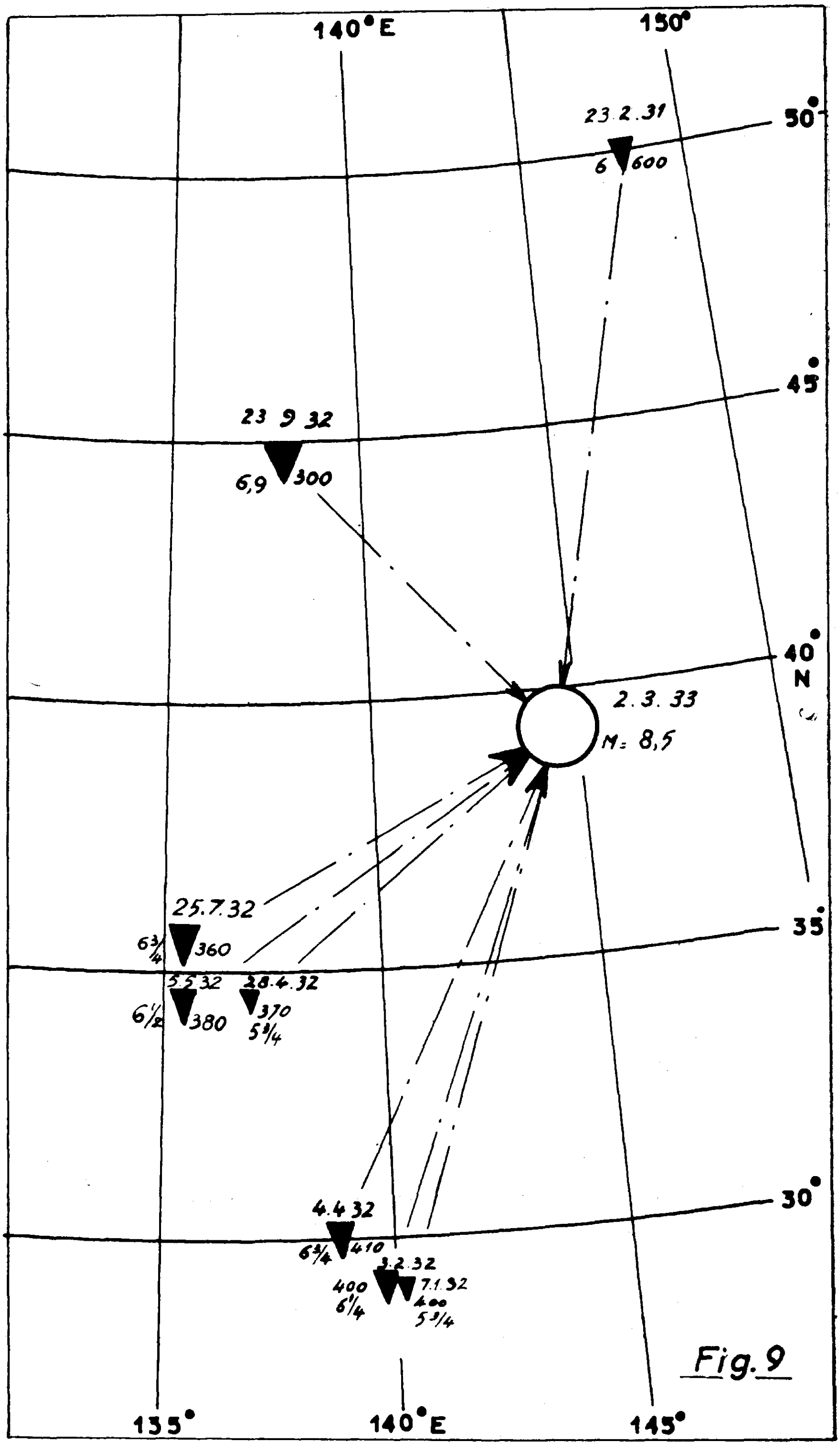
140°E
150°
50°
45°
40°
N
35°
30°
23.2.31
6
600
23 9 32
6,9
300
2.3.33
M= 8,5
25.7.32
6¾
360
5.5.32
6½
380
28.4.32
370
5¾
4.4.32
6¾
410
3.2.32
400
6¼
7.1.32
400
5¾
135°
140°E
145°

Fig. 9

celle d'un arc circum-pacifique à caractère océanique, tel que celui des Tonga. Les foyers se répartissent au voisinage d'une surface S conique dont le sommet pourrait être situé vers 40° N, 12° E à

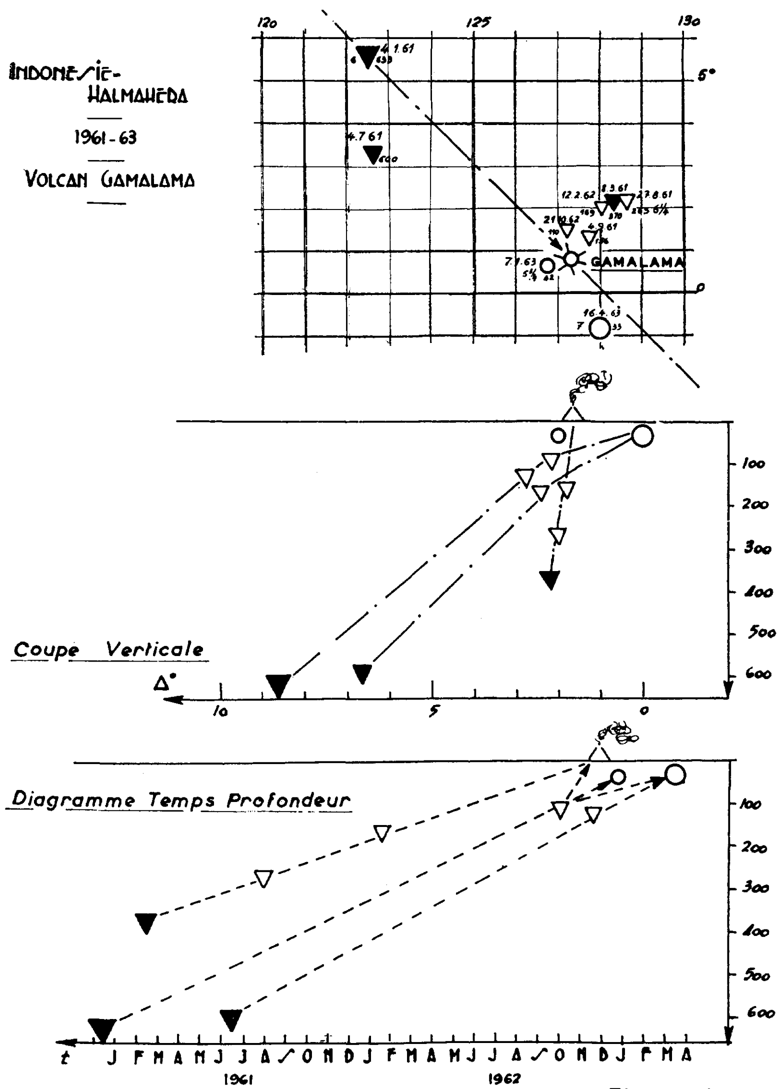

Figure 10

700 km de profondeur et dont la base serait constituée par l'arc calabrais des séismes normaux..... La surface S pourrait être une vraie surface de discontinuité ».

Il a été trouvé quelques cas de relations entre séismes intermédiaires et éruptions des volcans : Vésuve, Stromboli [*1]. Si la séismicité de cette région est faible (en comparaison de celle des Tonga) et les séismes profonds rares (du moins ceux assez forts pour être déterminés avec certitude) il est cependant remarquable que le séisme le plus profond détecté sous la mer Tyrrhénienne le 17 février 1955 (h = 450 km M 5 1/4) ait été suivi 2 ans après des grandes éruptions de l'Etna (mai 1957) et du Stromboli (août 1957). Chacune de ces éruptions avait été précédée 2 mois 1/2 auparavant de séismes situés sous la croûte (h = 60 km).

Région de la mer TYRRHENIENNE_1955_1957

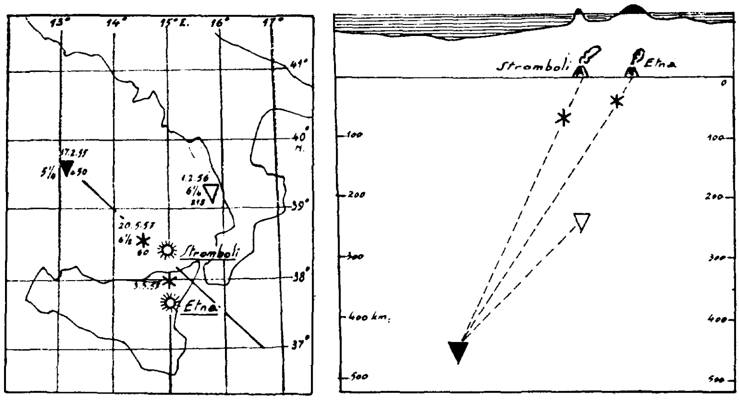

PLAN COUPE

d'après E. PETERSCHMITT (x 4)

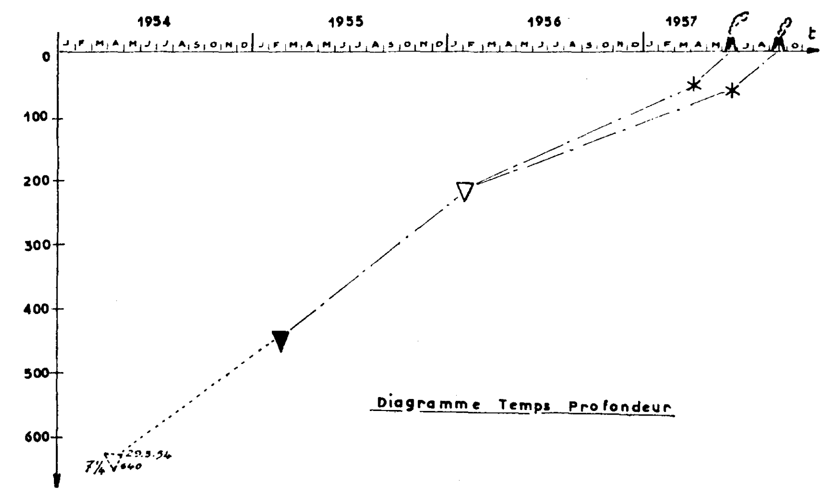

Figure 11

La faible magnitude du séisme profond (M = 5 1/4) ainsi que l'activité réduite de ce secteur pourraient expliquer le délai un peu plus long que ceux trouvés dans les cas précédents.

En poursuivant ces analogies on peut formuler l'hypothèse que le séisme extraordinaire d'Espagne du 29 mars 1954 (M = 7 1/2 h = 630 km, 36°9 N et 3°5 W) a été à l'origine de la succession des séismes et éruptions précédemment décrits.

En effet sur le diagramme temps-profondeur de la figure 11, le pointage de ce séisme extrapole la courbe ascendante indiquée.

Par analogie également on peut avancer que la fameuse éruption sous-marine de Faïal aux Açores du 27 septembre 1957 (38°58 N 28°75 W) qui a eu lieu peu après les éruptions de l'Etna et du Stromboli a eu pour origine ce même séisme profond d'Espagne, centré entre les Açores et la Sicile.

Conclusion

Les quelques exemples présentés dans ce bref exposé confirment l'existence de la montée d'un phénomène énergétique (à la vitesse moyenne de l'ordre de 1,5 km/jour) et qui déclancherait, dans les zones favorables, des séismes à des profondeurs successivement moindres.

L'aspect rayonnant de la diffusion de cette énergie à partir d'un « séisme » profond, rayonnement qui se retrouve également pour des séismes intermédiaires, la production de « séismes » très profonds dans des zones hors de toute structure orogénique classique posent des problèmes sur l'origine de ces « séismes » profonds et le phénomène énergétique qui en résulte.

R. D. Adams (Seismological Observatory, Wellington) termine son étude comparative des séismes profonds anormaux de 1960 en Nouvelle-Zélande et du séisme d'Espagne de 1954 en formulant l'hypothèse suivante [*5].

« Ces faits suggèrent que le mécanisme des séismes à foyers profonds est davantage expliqué par les conditions au foyer, telles que température et pression, que par une quelconque tension structurale associée aux phénomènes superficiels ».

Si la réalité de ce phénomène est entièrement confirmée par les études en cours, la prévision des séismes pourrait devenir une science exacte, comme la prévision météorologique dont le principe est identique : suivre à partir d'un réseau de stations la progression des perturbations et, compte tenu des lois de la Physique du Globe, en prévoir les trajectoires et les effets.

RÉFÉRENCES

[*1] BLOT (C.) et PRIAM (R.). Volcanisme et séismicité dans l'Archipel des Nouvelles-Hébrides. (Bulletin Volcanologique, T. XXVI, pp. 167-180. Napoli, 1963.)

[*2] REMY (J.-M.) et REICHENFELD (C.). Rapport préliminaire concernant l'éruption du volcan Lopévi (Nouvelles-Hébrides). Juillet 1960 (inéd. arch. Service des Mines — Port-Vila).

[*3] WILLIAMS (C. E.). Preliminary report on the Lopevi eruption, 10th July 1960 (impublished geological Survey records, Port-Vila).

[*4] PETERSCHMITT (E.). Quelques données nouvelles sur les séismes profonds de la mer Tyrrhénienne. (Annali di Geofisica, Vol. IX, n° 3. 1956, pp. 305-334, Roma.)

[*5] ADAMS (R. D.). Source Characteristics of some deep New-Zealand Earthquakes (N. Z. Journal of Geology and Geophysics, Vol. 6, n° 2, May 1963, pp. 209-220, Wellington).

— GUTENBERG and RICHTER (F.). Seismicity of the Earth. (Princeton University Press, 1954.)

— International Seismological Summary. (University Observatory Oxford.

— Bulletins du Bureau Central International de Séismologie (Strasbourg).

— Bulletins de l'U. S. Coast and Geodetic Survey (Washington D. C.).

ABSTRACT

The detailed study of seismicity in the region of the New-Hebrides in particular, and in the Southwestern Pacific in general, has shown a correlation between deep, intermediate, shallow earthquakes, and volcanic eruptions.

The intervals between deep earthquakes and shallow phenomena (earthquakes and volcanic eruptions), on the order of several months (and years), are functions :

— of the depth of the foreshocks,
— of their magnitude,
— of their distance in relation to shallow earthquakes and volcanoes.

The laws for the Southwestern Pacific seem verified for other regions of the globe where intermediate and deep foci exist : America, Japan, Indonesia, Indo-Koush, ...

The earthquakes of very great magnitude are preceded by deep earthquakes of a magnitude superior to 7, or by several deep earthquakes of a lesser magnitude.

ON NEOTECTONICS OF AFRICA IN CONNECTION WITH ITS SEISMICITY

by N. P. KOSTENKO

(Dept. of Geology, University, Moscow)

It is beyond the scope of this paper to present anything but the generalized outline of the main points to be investigated.

1. The distribution of areas of higher seismicity is characterized by the fact that they are confined to the definite recent structural conditions. In this respect there are separated : *a*) moutain-building areas — the Atlas and Arabio-African ones; *b*) separate boundary zones « mainland-ocean »; *c*) particular upheavals within the Mediterranean aquatorium connected structurally with the African Continent (*fig.* 1).

2. The Atlas mountain-building area represents a young or epigeosynclinal country consisting of a complex system of arch-folded and arch-blocked uplifts. The latter are being developed according to the rejuvenated mountain-structure types. High seismicity is confined to a fault zone of sublatitudinal and meridional strike with contrasting movements having different sign, the zone stretching along the Atlas coast from Oran to Philippville. This zone is characterized by an active development of a differently oriented complex system of faults. A zone of uplifts crossing over the Atlas mountain structure in SW direction from about the Gulf of Gabes to Algiers is characterized by less abundant epicentres. A very high concentration of great significance earthquake foci is perceived in the area traversing highly seismic zones (in the Algiers region) (*fig.* 1).

3. The Arabio-African mountain-building district is an epiplatform or rejuvenated mountainous country. Within it there are recognized great ellipsoidal upswells of a type of grandiose mega-brachy folds having extensive radius of curvature and mainly NE in strike.

Along their slopes and arches these are complicated by regional fault-like breaks and fissures. The regions of high seismicity are : 1) megabrachy folds changing abruptly in strike; 2) abruptly plunging periclinals; 3) closed together positive structural forms under the conditions of their upheaval and extension (*fig.* 2).

4. High seismicity characterizes new positive structural forms — *dams* separating individual aquatorium depressions. Among

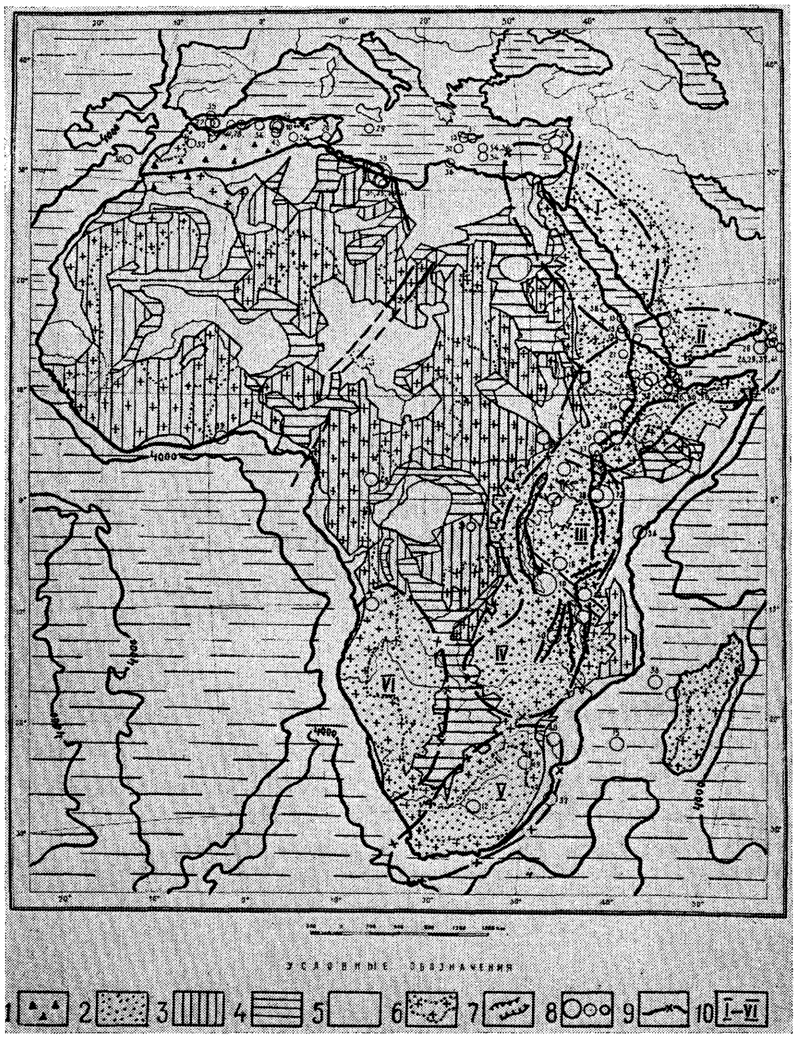

On neotectonics of Africa in connection with its seismicity.

Fig. 1 : The map table of the Neotectonics of Africa.

I. Significant Mountain Building Areas :

1. Epigeosynclinal or young mountains having arch-folded structure.
2. Epiplatform or rejuvenated mountains having arch-blocked structure.

II. Platform areas of unimportant Mountain Building :

3. Uplifts; 4. Slopes of conjugated uplifts and depressions; 5. Depressions; 6. The foundation exposures / Pre-Paleozoic and Paleozoic (not dismembered) /; 7. Main Breaks; 8. Earthquake epicentres (after G. P. Gorshkov); 9. Suppositious contours of megabrachy folds (I-VI); 10. I-Arabia, II-Abyssinia, III-Tanganyika, IV-Nyassaland, V-Drakenberg, VI-Angola.

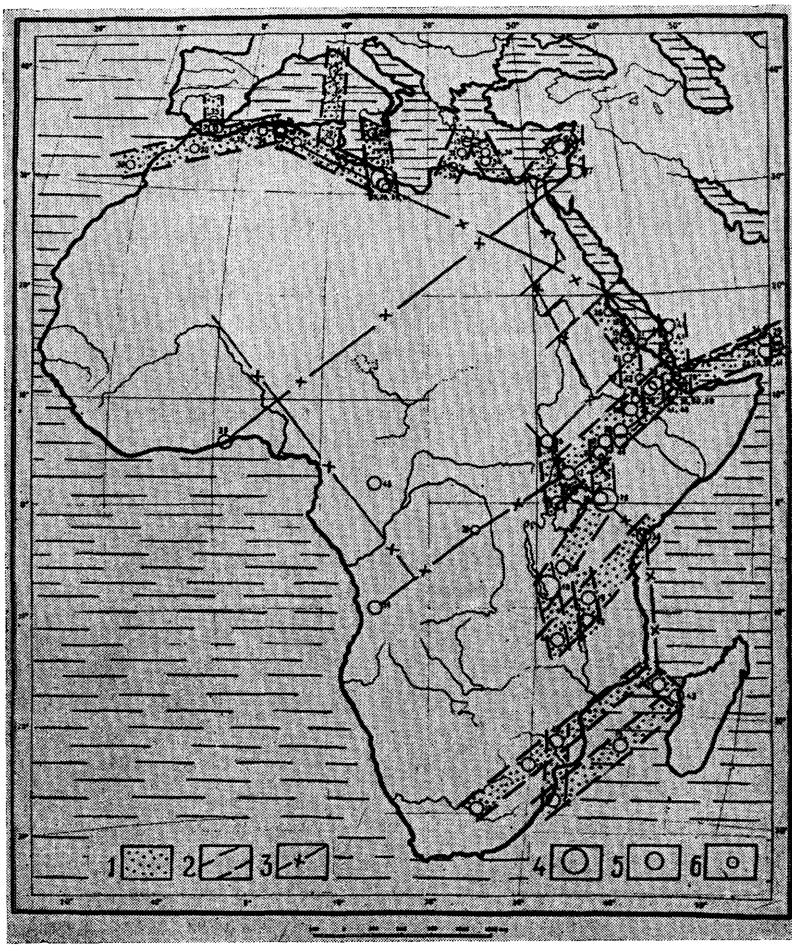

FIG. 2 : Map-table of the spatial distribution of high concentration of earthquakes. Conventional marks : 1. rough outlines of the areas of the concentration of earthquakes; 2. main directions showing significant earthquakes; 3. different comparable lines; 4-5-6. earthquake epicentres of class *b, c* (after G. P. Gorshkov, 1962).

them in the north of the African coast are recognized Gibraltar, Tripolitan-Sicilian, Cretan and Cyprian dams. In the NE the Madagascar dam is highly seismic. There are given maps of the bottom relief of sea and ocean depressions in their connection with orographic forms of adjacent continental areas.

5. Each of the above mentioned areas of high seismicity possesses peculiar features of recent development, general features being the unchanging confinement of high seismicity to actively developing

positive structural forms and breaks zones of a definite strike. Typical associations of ruptures and breaks of the African continent may be established by the comparative analysis of 1) fracture, rupture zones, 2) characteristic lineament of recent relief, 3) « pattern » of a hydrographic system, generalized coast lines, shelf, continental slope and the main uplands and depressions of the African continent as well (*fig.* 2).

There may be separated : The NE Red Sea direction defining generalized outlines of the Red Sea, the coasts of SW Africa near the Cape Mountains and other regions as well (*fig.* 3, strike diagrams).

The Atlas — the second, no less extensive NE direction is peculiar to generalized outlines of separate coast areas where the SW Atlas Mountain system plunges.

This (NE) direction determines the mainland outlines (of considerable extension) along the Drakenberg Mountains and other coastal areas as well. Within the northern coast, shelf and continental slope of Africa the Mediterranean, that is, W-NW strike is characterized by its considerable extension. It determines the direction of low-lying coast of Africa in the Libyan desert from the Gulf of Gabes to the mouth of the Nile. Both the Mozambique-submeridional and the Madagascar directions stretch in the SE of Africa within the Mozambique Strait area and in other regions. The Aden sublatitudinal E-NE strike is less common. It characterizes the southern coast of the Gulf of Aden in the Somali region — the Atlas coast from Gibraltar to Bizerte, and some other places. In this way it is universally established that the outlines of the continental slope in their more gentle and generalized form repeat the coastline contours.

6. The correlation of the configuration of lowlands and uplands abutting against the coastal zone evidences that the above mentioned main strikes determine not only the contours of the major continental elements but at the same time they predeterminate the river valley outlines. Under the conditions of a most expansive foundation of « hard » rocks the hydrographic pattern adjusts to the fissured and ruptured systems as the most favourable ones with regard to denudation. Under given conditions, therefore, the analysis of the hydrographic pattern indicates indirectly the arrangement of a rupture system which has been actively developing in recent time. This regular construction suggests that the relief outlines of the whole African continent are, in the main, determined

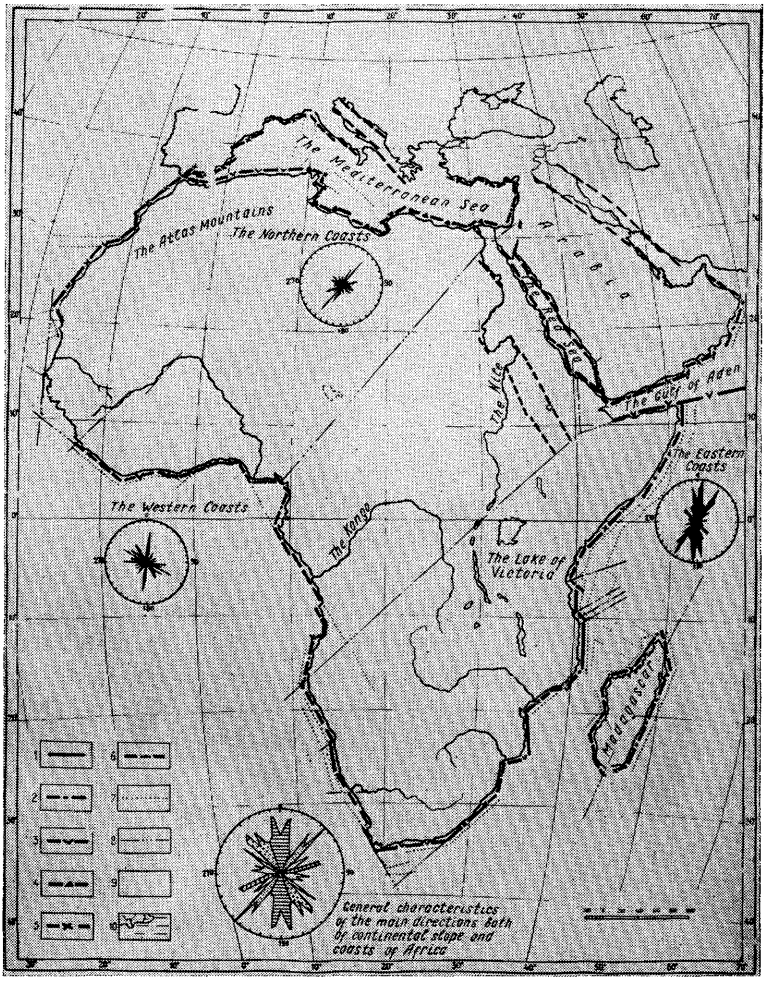

FIG. 3 : map-table of the main strike of the coast of Africa.

I. Meridional and related ones :
1. nearly meridional — Mozambique; 2. N-NE — Madagascar.
II. Latitudinal and sublatitudinal :
3. NE Aden; 4. W-NW Mediterranean.
III. Diagonal :
5. NE Atlas; 6. NW the Red Sea; 7. Generalized strikes of the continental slope; 8. different comparable lines; 9. dry lands; 10. sea and ocean depressions.
Special marks showing the direction of coasts and continental slopes adjoining them (in graphs) : 1. Mozambique; 2. Atlas; 3. Aden; 4. the Red Sea.
Note : The main directions have been defined according to the mean values of the shelf outer rim and the upper part of the African mainland continental slope.

by regional deep-seated ruptures of the above mentioned directions.

In the south of Africa of great importance are the breaks of the Mozambique strike together with the Atlas and the Red Sea ones. In the north of Africa prevail Mediterranean and Aden sublatitudinal strikes in combination with the Mozambique one.

7. Comparing the outlines of upheaval and the depression zones of the platform areas of Africa permits establishing the configuration similitude of the largest structures of the Atlantic Ocean and the African continent due to the regular changes in strike within the equatorial latitudes. To illustrate this statement it is necessary to compare the changes in strike of great oceanic depressions such as the Angola, the Guinea, North African and as well as the Atlantic Range with a general strike of the continental slope of Africa. Within the continent the general « pattern » of arrangement of upheavals and depressions retains the same character : The North African zone of upheavals — Sierra Leone, Cameroons and Angola repeats the strike of both the western coast and the continental slope of Africa. The central zone of hinterland depressions parallels them. (Senegal, Tchad, Congo-Kalahari). The same plan of uplifts persists in Arabio-African zone but is less clear-cut. Within the continent the upbuilding of the uplift and the depression zones which in their outlines are very near to recent ones (having sharply expressed changes from sublatitudinal to submeridional strike) seems to date from the Paleozoic. This suggests that the recent outlines of the above-mentioned large uplifts and depressions of the Atlantic Ocean are ancient and have already existed as far as the Upper Paleozoic.

Their hypsometric position is not clear and it must have been somewhat higher.

The study of the « continent-ocean » boundary zone suggests that apart from the similitude of a general plan of uplifts and depressions there are marked orographic and some seemingly genetic relation to recent structural forms of the continent and the main uplifts and depressions in the boundary zone of the ocean areas.

The Atlas mountainous country runs as a submarine upland with volcanic edifices (Cape Verde Islands and, perhaps, Canary Islands).

The uplift of the platform area of Africa is connected with the submarine rampart and with the main Atlantic trunk in the area of its sharp change of strike in the equatorial latitudes.

Megabrachy fold systems of the Arabio-African rejuvenated mountainous country are connected with linear ranges — Walfish and Cape uplifts and with submarine uplift system in the Mozambique area uniting Africa and Madagascar.

EINIGE MÖGLICHKEITEN DER FORTFÜHRUNG SEISMOLOGISCHER ERDKRUSTENFORSCHUNG DURCH WEITERE GEOLOGISCH-GEOPHYSIKALISCHE UNTERSUCHUNGSMETHODEN

von ROBERT LAUTERBACH (Leipzig)

Die seismologische Erforschung der Erdkruste und des oberen Mantels strebt in erster Linie die Ermittelung der *Tiefenlage der wichtigsten Diskontinuitäten* an : in Mitteleuropa sind dies die FÖRTSCH-Diskontinuität (etwa 5 500 m/s gegen etwa 6 000 m/s), die CONRAD-Diskontinuität (etwa 6 000 m/s gegen etwa 6 500 m/s), die « CM-Diskontinuität » nach LIEBSCHER bei DOHR — 1962 — (6 500 m/s gegen 7 100 m/s) und die MOHOROVIČIĆ-Diskontinuität (7 100 m/s gegen etwas über 8 000 m/s).

Weiterhin ergibt sich die Notwendigkeit, der Untersuchung des *Reliefs dieser Diskontinuitäten* Aufmerksamkeit zuzuwenden, um damit die feinere Struktur der Erdkruste und der Manteloberfläche zu erfassen; eine Frage, die zugleich ökonomische Perspektiven besitzt (REICHENBACH und SCHMIDT, 1959).

Eine Reihe von Autoren hat sich erfolgreich mit der Frage nach den Zusammenhängen zwischen großen regionalen gravimetrischen und magnetischen Anomalien einerseits und den seismisch nachgewiesenen Reliefstrukturen der Diskontinuitäten andererseits befaßt. Dies geschieht besonders intensiv, seit bei reflexionsseismischen Routinemessungen auswertbare Reflexionen langer Laufzeit gewonnen werden (SCHULZ — 1957 — und DOHR — 1959, 1962 —). Auch bei speziellen tiefenseismischen Sondierungen wurden *Isohypsenpläne von Schichtgrenzen* der Erdkruste entworfen (vgl. z. B. WEIZMAN u. a. sowie GALPERIN u. a. — 1962 —). Dabei ergaben sich mehrfach deutliche Zusammenhänge zwischen der Deformation der Diskontinuitäten und mehr oder weniger vertikalen *tektonischen Bruchstrukturen* der Erdkruste.

Ein besonders treffendes deutsches Beispiel hat DOHR (1959) vom oberen *Rheintalgraben* — Gebiet veröffentlicht. Dieses nach dem Gang seiner Erforschung fast als klassisch zu bezeichnende, NNO (rheinisch) streichende Lineament wird sehr wahrscheinlich von einer trogartigen *Einsenkung der* CONRAD-*Diskontinuität* begleitet. Das zeigt, daß der oberflächlich gegebene tektonische Baustil bis in größere Krustentiefe der Tendenz nach anhält. Hierzu kann ergänzend noch festgestellt werden, daß sich diese Struktur der CONRAD-Diskontinuität überraschend gut mit einem regionalen *magnetischen Minimum* der Vertikalkomponente deckt (nach Ergebnissen der früheren Kommission zur Geophysikalischen Reichsaufnahme unter Leitung von O. BARSCH).

Das Interesse an der Weiterverfolgung dieser Zusammenhänge ist inzwischen noch gestiegen, seit zahlreiche Autoren die Wechselhaftigkeit der strukturellen Ausbildung besonders der CONRAD-Diskontinuität, aber teilweise abgeschwächt auch noch der MOHOROVIČIĆ-Diskontinuität feststellen konnten. Die Klärung dieser Fragen gewinnt damit immer mehr an Bedeutung nicht allein für die Erforschung des Großbaues der Erdkruste schlechthin, sondern auch für ökonomisch-geologische Probleme, auf die hier nicht eingegangen werden kann. Es sind jedoch bereits Ansätze vorhanden und weitere Beispiele dafür zu erwarten, daß die Aufsuchung von Lagerstättenbezirken u. U. rascher auf dem nur scheinbaren Umweg über die Tiefenerkundung der Erdkruste zu ermöglichen ist als durch konventionelle geologische und geophysikalische Arbeiten allein.

Dabei spielt der *Zusammenhang zwischen Struktur der krustalen Schichtgrenzen und Lineamenten* eine bedeutende Rolle. Tiefreichende Bruchzonen in der Erdkruste sind Bereiche mehr oder weniger starker Stabilitätsverminderung insbesondere der oberen Erdkruste. Das aber scheint angesichts der permanenten statischen und vor allem dynamischen Beanspruchung der Erdkruste eine besonders wichtige Voraussetzung für die Ausbildung der genannten Strukturen tieferer Diskontinuitäten zu sein. Hierzu sei lediglich ein *Beispiel* angeführt.

Nach CLOOS (1948) ist in *Abbildung 1* die Halbierung der antipazifischen Erdkalotte durch die große « rheinische » Geofraktur wiedergegeben. In Mitteleuropa liegt an der auffallenden Stelle der Verzweigung (und z. T. Kreuzung) dieser planetaren Bruchstruktur das *Flechtinger oder Magdeburger Schwerehoch* (« Fl.-H. » in *Abbildung 1*). Verfasser hat diese Anomalie auf die Möglichkeiten ihrer Interpretation näher geprüft (LAUTERBACH — 1962a, 1963 —). Sie ist offenbar das Ergebnis einer *Aufwölbung der* MOHOROVIČIĆ-*Diskontinuität* an der Stelle der *Kreuzung zweier tiefreichender Lineamente* (*Abbildung 2, Skizze 4*). Eines davon hat rheinische Richtung und ist eine der Fortsetzungen des bereits erwähnten Oberrheintalgraben-Lineamentes. Hier wie dort ist die CONRAD-*Diskontinuität* offenbar *eingesenkt*. Die Skizzen 1, 2 und 3 in Abbildung 2 sollen die denkbare Art der Herausbildung dieser krustalen Struktur darstellen, wenn man die verschiedenen tektonischen Entwicklungsphasen mit Wechsel von Einengung und Zerrung berücksichtigt.

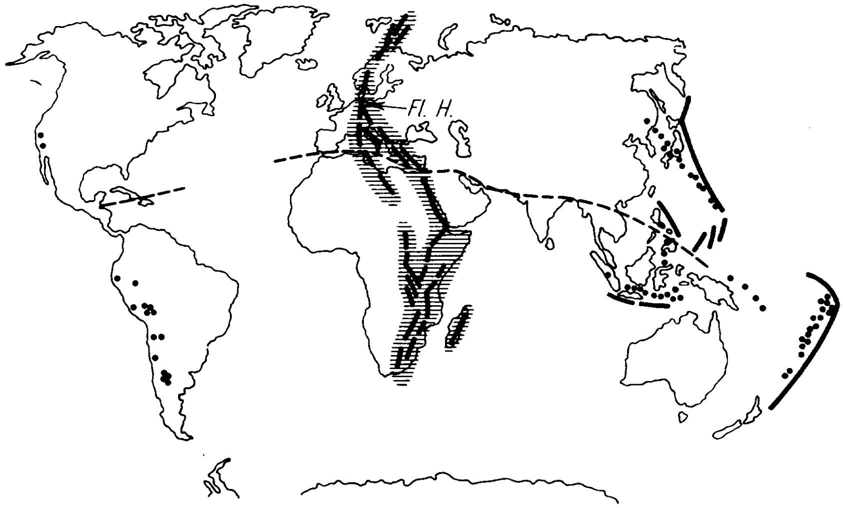

Abbildung 1 : Die Halbierung der antipazifischen Erdkalotte durch die europäisch-afrikanische Geofraktur nach Cloos (1948). Fl. H. = Lage des Flechtinger (Magdeburger) Schwerehochs. Schraffiert : die mediane Bruchzone. Starke Linien : Tiefseerinnen. Punkte : Tiefherdbeben. Gestrichelte West-Ost-Linie : Grenze zwischen Nord- und Süderde.

Dieses Beispiel zeigt die Bedeutung der *Verknüpfung geophysikalischer und tektonischer Krustenforschung*. Die in erster Linie geologisch nachweisbaren Lineamente sind Zonen der Auslösung und Verknüpfung untereinander ähnlicher Reaktionsformen der Erdkruste. Ein in einigen Punkten gutes (in anderen unbrauchbares Modell) hierzu ist die Ausbildung von Salzstrukturen als Folge von Brüchen des Hangenden.

Lineamente sind gleichzeitig Zonen erhöhter seismischer Aktivität der Erdkruste und insofern von ursprünglicher Bedeutung für die Erforschung des Baues der Kruste (vgl. z. B. Lauterbach — 1953/54 —).

Eine besondere seismische, tektonische und schließlich auch strukturbildende Aktivität weisen *meridionale bis submeridionale Lineamente auf*. In allen Kontinenten findet man sie verbreitet. Die Verbreitung und ihre große Rolle bei der Herausbildung der kontinentalen wie ozeanischen Strukturen der Kruste verdanken sie zweifellos der Tatsache, daß sie als Folge der Deformation der rotierenden Erde erdgeschichtlich frühzeitig angelegt und

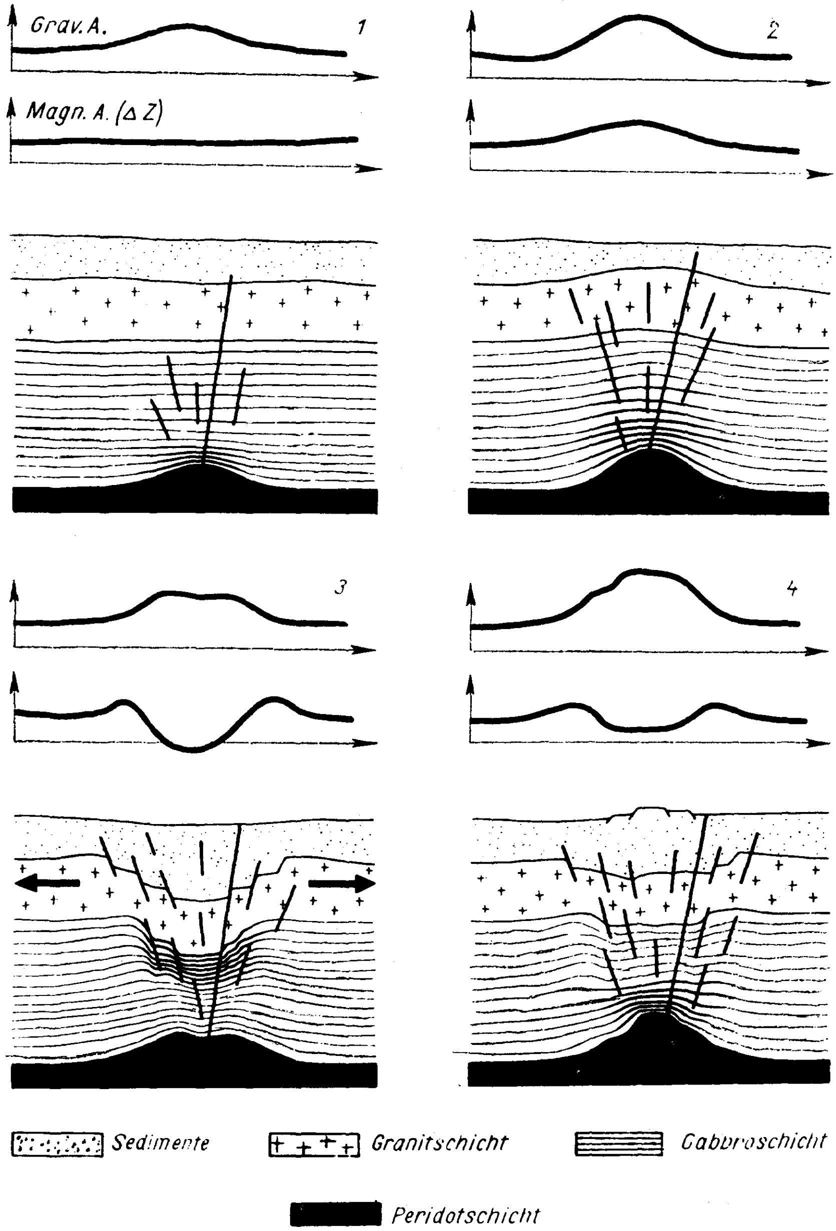

ABBILDUNG 2 : Denkbarer Werdegang des Flechtinger (Magdeburger) Massivs im Bereich der Kreuzung zweier Geofrakturen unter der abwechselnden Einwirkung kompressiver und distraktiver tektonischer Tendenzen. Das Massiv ist als Schwerehoch Kernstück eines rhenotypen Lineamentes, es wird von magnetischen ΔZ - Anomalien flankiert. Skizze 1 bis 3 : möglicher Werdegang, Skizze 4 : Interpretation der bislang vorliegenden seismischen, gravimetrischen und magnetischen sowie thermischen Ergebnisse.

überall bis in die Gegenwart mobil erhalten blieben (vgl. z. B. WORONOW, 1962).

Lineamente werden ganz allgemein und besonders wenn sie vom letztgenannten Typ sind — wegen der damit notwendigerweise verbundenen Distraktivtendenzen — häufig als *Aufstiegswege von Magmen* aus der Tiefe benutzt. Von besonderem Interesse ist hierbei der Stoff der *Gabbro* — als auch der *Peridotitschicht* und gegebenenfalls noch tieferer Schichten des Erdmantels.

Die *Interpretation gravimetrischer* wie auch *magnetischer Anomalien* in Zusammenhang mit seismischer Krustenforschung wirft eine Reihe noch offener Fragen auf. Bleiben wir bei dem stellvertretend für zahlreiche andere Ergebnisse behandelten Beispiel der Abbildung 2.

Hier wäre es notwendig, folgende Probleme zu klären :

1) Ist die Dichtedifferenz an der MOHOROVIČIĆ-Diskontinuität tatsächlich so groß, daß sie für die Ausbildung der gravimetrischen Anomalie von dominierendem Einfluß ist? Dies wird zwar häufig bei Interpretationsversuchen vorausgesetzt, indes fehlt noch eine umfassende Untersuchung, weil es naturgemäß schwer ist, die von der Erdoberfläche aus zugänglichen Sendboten der Tiefe als solche zu identifizieren bzw. den Grad ihrer Juvenilität zu ermitteln. Hinzu kommt sodann die schwierige Klärung der Druckabhängigkeit der Dichte und des stofflichen Bestandes.

2) Warum wird diese gravimetrische Anomalie nicht von einer magnetischen Anomalie begleitet, wie dies in anderen Fällen durchaus zutrifft? Statt dessen wird sie von schwachen magnetischen Störungen gesäumt. Liegt dies in erster Linie (wie hier vorausgesetzt) an der Tiefenlage der CONRAD-Diskontinuität mit Einsenkung unter die Curietemperatur-Isothermalfläche des Magnetits? Oder weist die Gabbrofamilie in ihrem mittleren Stoffbestand einen prozentual hohen Anteil schwach magnetischer Glieder auf?

Diese und weitere Fragen sind für die Untersuchung des nach unten zunehmend basischer werdenden magmatischen bzw. magmatogenen Stoffes der Erdkruste von besonderer Wichtigkeit.

Als Schlußfolgerung aus diesen Beispielen, die stellvertretend für eine größere Zahl von in Bearbeitung stehenden Fragen herausgegriffen wurden, ergibt sich z. B. die Notwendigkeit der Klärung,

1) ob man juvenile, also nicht hybride basische Produkte (meist als magmatische Förderung in bzw. aus Lineamenten) als solche identifizieren kann und

2) welche petrophysikalischen Eigenschaften sie aufweisen.

Zu Punkt 1 läßt sich nunmehr eine Antwort geben. Mehrjährige petrophysikalische Untersuchungen des Instituts für Geophysikalische Erkundung an der Karl-Marx-Universität Leipzig zeigen, daß sich die Gamma-Aktivität *basischer Vulkanite* zur Ermittelung des Grades ihrer *Tiefenherkunft* am besten von allen petrophysikalischen Untersuchungsmethoden eignet. Allerdings genügt nicht die integrale Aktivitätsmessung, es bedarf vielmehr der *spektralen Untersuchung der Gamma-Strahlung* auf ihre U/Ra-, Th- und K^{40}-bedingten Anteile. Wie bereits berichtet (LAUTERBACH — 1962 b —), ist diese schwierige Aufgabe — insbesondere was die Reproduzierbarkeit der Ergebnisse anlangt — mit mäßigem technischem Aufwand und zudem noch geringer Probenmenge (1 Handstück zu 400-500 g) in obigem Institut gelöst worden. Das Ergebnis ist sehr interessant : Aus großen Serien von gamma-spektrometrischen Aufnahmen sei in *Abbildung 3* ein Beispiel anhand dreier Spektren gezeigt : Basalte (aber auch Diabase oder Melaphyre usw.) die nach der gesamten geologisch-tektonischen Situation sehr rasch aus großer Tiefe aufgestiegen sein müssen, zeigen eine besonders geringe K^{40}-Aktivität (1,46 MeV), aber auch verminderte RaC′-(1,12 MeV) und MsTh2-Aktivität (i. M. 0,93 MeV) (vgl. *Abbildung 3*, rechts). Hierzu gehört z. B. der Plateaubasalt aus dem Hochland von Dekhan (Indien) und mehrere Ozeanite. Je längere Verweilzeit der basischen Schmelze offenbar in der oberen Kruste zur Verfügung stand, desto weiter entfernen sich die Gamma-Spektren der vulkanischen Erstarrungsprodukte von diesem Prototyp (*Abbildung 3*, Mitte und links). Eine Basaltprovinz des letzteren Typs ist z. B. die der Eifel.

Zahllose Einzeluntersuchungen zeigen somit, daß es mit einem relativ hohen Grad von Wahrscheinlichkeit (ermittelt an wohl definiertem und bestimmtem Vergleichsmaterial aus Institutssammlungen) möglich ist, die relativ am wenigsten veränderten basischen Magmatite zu ermitteln. Dabei wurde den Vulkaniten deshalb der Vorzug gegeben, weil sie einer geringeren magmatischen Differentiation unterlagen als die entsprechenden Plutonite und weil schließlich auch die sialische Beeinflussung hier — je nach den Aufstiegsbedingungen — kleiner bleiben kann.

Somit nun war es möglich, besser zielgerichtet an die Untersuchung der weiteren *petrophysikalischen Eigenschaften* dieser Gesteine heranzugehen. Durch einen Mitarbeiter des Verf., P. FABIANEK, wurde zunächst mit einer statistischen Bearbeitung der *magnetischen Suszeptibilität basischer Magmatite* begonnen. Die notwendigen sehr großen Reihen und die infolgedessen nicht immer leichte Beschaffung von Material zunächst mit Schwerpunkt aus Europa sind die Ursache dafür, daß diese Arbeit noch nicht abgeschlossen ist. Aus einer Zwischenbilanz kann man jedoch schon jetzt folgendes entnehmen :

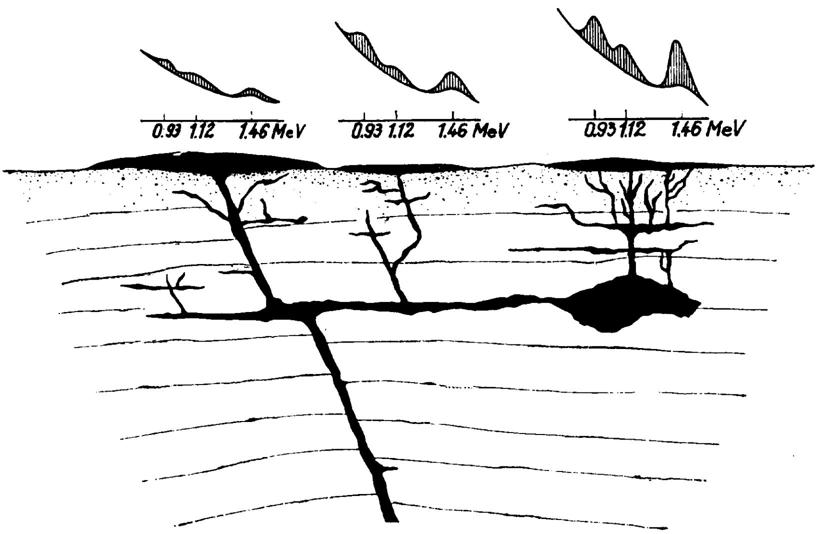

ABBILDUNG 3 : Drei Gamma-Spektren (Ausschnitte von 0,8 bis 1,6 MeV) von verschiedenen Basalttypen. Rechts : Plateaubasalt; links : hybrider Basalt; Mitte : Übergangstyp. Folgende Gamma-Linien sind dargestellt :
0,93 MeV : MsTh 2. — 1,12 MeV : RaC'. — 1,46 MeV : K^{40}.
Plateaubasalte und Ozeanite sowie andere simatische junge und alte Vulkanite (Diabase, Melaphyre) zeigen geringe K^{40}-, Ra- und z. T. Th-Aktivität. Sialisch beeinflußte basische Vulkanite sind durch starken Aktivitätsanstieg gekennzeichnet. Damit ist die Identifizierung tiefreichender Förderzonen mit Lineamentcharakter möglich.

66 % aller untersuchten *Gabbros* besitzen eine magnetische Suszeptibilität zwischen 0 und 100.10^{-6}. Ein Nebenmaximum findet sich im Bereich von $1\,000$-$3\,000.10^{-6}$ (nur 6 %).

42 % aller untersuchten *Basalte* zeigen magnetische Suszeptibilitätswerte zwischen $1\,000$-$3\,000.10^{-6}$. Nur 3 % zeigen Werte jenes Bereiches, in dem 66 % aller Gabbros liegen (0 bis 100.10^{-6}).

Peridotite zeigen ein weniger klares Bild, neigen in der Verteilung der Suszeptibilitätswerte aber wohl mehr den Basalten zu : 27 % der untersuchten Gesteine liegen im Bereich von 500-$1\,000.10^{-6}$, nur knapp 6 % im Intervall von 0-100.10^{-6}, wo sich das Gabbromaximum befindet.

Nach dem aus verschiedenen Gründen noch unzureichenden Ergebnis, das keine schematische Deutung zuläßt, ergibt sich aber durchaus die Möglichkeit, daß *Aufwölbungen der Gabbroschicht keine magnetischen Anomalien hervorrufen müssen.* Es zeigt sich ferner, daß die Reihe Gabbro-Peridotit-Basalt eine Reihe der Zunahme der magnetischen Suszeptibilität der entsprechenden Oberflächengesteine ist. Es ist nicht ausgeschlossen, daß es sich hier gleichzeitig um eine Tiefensequenz handelt.

Die jetzigen Resultate deuten an, daß die *gamma-spektrometrische Sortierung* nach stärker juvenilem und mehr hydridem basischen Material voraussichtlich ein noch klareres Bild der petrophysikalischen Eigenschaften von basischen Tiefengesteinen geben wird. Dies deshalb, weil mit dieser Methode die Berechtigung bzw. Unzulässigkeit der Übertragung von Schlußfolgerungen aus Gesteinsuntersuchungen von Oberflächenmaterial auf die tiefen Schichten kritisch überprüft werden kann.

Die Gamma-Spektrometrie von basischen Magmatiten, insbesondere von Vulkaniten (Basalten, Diabasen, Melaphyren u. s. w.) beginnt sich bereits als Hilfsmittel des Nachweises tief reichender Förderzonen von Lineamentcharakter zu bewähren. Sie gibt damit *Hinweise auf Schwächezonen* der Erdkruste, die ihrerseits für die Ausbildung von *Reliefstrukturen seismischer Diskontinuitätsflächen* eine große Rolle gespielt haben.

Literaturverzeichnis

Cloos (H.). Grundschollen und Erdnähte. Geologische Rundschau, *35*, 2, Stuttgart 1948.

Dohr (G.). Über die Beobachtungen von Reflexionen aus dem tieferen Untergrunde im Rahmen routinemäßiger reflexionsseismischer Messungen. Z. f. Geophysik, *25*, H. 6, 1959.

Dohr (G.). Untersuchungen über den Bau der Erdkruste in Westdeutschland durch reflexionsseismische Messungen. Bolletino di Geofisica teorica e applicata, Vol. IV, Nr. 14, 1962.

Galperin (E. I.), Kosminskaja (I. P.), Krakschina (R. M.). Hauptcharakteristiken tiefer Wellen, registriert bei seismischen Tiefensondierungen im zentralen Teil des Kaspi-Sees. Glubinnoje Seismičeskoje Sondirowanije Semnoj Kory w SSSR, Leningrad, 1962.

Lauterbach (R.). Beiträge zur tektonischen Deutung der geomagnetischen Übersichtskarte der Deutschen Demokratischen Republik. Wissenschaftliche Zeitschrift der Karl-Marx-Universität Leipzig *3*, Math.-Nat. Reihe, Heft 3, 1953/54 und Gerl. Beitr. z. Geophysik, *64*, 1955.

Lauterbach (R.). Rhenotype Strukturen im Bilde geologisch-geophysikalischer Untersuchungsergebnisse Mitteleuropas. Berichte der Geologischen Gesellschaft in der DDR, Band 6, Heft 3, 1962 a.

Lauterbach (R.). Gamma-Spektrogramme von Basalten und anderen natürlichen Gesteinen ohne erhöhte Radioaktivität. Geophysik und Geologie, Folge 4, Leipzig, 1962 b.

LAUTERBACH (R.). Das Flechtinger Massiv, Abh. d. Klasse für Chemie, Geologie und Biologie der Deutschen Akademie der Wissenschaften, Berlin, 1964, Festschrift f. Prof. D[r] DEUBEL.

REICHENBACH (R.) und SCHMIDT (G.). Results of Surface Reflection Seismic Measurements in the Siderite District of the Siegerland. Geophys. Prospecting VII, 3, 1959.

SCHULZ (G.). Reflexionen aus dem kristallinen Untergrund des Pfälzer Berglandes. Z. f. Geophysik, *23*, 1957.

WEIZMAN (P. S.), KOSMINSKAJA (I. P.), MICHOTA (G. G.), TULINA (J. W.). Hauptcharakteristiken tiefer Wellen, registriert in den Gebieten des nördlichen Tien-Schan, Pamir-Alai und südwestlichen Turkmenien. Glubinnoje Seismičeskoje Sondirowanije Semnoj Kory w SSSR, Leningrad 1962.

WORONOW (P. S.. Über die Abhängigkeit des morphologischen Strukturplanes der Arktis und Antarktis von den Rotationskräften der Erde. Geografitscheskij Sbornik, XV Astrogeologija, Ak. Nauk SSSR, 1962.

ON THE COMPOSITION OF MICROSEISMS AND SOME OBSERVATIONS ON THEIR SOURCES

by V. N. TABULEVICH and E. F. SAVARENSKY

The first attempt to locate microseismic sources using amplitude relations of three remote seismic stations was made by GILMORE [1]. Due to considerable discrepancies this method, however, has received no further development. A somewhat different approach to amplitude location was suggested by authors of present paper [2, 3, 4] and applied to conditions of microseisms of the Caspian sea and in the Oceans. The choise of stations suitable for the location of sources of microseismic excitation was based on the principle of frequency synchronism.

Comparison of microseismic vibrations in two reception points led to a relation of the form :

$$\frac{A_1}{A_2} = \frac{r_2^{n_2}}{r_1^{n_1}}, \tag{1}$$

where $A_{1,2}$ are averaged amplitudes of microseisms in reception points 1, 2, $r_{1,2}$ — distances between points of reception and source of microseisms and $n_{1,2}$ — some exponents. Taking pairs of reception points, which satisfy the frequency synchronism condition, an area of circle intersection is obtained, which is considered as a source of microseismic excitation. Originally the exponents were selected to obtain a minimum of the area of circle intersection. Actually a considerable number of constructions showed n to vary from 3/2 to 1.

Now we turn to the determination of n from other considerations.

There is a widespread opinion, that microseismic vibrations are composed of surface waves of the Rayleigh and Love types only. A justification of this view is usually seen in the fact, that their amplitudes decrease, as $r^{\frac{1}{2}}$, whereas the amplitudes of body waves decrease more rapidly.

Considering earthquakes — processes of impulsive excitation of the earth's crust — it is not necessary to accept hypotheses on the composition of the vibrations, because the latter is uniquely determined by the phases of arrival of various types of waves.

Unlike to earthquakes, however, microseismic vibrations are more or less stationary phenomena. The investigator deals with a *resultant* vibration which is a superposition of all types of body, surfacional, reflected and secondary waves, polarized *randomly* in space.

There exist any procedures, allowing a unique spliting of this process into physically real wave components and hence giving a prove of the hypotesis about the surfacional nature of microseisms. It is possible, however, to consider phenomena of impulsive excitation of the earth's crust, which are analogous to microseisms. It should permit a greater certainity of judgements on this subject.

Phenomena of this kind to be considered are particularly earthquakes with shallow sources. Records of even remote earthquakes permit to discover not only surfacional waves, but also body waves adequate to the distance of the source. The process of microseismic excitation can differ only quantitatively from the excitation of the earth's crust by earthquakes with shallow sources. In both cases an action of compressional waves in air and in water on the earth's crust takes place (see, for instance [5]).

Suppose now, that the source of vibrations acts in a definite point of the earth's crust and is of a periodic (microseisms), rather than of an impulsive (explosion, earthquake) nature. The investigator, in attempting to determine the azimuth of the source, is inclined to ascribe the bulk of the vibrations to surfacional Rayleigh waves of an amplitude A_{RH}. The actual displacement of a point, however, will be determined by the geometrical sum of the projections of waves vectors of body (P_H, S_H) and surfacional (R) waves on a horizontal plane :

$$\bar{A}_H = \bar{A}_{RH} + \bar{A}_{SH} + \bar{A}_{PH}.$$

Figure 1 shows horizontal wave vector P_H, S_H, L_H and R_H actually recorded by seismic station Makhachkala in the case of an earthquake in the Golf of Aden December 21, 1959. Consider this case to concretize assumptions mentioned above. From figure 1 b it may be already seen, that the vector S_H gives rise to considerable azimuth distortion. For our purpose it is reasonable to suppose the possibility of a case, when the moduli of the wave vectors are in the same relations as in figure 1 a, but their spacial pattern is essentially more distorted, for structural and geographical reasons.

For estimation purposes take, that $\bar{A}_{PH}$ and $\bar{A}_{SH}$ ($\bar{A}_{PH} \ll \bar{A}_{SH}$) have the same direction. Then $\bar{A}_{PH} + \bar{A}_{SH} = | A_{PH} + A_{SH} |$. Suppose further that the polarization planes of surfacional and body waves form in space an angle $\pm \varphi$ (*fig.* 1 *c*). To determine the fraction of

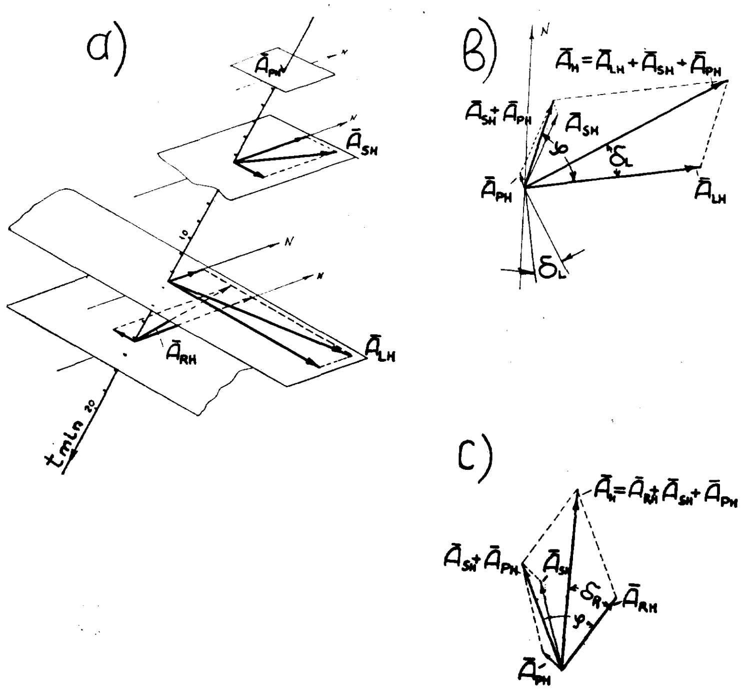

FIG. 1. — Distortion of the azimuth of a source of microseisms in the case of simplifying assumptions on the composition of vibrations.

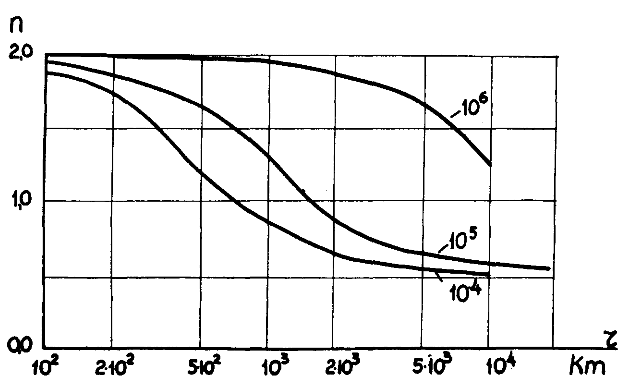

FIG. 2. — Theoretical relation of *a/b* from distance.

azimutal distortion introduced by body waves P_H and S_H interacting with R waves :

$$\operatorname{tg} \delta_R = \frac{(A_{SH} + A_{PH}) \sin \varphi}{A_{RH} + (A_{PH} + A_{SH}) \cos \varphi} . \tag{2}$$

The distortion angle will be $\pm\ \delta_R$ or $2\ \delta_R$.

A similar distortion arises, when P_H, S_H and L_H vibrations are ascribed exclusively to L_H-vibrations. The resultant amplitude of vibrations will be determined by the sum of the vectors $\overline{A}_H = \overline{A}_{LH} + \overline{A}_{PH} + \overline{A}_{SH}$, and

$$\operatorname{tg} \delta_L = \frac{(A_{PH} + A_{SH}) \sin \varphi}{A_L + (A_{PH} + A_{SH}) \cos \varphi} .$$

Here again appears an angle of distortion $\pm\ \delta_L$ or $2\ \delta_L$.

Generally the distortion will be :

$$\overline{A}_H = \Sigma\ \overline{A}_{LH} + \Sigma\ \overline{A}_{RH} + \Sigma\ \overline{A}_{PH} + \Sigma\ \overline{A}_{SH},$$

where $\Sigma\ \overline{A}_{PH}$ and $\Sigma\ \overline{A}_{SH}$ is the geometrical sum of the whole complex of reflected and refracted wave vectors, respectively. For our illustrative purposes such cases will be not considered.

In order to determine the azimuth distortion of a microseismic source ($2\ \delta$) as a function of distance, a number of records of earthquakes with shallow sources was considered. For sources of microseisms with distances less than 45 deg. $2\ \delta$ = 45-90 deg. Only for distances up to 80 deg. the relative role of surfacional waves increased to give azimuth distortions $2\ \delta$ of 10-20 deg.

Hence, the bulk of microseisms, recorded even at considerable distances, is apparently to some degree composed of body waves. The Phase-location Method of determining a microseismic source precludes the prospecting of a procedure of finding the individual phases of the variety of the arriving waves whereas the Amplitude-location Method requires the knowledge of the fraction of body waves in the wave train. Consider this question in more detail.

(a) *In the case of impulsive excitation* definite types of vibrations due to dispersion diverge in the form of different wave trains, the time of arrival of wich corresponds to their phase velocities. In the absence of dissipative forces, the energy of the i-th wave train, passing a fixed surface S_i which has the form of a wave front, will invariant :

$$E_i = \text{Const} = C_1 \oint_{Si} d\ S_i \int_{-\infty}^{+\infty} \dot{u}_i^2\ dt = C_2 \oint_{Si} dS_i \int_{-\infty}^{+\infty} \Phi_i^2(\omega)\ d\omega .$$

Here $C_{1\cdot 2}$ are constants, $\Phi_i(\omega)$ — the frequency spectrum of the i-th wave train, $\dot{u}_i$ — the instantanous velocity of the vibration.

In the case of surfacional waves we can assume S_i to be cylindric surfaces. Hence, we have :

$$E_i = \text{const} = C_1\, r \int_{-\infty}^{+\infty} \dot{u}_i^2\, dt = C_2\, r \int_0^{\infty} \Phi^2 (\omega)\, d\omega$$

$$\frac{\text{const}}{r} = \int_{-\infty}^{+\infty} \dot{u}_i^2\, dt \approx C_3\, \omega_i^2\, \tau_i \sum_{n=1}^{N} A^2_{ni} = \frac{N_i^3}{T_i}\, \overline{A}_i^2 \;,$$

$$\overline{A}_i = \frac{1}{N} \sqrt{\sum_{n=1}^{N} A^2_{ni}} \;. \qquad (3)$$

Consequently, the decrease of amplitudes with distances will obey the relation :

$$\overline{A}_i = \frac{\text{const}\ T^{\frac{1}{2}}}{N^{3/2}\, r^{\frac{1}{2}}} \qquad (4)$$

In the case of body waves the form of a wave front can not be taken as a constant and it is impossible to perform the operation $\oint_{Si} d\, S_i$. Therefore we shall make the assumption, that the « surface » of the wave front varies as r^{2k}.

$$E_i = \text{const} = C_1\, r^{2k} \int_{-\infty}^{+\infty} \dot{u}_i^2\, \text{dt} = C_2 r^{2k} \int_{-\infty}^{+\infty} \Phi^2 (\omega)\, d\omega$$

and

$$\frac{\text{const}}{r^{2k}} = \int_{-\infty}^{+\infty} \dot{u}_i^2\, \text{dt} = C_3\, \omega_j^2\, \tau_i \sum_{n=1}^{N} A^2_{ni} = \frac{N_i^3}{T_i}\, A_i^{-2} \qquad (5)$$

In order to compare wave trains of different types of waves by their energies, for the sake of the introduction of an analogy with microseisms, it is possible to reduce the periods and durations of different wave trains to an arbitrary reference wave train, for instance to the S-train, equalling the energies :

$$N_i^3\, T_i^{-1}\, A_j^2 = N_i^3{}_{\text{ref}}\, T_i^{-1}{}_{\text{ref}}\, A_i^2{}_{\text{ref}}$$

Hence, any wave train can be reduced to an arbitrary reference wave train by changing its RMS amplitude by means of the relation :

$$\overline{A}_{i\ \text{ref}} = \overline{A}_i \sqrt{\frac{T_{\text{ref}}}{T_i}} \;\; \sqrt{\left(\frac{N_i}{N_{i\ \text{ref}}}\right)^3} \;. \qquad (6$$

Using (4) and (5), the amplitude-distance relation of microseims, equivalent to impulsive processes, can be obtained :

$$A = \frac{aT^{\frac{1}{2}}_{ref}}{r^2 N^{3/2}_{ref}} + \frac{bT^{\frac{1}{2}}_{ref}}{r^{\frac{1}{2}} N^{3/2}_{ref}}$$

It can be shown, that N_{ref} and T_{ref} can be chosen arbitrarly, for instance T_{ref} can be taken characteristic for microseisms.

As to the values of k, in the investigations of Yu. V. Risnichenko, I. P. Pasechnik, V. I. Khalturin and N. B. Urusoff [6, 7, 8] the question of the variation at different periods of the effective divergence coefficient is minutely considered. The k-values are found to vary from 1,5 to 3. A theoretical analysis [10] leads to the value $k = 2$. The dispersion factor $T^{\frac{1}{2}}N^{-3/2}$ in our formula takes this phenomenon into account, so we accept $k = 2$. Further, putting, $A = CA_{ref}\, T^{\frac{1}{2}}_{ref}\, N^{-3/2}_{ref}$ we obtain finally :

$$A_{equi} = \frac{a}{r^2} + \frac{b}{r^{\frac{1}{2}}} = br^{-1/2}\left(1 + \frac{a}{b}\, r^{-1,5}\right) \qquad (7)$$

(b) *A case of microseisms, propagating from a single source,* assumed to be stationary and harmonic. The periods of different wave types are equal to the period of the exciting force. Consequently, microseisms and impulsive processes are equivalent, if reduced to a reference wave train by means of (3) and (6). In this case obviously the formula (7) is directly applicable. The decomposition of the whole process into body and surfacional components is however impossible without recourse to analogies.

Equation (7) can be presented in a equivalent form :

$$A = cr^{-n}$$

$$\frac{d\,(ln\, A)}{d\,(ln r)} = -\, n$$

After taking the logarithm of (7)

$$ln\, A = ln\, b - \frac{1}{2}\, ln\, r + ln\left(1 + \frac{a}{b}\, r^{-1,5}\right)$$

and finding the derivative we obtain finally :

$$\frac{d\,(ln\, A)}{d\,(ln r)} = -\,\frac{1}{2} - 1,5\,\frac{\frac{a}{b}\, r^{-1,5}}{1 + \frac{a}{b}\, r^{-1,5}} \qquad (8)$$

It can be seen, that at $r \to \infty$ the slope n tends to $-\frac{1}{2}$, whereas at short distances it tends to -2.

In a recent work (2) we have found, that in determining a source of microseisms within a limited area ad using an empyrical relation for N, the latter varies from $-3/2$ to -1. Expression (8) confirms theoretically this empyrical statement. Actually the quantity a/b should be regarded as a simple parameter. A most satisfactory agreement with empyrical values of n (*fig.* 3), found in papers [2, 3, 4] is obtained by putting $a/b = 10^4$-10^5.

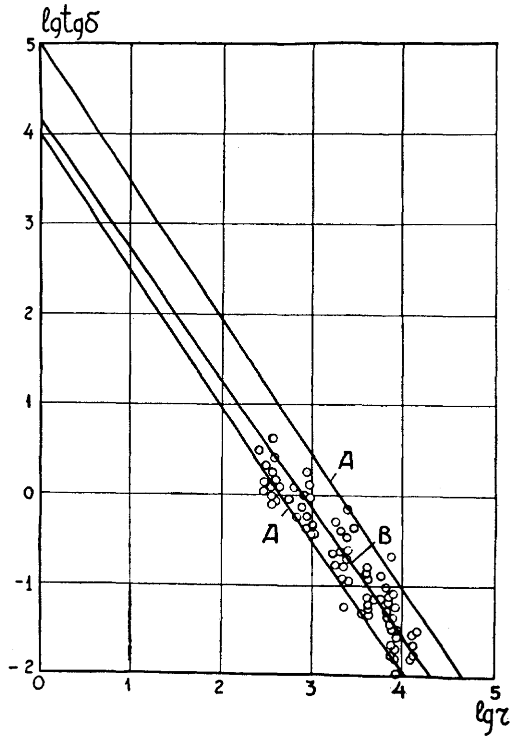

FIG. 3. — Observed and computed relation between the tangent of the angle of azimutal distortion and the distance.
A : computed.
B : observed.

Finally consider n from a somewhat different aspect. Suppose that the body and surface waves vectors form an angle, as it was above in the case of azimutal angle distortion. From (7) and (8) it follows that

$$\lg \operatorname{tg} \delta = -1{,}5 \lg r + \lg \frac{a}{b} + \lg \frac{\sin \varphi}{1 + \frac{a}{b} \cos \varphi \, r^{-1{,}5}} \qquad (9)$$

On the other hand, the lot of points, obtained by the analysis of earthquakes using relations (2), (3), (4) and (7) was plotted on figure 5, in assumption of $\varphi = \pi/2$. Constructions, performed for $\varphi = \pi/4$ and $\varphi = \pi/6$ had shown any new features in comparison with $\varphi = \pi/2$.

It may be seen, that the lot of points is located within a rather stretched ellypsis, having a slope of its greater axis equal to — 1,5, the latter cuts the ordinate axis approximately in point 10^4-10^5. In logarithmic coordinates, however, the plot of expression (9) will be a straight line, intersecting the ordinate axis in point a/b and having a negative slope of 1,5 (lines AA, *fig.* 5).

Hence, a confirmation of the empyrical distance relation of the exponent n, based exclusively on various cases of microseisms is obtained on one hand, and a similar result followed from an identification of earthquakes with microseisms — on the other. Such concordance of numerical values obtained by two perfectly different ways seems to be a confirmation of the interpretation chosen.

***

Using the amplitude location method of determining the coordinates of a microseismic source, we succeded to find, that intensive microseismic storms arise in areas of collison of swell waves with an oppositely directed wind. Actual observation of sources of microseismic excitation were carried out by authors in the Caspian sea. For this purpose, data of sea roughness observations of coastal hydrometeorological stations and open sea observations by vessels of the Caspian lines 1956-1958 were used. The microseisms were recorded by seismic stations « Makhachkala », « Lenkoran », « Kirovabad », « Shemakha », « Kysyl Arvat ».

A statistical comparison of periods of sea waves T_w with the periods of microseisms is shown in figure 4 by means of regression lines RR and CC. The correlation coefficient is 0,73. Periods of sea waves were measured by hydrometeorological station « Nizovaya Pristan » and microseismic data of Caspian seismic stations recording synchronous periods were used. The obtained statistical ratio $T_{ms}/T_w = 0,5$ is in excellent concordance with theory [11] and may be seen as a confirmation of the fact, that microseisms are due to sea waves with the frequencies considered. The slopes of the regression lines RR and CC are 0,35 and 0,65 and give the variation $T_{ms}/T_w = 0,5 \pm 0,15$. It should be mentioned, that the periods of sea waves, recorded by hydrometeorological stations

Makhachkala, Derbent and stations of the eastern coast result a ratio T_{ms}/T_w differing from 0,5. Apparently this discrepancy can

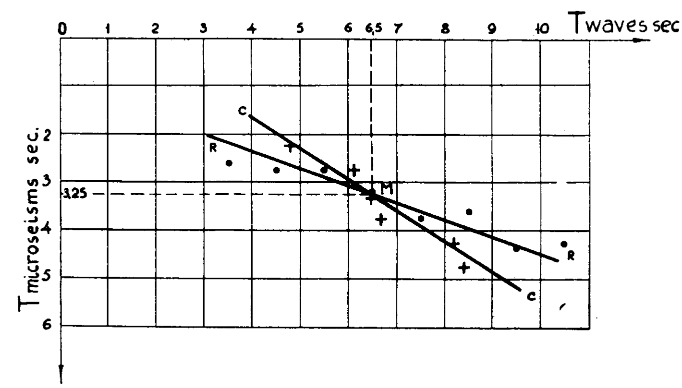

FIG. 4. — Regression lines of periods of microseisms and sea waves.

be related to shallow areas of the sea, to dispersion of sea waves and remoteness of the observation points from their excitation sources.

Observations of wave heights *h* carried out by vessels during microseismic storms between the latitudes 40-45 degrees and of amplitudes of microseisms A_{ms}, recorded by seismic station Makhachkala, gave a correlation coefficient $r = 0{,}56$.

Comparing *h* and A_{ms} in the case of a unilateral wind and sea waves, we see, that propagating sea waves of considerable height (h = 5-7 meters) do not give an increase of microseismic amplitudes excessive to the general microseismic background (A_{ms} = 1-1,5 microns).

Consider now the sequence of wind strength variation, sea roughness and the micrcseisms during the passage of a cyclone. The data available permit to select several cases, which show a complete representation of the phenomena studied and imply only a single microseismic source. Figure 5 shows a wave picture characteristic for the Casoian sea which arose by 18 hours GMT June 25 1956. It was due to a SE — wind of a long duration, connected with a cyclone moving over the European part of the Soviet Union. By 18 hours its low pressure area was located with its eastern wing over the Caspian, whereas its western part remained ashore. Over the medium area of the Caspian stable SE-winds were observed. The majority of coastal hydrometeostations reported their data by 15 hcurs. Figure 5 shows observations at 15 hours with dotted lines, and at 18 hours with continuous lines. The direction of wave development is shown by arrows. At each point of observation the numerator of a fraction shows the wave height and the denominator their period in seconds. For the sake of obviousness the heights and the wavelengths are depicted proportionally. From figure 5 it may be seen that the most intensive

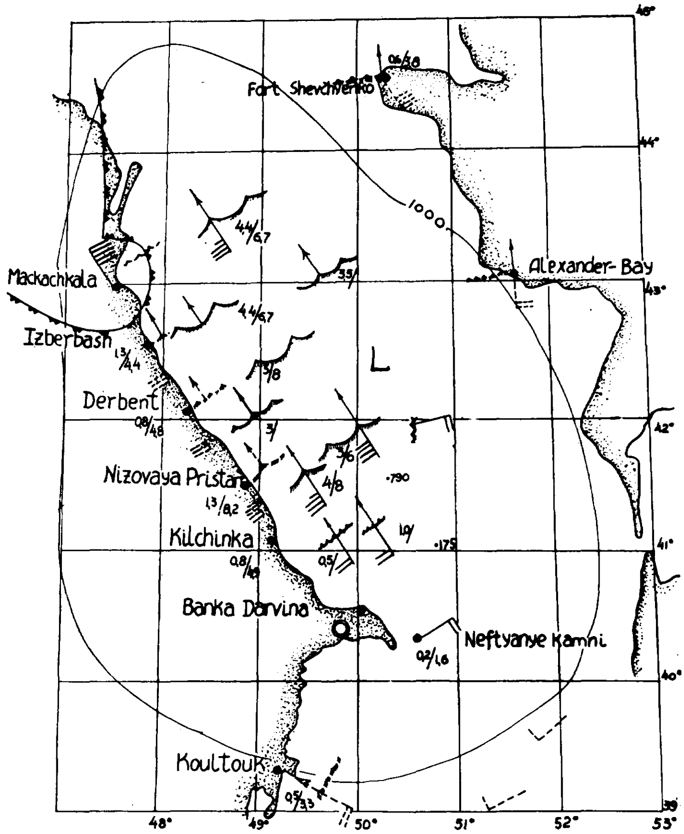

FIG. 5. — Hydrometeorological conditions on the Caspian 18 hours GMT June 25, 1956.

roughness was developed in the area of the Derbent depression and reached approximately the 43 latitude in the southern part of the sea, nearer to Iran, at 15 hours a weak choppines was recorded with winds with a force 2, which by 18 hours could not give rise to high waves. In the northern part of the Caspian and at the eastern coast also weak winds and insignificant choppines were observed. Hence, by 18 hours we have a a single SE-wave movement in the medium part of the Caspian.

At 18 hours a cold front, moving southward, reached the moutain barrier of the Mean Caucasian Ridge and proceeded to move in a SE-direction. Before 18 hours the movement of the cyclone was considerably slower. Since 18 hours the processes develop rather acively. The velocity of the depression center increases, the atmospheric pressure lowers, the winds strenthen. The first squall of the NW-wind begins at the Makhachkala shore. The increasement of the wind strength is nearly instantanous, ressembling a shock. At 18 hours all vessels report, SE wind, but meanwhile in Makhachkala already arises à NW wind of a force 10. 18 hours is a last term for the appearance of the cyclone above the sea. Figure 6 allows to trace the development of a microseismic storm, due to phenomena mentioned above. Between 15 and 18 hours only a general microseismic background can be observed, their amplitudes do not exceed 1,2 microns. At 18 hours 10 min the seismic station Makhachkala begins to record an increasement of periods and amplitudes of microseisms (from 2 to 3,5 sec and from 1,2 to 12 microns, respectively). In Makhachkala the first maximum of the amplitudes of microseisms is observed at 19 hours 20 min, that is, 1 hour 10 min after the beginning of the process, the period of microseisms at this moment equals 2,8 sec. The seismic stations « Grozny », « Kyzyl Arvat », « Kirovabad » record a single maximum of microseismic amplitudes at 21-22 hours with periods 3,5 sec, whereas simultaneusly in Makhachkala arises a second maximum. A comparison of all the data mentioned shows indeed, that only a shock of a NW wind collapsing with an oppositely directed swell of a SE direction gives rise to an increasement of microseismic amplitudes and periods.

It has been shown by Miche and Longuet-Higgins, that the origin of microseisms is possible due to standing sea waves. How can standing waves arise in the example considered above of the storm June 25-26? Before all we eliminate the built-up of a standing wave due to reflections from steep banks and to interference of waves originating from different sources. Indeed, 18 hours June 25 in the Medium Caspian only progressive waves of a height 4-5 meters in the SE direction had arosen. This phenomenon by itself somewhat increased the general background of microseisms, but did not give rise to an intensive growth of microseisms. The lack of correlation between unilateral wind, sea roughness and microseisms was already shown in paper [2]. Naturally it is rather improbable to suppose the appearance of reflected waves on the flat, sandy banks of the Caspian. Again, there are any reasons to suppose, that before 18 hours several wave trains of different directions should have arosen, which should be capable to create a standing wave : the meteorologic conditions testify only a SE stormy wind and SE wave movement.

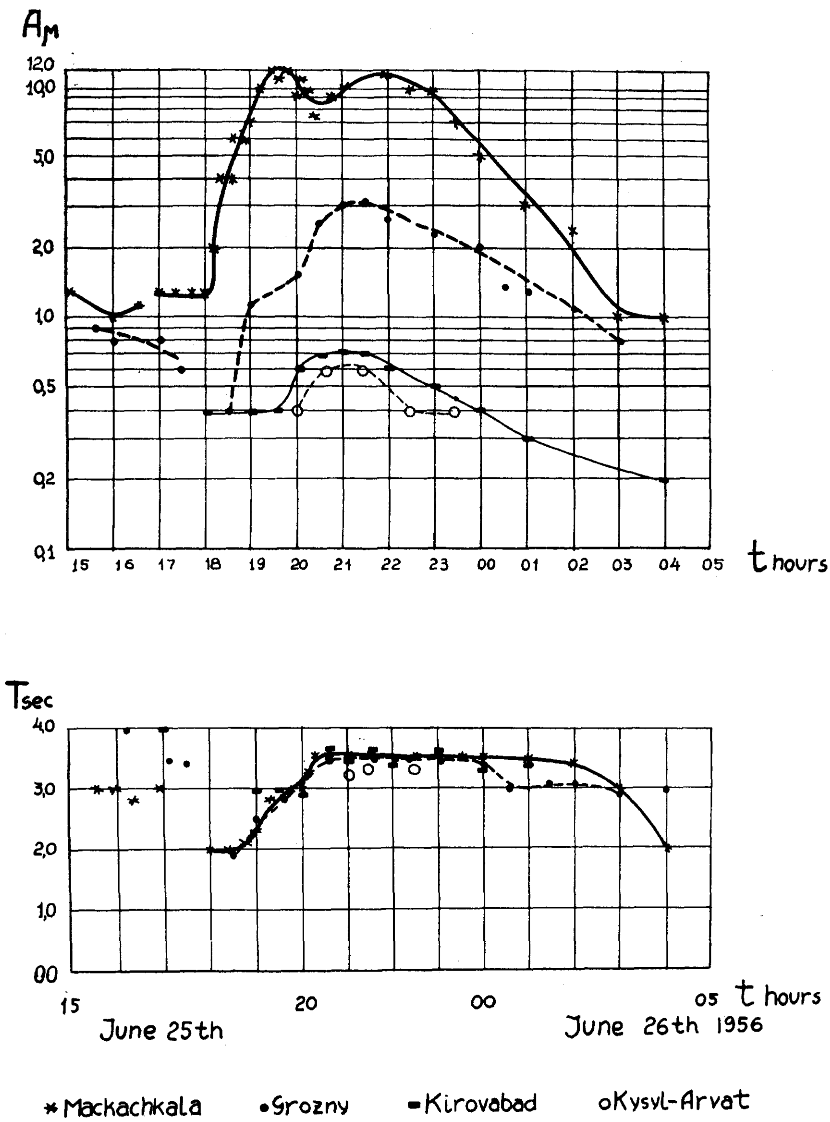

FIG. 6. — Microseismic periods and amplitudes June 25-26, 1956.

Figure 7 represents hydrometeorologic observations 21 hours June 25 (coastal stations) and 00 hours June 26 (ship observations). We see, that the low pressure area has proceeded to the SE, the cold front has moved over the sea and a stormy NW wind of a force 8-10 has already created progressive waves. June 26 00 hours all vessels report a same direction of progressive waves and wind. From the graph of microseisms (*fig.* 6) it may be seen, that 00 hours the microseismic storm quitens and 03 hours the amplitudes of

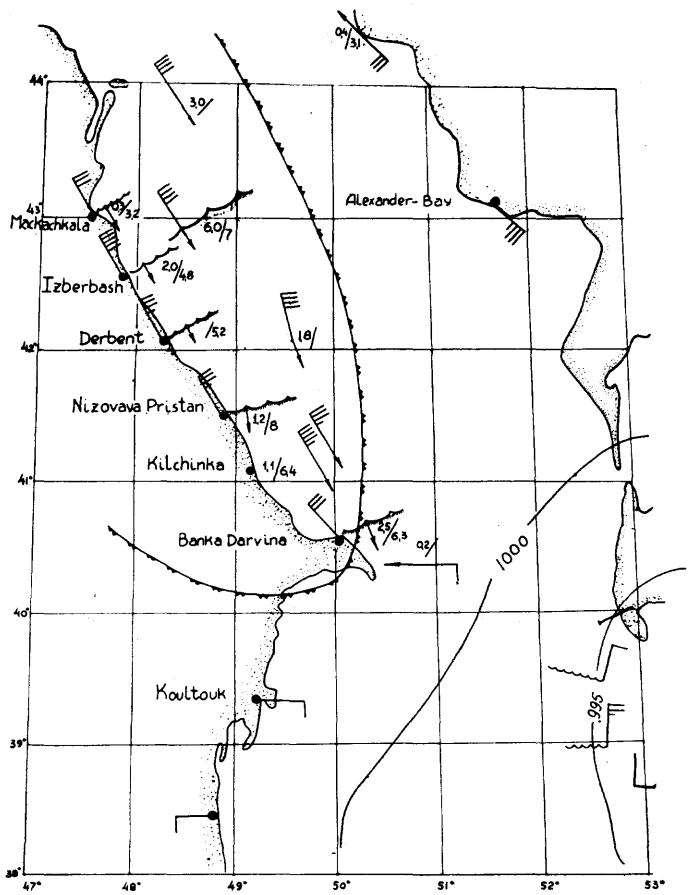

FIG. 7. — Hydrometeorological conditions on the Caspian 21 hour, June 25 and 00 hours, June 26, 1956.

microseisms of all the stations do not exceed the level of the usual background. The whole microseismic storm passed during 6 hours. It began at the moment of the displacement of the depression center above the surface of the aquatorium and the encounterment of the NW wind with a SE directed swell. A combination of this phenomena only could give rise to a microseismic storm. The formation of a standing wave could occur only during an interaction of a SE directed swell with an oppositely directed NW wind.

Frequency spectra of oppositely directed waves

Longuet-Higgins [11] has shown in his theory of the origin of microseisms, that the pressure acting on the bottom of the sea arises due to superposition of components of equal frequencies in oppositely directed wave groups

$$\frac{F}{\rho} = - K\, 4\,(\pi/k)^2 \int_{-\infty}^{\infty}\int_{-\infty}^{\infty} A_+ \, A_- \, \sigma^2 \, e^{2i\sigma t} \, du \, dv \qquad (10)$$

where $A_+(u, v)$, $A_-(u, v)$ are amplitudes of opposite wave components, $u, v,$ — the particle velocities in the direction of the x, y axes $k = \dfrac{2\,\pi}{(u^2+v^2)^{1/2}\,\lambda}$, λ — the wave length

$$\sigma^2 = (u^2 + v^2)^{\frac{1}{2}}\, gk\, th(u^2 + v^2)^{1/2}\, kH$$

σ — angular frequency of the resultant wave, g — the acceleration of gravity, H — sea depth.

Suppose an unilateral wind to develop a stationary wave movement in the aquatorium (*fig.* 5). Consider a sea district someone. It is known, that sea waves are not monochromatic, but have a definite spectrum of periods [12]. Suppose a possible unidimensional statistic spectral function A(T) in the form of an unsymmetric Pearson's distribution :

$$A = T^{m_1}\,(T_{max} - T)^{m_2} \qquad (11)$$

In our case the predominating period is approximately 7-8 sec. It is improbable to expect remarcable values of A having periods exceeding 10 sec. These conditions can be realized with $m_1 = 2$, $m_2 = 0{,}5$. This distribution is shown on figure 8 (curve A_+). Suppose, that the wind at $t = 0$ in the original direction has ceased and that immediatly an oppositely directed wind of constant force has arosen, as it was in the cases represented in figures 5 and 7. Let for the sake of simplicity the principle of superposition be valid for the waves of the direct and opposite direction. Suppose finally, that the spectrum A_+ remains costant and that the opposite wind creates only monochromatic waves, developing with the time

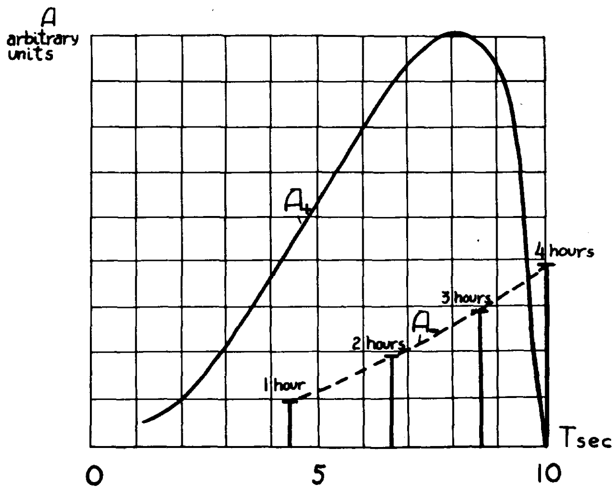

FIG. 8. — Interaction between frequency spectrum of the swell and a wave movement created by opposite wind.

in accord with the empyrical formulas of V. V. SHULEIKIN [12]

$$\lambda = B_1\, t^{1,2} \; ; \quad \frac{A_-}{\lambda} = B_2\, t^{\,0,2} \; . \; .$$

It may be readily obtained :

$$T = \frac{\lambda}{\sqrt{\dfrac{g\,\lambda}{2\,\pi}}} = \text{const}\; t^{0,6} \;\; ;$$

$$\lg T = \text{const} + 0{,}6 \lg t \qquad (12)$$

$$A_- = \text{const}\;\; t$$

In attempting to communicate greater reality to the present example, we assume that in 4 hours T_- reaches 10 sec and A_- 4 meters; then (12) and (13) give variations of the parameters of the opposite wave motion :

t_{hours}	1	2	3	4
T_{sec}	4,35	6,6	8,5	10
$A_{-\text{meters}}$	1	2	3	4
$T_{\text{ms sec}}$	2,17	3,3	4,2	5

For computation of variations of the periods and amplitudes formula (10) was used. For our case this relation can be simplified and takes the form :

$$F = \text{const}\ A_+\ A_-\ (t)\ \frac{1}{T^2}\ e^{4i\frac{\pi}{T}t}\ .$$

Figure 9 shows computed and recorded periods and amplitudes of microseisms for the seismic station Grozny. It may be seen, that the explanation proposed describes the variation of microseismic amplitudes fairly well. The period curve, however, diverges

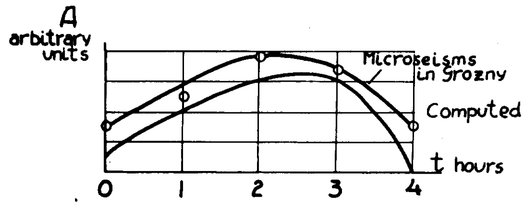

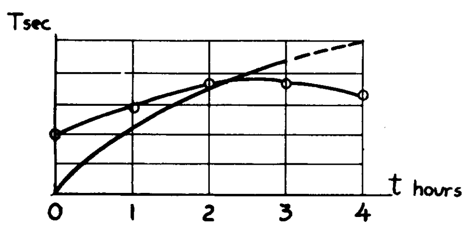

FIG. 9. — Comparison of computed and observed variation of periods and amplitudes of a microseismic storm June 25-26, 1956.

with observed values and has no descendent branch. This divergence could be eliminated, if the whole spectrum of the opposite wave movement should be considered, rather than a single component, and the attenuation of the waves should be taken into account.

DISCUSSION

The mechanism of microseismic generation, proposed by Longuet-Higgins can not be regarded as a uniquely possible. Theoretically a variety of situations leading to microseismic storms is conceivable. Nanda, for instance, determines the force acting on the sea bottom, created by interaction of an amplitude-modulated wave motion and an opposite wind [13] :

$$F = \text{const}\ (L/2\ HN^{\frac{1}{2}})\ \Omega\ \rho_a\ ua^2\ \text{Cos}\ \omega t \qquad (14)$$

where l- lenth of wave front, H-sea depth, ρ_a -air density, u_a wind velocity, ω -angular frequency of waves, Ω -area of the storm, 1/N -its part vibrating in phase.

According to Nanda's estimates, this force is by two orders smaller than Miche's force [11], great enough, however for generating microseisms. The force is inversely proportional to the sea depth, so the effect of rapid attenuation of microseisms generated in deep areas becomes explainable.

The phenomenon of change of wind direction by 180 degrees parallel to the western coast of the Caspian, depicted on fig-s 5 and 7, associated by a microseismic storm, is at the first sight in favour for Nanda's theory. Nevertheless, in the case considered a doubling of frequencies of microseisms with respect to the swell is indeed evident, which is a striking diagnostic symptom of Miche-Longuet-Higgins's mechanism. The distinct effect of increasement of the periods of microseisms during microseismic storms is also difficult to account for, from the point of view of Nanda's mechanism.

The inverse proportionality to H contained in expression (14) in our case contradicts to the fact, that one of the deepest districts of the Caspian is to be considered as the source of microseisms (the depth of the Derbent depression is 790 meters) [2].

Usually in analysing applications of Longuet-Higgins theory, doubts were expressed [13 and oth.] that actually the arising of significant areas of standing waves, vibrating in phase should be improbable. During visual observations of Caspian roughness on sea a few kilometers abeam of Makhachkala the authors of present paper succeeded to witness a quite favourable case of sudden change of wind direction associated with the movement of a cyclone eastward. The interaction of opposite wind and swell came to a gradual change of the wave pattern. On the original swell, rolling in the straight direction, opposite wave processes were imposed, which gave a standing wave pattern of spectrum components. The period of these waves increased with time under the influence of opposite wind. Pure standing waves were not to observe. This, however is in any case in contradiction with Longuet-Higgins theory, which requires only, that the spectrum should cotain oppositely directed components. The perceivable pattern of wave movement may ressemble a propagating one, but contain nevertheless standing components.

Hence, the case considered above apparently is controlled by the mechanism of Longuet-Higgins.

References

[1] Gilmore (M. H.). Amplitude distribution of storm microseisms. Symposium on microseisms. Nat. Res. Council. Publication 306, 1953. Washington D. C.

[2] Tabulevich (V. N.). On the nature of microseisms of the Caspian basin. Izvestiya AN SSSR, # 11, 1959. (In Russian).

[3] Tabulevich (V. N.). On some cases of microseismic excitation in the Atlantic and Pacific oceans. Doklady AN SSSR, 31, 4.814, 1960. (In Russian).

[4] Tabulevich (V. N.), Savarensky (E. F.). On the question of correlation between microseisms, meteorological situation and sea roughness. Studia Geoph. et Geod. 6 (1962).

[5] Hieblot (J.), Rocard (J.). Contribution à la théorie des microséismes. Ann. de Géoph. 15, 539, 1959.

[6] Risnichenko (Yu. V.). On the possibilities of calculation of maximum earthquakes. Proceedings of the Institute of Physics of the Earth, # 25 (192). (In Russian).

[7] Pasechnik (I. P.). On the determination of attenuation parameters of waves P_n and S*. Izvestiya AN SSSR, Geoph. series, # 12, 1960. (In Russian).

[8] Khalturin (V. I.), Urusova (N. B.). Estimate of the absorption of longitudinal and transversal waves in the earth's crust by observations on local earthquakes. Proceedings of the Institute of the Physics of the earth. # 25 (192).

[9] Monakhoff (F. I.). A microseismic method of sea storm tracing. Vestnik AN SSSR, # 9, 1955. (In Russian).

[10] Savarensky (E. F.), Kirnos (D. P.). Elements of seismology and seismometry. Moscow, 1955. (In Russian).

[11] Longuet-Higgins (M. S.). A theory of the origin of microseims. Trans. Phil. Roy. Soc. A 243, 1950.

[12] Shuleikin (V. V.). Short course of sea physics. Leningrad, 1959. (In Russian).

[13] Nanda (J. N.). The origin of microseisms. Journ. of Geoph. Res. Vol. 65, 6, 1815, 1960.

Toulouse. — Imprimerie EDOUARD PRIVAT — 34-9-64

PRINTED IN FRANCE